The use of satellite remote sensing to determine the spatial and temporal distribution of surface water on the Eastern Shores of Lake St Lucia

by

Franko Sokolic

Submitted in fulfilment of the academic
requirements for the degree of
Master of Science in the
School of Environmental Sciences
University of KwaZulu-Natal

Durban
2006

Abstract

The Eastern Shores of Lake St Lucia forms part of the ecologically important Greater St Lucia Wetland Park, designated a World Heritage Site in 1999. The landscape is characterised by surface water, a high water table and numerous wetlands. Little is known about the distribution and temporal fluctuations of this surface water and its relationship to the wetlands. This study uses remote sensing to examine the relationship by mapping the extent of seasonal, ephemeral and permanent surface water on the Eastern Shores.

Much of the surface water occurs in conjunction with emergent vegetation and is not easily mapped using hard classification methods. Neither a cluster analysis nor a maximum likelihood classification were able to map the subtle variations of the water-vegetation mix. Much more successful was the application of spectral mixture analysis using image endmembers of water, woody vegetation and non-woody vegetation. This technique was applied to seven Landsat Thematic Mapper images from 1991, 2001 and 2002. Steep slopes, forests and bare sand were masked out prior to classification.

Maps of water extent were produced for each of the seven study dates. Mapping accuracy was verified against rainfall, with high correlations being obtained against rainfall accumulated over six months and longer. Long-term rainfall patterns were reflected in the surface water distribution, with inundation being more extensive when accumulated rainfall was high. Fire scars reduced the accuracy of the spectral mixture analysis but these scars could be identified from the thermal image bands. The largest open water body in the study area was Lake Bhangazi. Large extents of surface water were also found in the Mfabeni swamp and the wilderness area to the north where water concentrations of 90% were measured during wet periods. Surface water present near Brodies Crossing during wet periods was less evident when rainfall was lower. No inundation was recorded in the areas to the west and south-west of the Mfabeni swamp or in the southern parts of the study area.

The techniques used in this study were developed into a water mapping protocol that uses image endmembers and spectral mixture analysis to measure water concentration.

Preface

The experimental work described in this dissertation was carried out in the School of Environmental Sciences, University of KwaZulu-Natal, Durban, from August 2002 to December 2005, under the supervision of Professor William Ellery.

These studies represent original work by the author and have not otherwise been submitted in any form for any degree or diploma to any University. Where use has been made of the work of others it is duly acknowledged in the text.

Signed:

F. Sokolic (candidate).

Signed:

Professor W.N. Ellery (supervisor).

Acknowledgements

Funding for this project was provided by the Norwegian Programme for Development, Research and Higher Education (NUFU). Were it not for this generous financial support, this project would not have been possible.

Much of the credit for this work must go to Fred Ellery, supervisor and friend, who first persuaded me to undertake this research. Your enthusiasm, support and advice were invaluable and greatly appreciated. Your love for wetlands is infectious and I hope that through this study I have been able to provide you with a unique perspective on these fascinating systems. Just remember, though, that despite the power of remote sensing nothing beats sloshing through wetlands and getting your feet wet!

Finally, much appreciation must go to Shirley Brooks, who provided considerable support, both emotional and academic. Your input into this project was far greater than you realise!

Table of Contents

List of Figures

List of Tables

1. INTRODUCTION

1.1 RATIONALE FOR THE STUDY

Water is a scarce and unevenly distributed natural resource that belongs to all South Africans. In viewing water as a commodity that must be managed sustainably and in a manner benefiting both users and the environment, the National Water Act (36 of 1998) provides guidelines for determining the national water reserve and also establishes a framework for managing it. The management principles prescribed in the Act are particularly important for the Eastern Shores of Lake St Lucia where, in contrast to its scarceness elsewhere in South Africa, water is relatively abundant. Most of this water is associated with wetlands that are considered to have great ecological value. In 1986 this value was recognised when the St Lucia wetland was declared a wetland of international importance in terms of the Ramsar Convention. More recently, the proclamation of the Greater St Lucia Wetland Park as a World Heritage Site in 1999 has resulted in international protection being afforded the area.

In mapping the surface water on the Eastern Shores, this study will address a number of important issues. Foremost among these is the issue of wetland delineation. The National Water Act (1998) defines a wetland as:

> "...land which is transitional between terrestrial and aquatic systems where the water table is usually at or near the surface, or the land is periodically covered with shallow water, and which land in normal circumstances supports or would support vegetation typically adapted to life in saturated soil" (National Water Act, 1998, Chapter 1, clause 1(xxix)).

There are a number of reasons why wetlands are important. Firstly, they provide value in the form of animal, plant and mineral resources. These include products like peat, reeds and fish. Secondly, wetlands provide indirect benefits such as flood attenuation, erosion control and the enhancement of water quality (DWAF, 2003). The most noticeable features of wetlands are the presence of water close to or at the surface, distinctive soils, and vegetation tolerant of saturated soils. Water, and the fluctuating level thereof, is the main factor leading to wetland formation. The depth and duration of flooding in a wetland is

directly responsible for the creation and maintenance of different wetland habitats (Keddy, 2000) and is described by the hydroperiod, which varies from permanently to intermittently flooded. With respect to wetland soils, saturation causes them to be oxygen deficient, resulting in increased solubility and leaching of metals such as iron and manganese from the soil (DWAF, 2003). This gives wetland soils a distinctive grey colour and also leads to the formation of brightly coloured mottles (yellow/orange/red) where leached metals (especially iron) are locally deposited in the zone of seasonally saturated water. Vegetation, the third important wetland feature, is adapted to flooding and a lack of oxygen in the root zone (Keddy, 2000), and is often used as an indicator of the presence of a wetland.

Hydrology is the main driver in the formation of wetlands. However, it is rarely used to delineate wetland boundaries as it takes years of careful observation to determine the hydroperiod (DWAF, 2003). For this reason, wetlands are usually delineated by examining the other two features, soil and vegetation. Unfortunately, the reworked marine sediments of the coastal plane are often iron-deficient, causing these soils to have a pale profile, even outside of wetlands (DWAF, 2003). Using the third characteristic, wetland vegetation, to delineate wetlands, requires not only expert knowledge but relies on the presence of undisturbed vegetation. These conditions are not always met. Furthermore, the relationship between wetland vegetation and the hydroperiod is poorly understood (Ellery, 2006a, pers. comm.) leading to uncertainties in delineating wetlands from vegetation alone. By mapping the distribution and fluctuation of surface water (and hence, the hydroperiod), this project may help to overcome the limitations of using soil and vegetation as wetland indicators. This allows wetlands to be delineated by means of the principal driver of wetland formation, and not surrogate indicators such as soil and/or vegetation.

The second important contribution this study makes is towards the determination of South Africa's water reserve. The reserve, as defined by the National Water Act (1998), consists of two parts: the basic human needs reserve and the ecological reserve. The former provides for the requirements of individual citizens while the latter describes the amount of water required to protect aquatic ecosystems. The reserve refers to both the quantity and the quality of the water resource. The Act stipulates that the water reserve should be determined for all significant water resources, be they estuaries, watercourses, aquifers, or surface water. While this is relatively easy to do for rivers and lakes, based on a well-tested methodology using bio-indicators, providing an accurate determination of the reserve for

wetlands is rather more difficult. In the case of the Eastern Shores, where the proclamation of the Greater St Lucia Wetland Park recognised the importance of the region's wetlands, little is currently known about the distribution of the surface water associated with these wetlands. While good groundwater and rainfall data are available for the Eastern Shores, knowledge of the location, extent, and persistence of wetlands is limited. This study provides a means of determining this reserve, not only though the mapping of surface water associated with wetlands, but also by establishing links between surface water and rainfall.

By mapping surface water and allowing the water reserve to be determined, this study also makes a contribution towards gaining a better understanding of wetland structure and its relationship with biodiversity. Wetland biodiversity is affected by the interconnectedness of wetlands, which in turn is determined by fluctuating water levels. Biodiversity tends to be higher in areas exposed to seasonal wetting and drying than in areas where conditions are more stable (Vrdoljak, 2004). This is because water bodies and wetlands that become isolated as water levels drop, form habitat islands in which the exchange of aquatic species with other water bodies is restricted. Having a mosaic of such habitat islands and/or interconnected wetlands leads to increased landscape-level heterogeneity, resulting in increased biodiversity (Vrdoljak, 2004). Furthermore, mapping the spatial distribution of surface water also allows the location of aquatic refugia to be determined. These are hydrologically stable areas that are extremely important in times of drought as they provide a stable environment in which aquatic biota are able to survive (Vrdoljak, 2004). Once the drought has passed and water bodies become reconnected, these species move out from the refugia and recolonise water bodies and wetlands from which they had disappeared during the drought. Through shedding light on the openness and spatial distribution of surface water systems on the Eastern Shores over time, this study provides a means of understanding wetland structure and its relationship with biodiversity.

The final aspect to which this study addresses itself is wetland management. The National Water Act (1998) places a strong emphasis on the management of water and provides clear guidelines for the establishment of catchment management agencies. These guidelines also apply to the Eastern Shores study area, which, as part of a World Heritage Site, is already subject to strict environmental controls. Managing this environment effectively can only be done by understanding the various components that comprise the system, as well as the interactions between them. By mapping the surface water of the Eastern Shores and by

determining its linkages with other environmental components, this study aims to increase this environmental understanding, thereby contributing to better management practices and to the effective protection of the environment.

This study, then, makes a meaningful contribution to wetland management, the delineation of wetlands, the establishment of the water reserve, and also sheds light on wetland structure and biodiversity. In the study, satellite-based remote sensing is used to map surface water on the Eastern Shores. There are a number of reasons why remote sensing is employed. Firstly, the Eastern Shores covers an area of almost 250 km^2, making ground-based mapping of wetlands and water bodies very difficult and time consuming. This is not only because of the large size of the area, but also because many areas are remote and inaccessible. In addition, dense wetland vegetation often hides the presence of water from ground-based observers, even in areas that are readily accessible. A final difficulty in conducting ground-based mapping is that much of the surface water on the Eastern Shores is episodic or ephemeral in nature. Because of this, surface water might no longer be present when an area is mapped. These problems are overcome by using remote sensing, which allows large areas of the earth's surface to be mapped reliably and repeatedly. Remote sensing has proved a cost effective technique (Thompson *et al.*, 2002), allowing the spatial and temporal characteristics of features on the earth's surface to be studied. Furthermore, archived satellite images are a valuable resource that can allow the hydrological regime on the Eastern Shores to be examined in detail.

In this study, various image classification techniques are applied to a time-series of Landsat images in an attempt to determine the best means of mapping surface water in the study area. A digital elevation model and vegetation index are used to aid the delineation of water bodies, and the most accurate technique is developed into a water mapping protocol.

1.2 AIM AND OBJECTIVES

With this background to the problem in mind, the aim of this study is to:

> Use satellite remote sensing to ascertain the spatial and temporal distribution of surface water on the Eastern Shores of Lake St Lucia.

It is important to note that the aim of this project is to map the distribution of surface water and not wetlands. However, given that the duration and frequency of flooding are important defining characteristics of wetlands, determining the presence of water, particularly when it occurs in conjunction with emergent vegetation, allows the presence of wetlands to be inferred.

In order to achieve the aim of the project, a number of objectives have been set:

- Assess the suitability of available remotely sensed products
- Acquire satellite images suitable for mapping surface water
- Geometrically and radiometrically correct the chosen satellite images
- Develop a set of spectral signatures to detect the presence of surface water on the Eastern Shores
- Map the distribution of surface water on the Eastern Shores
- Develop a protocol for mapping the distribution of surface water

The last two objectives refer to key products of this study. By mapping the distribution and temporal fluctuations of surface water, insight is gained into the characteristics and distribution of wetlands, while at the same time enabling correlations between surface water, groundwater and rainfall to be assessed. In addition to the maps, the mapping protocol provides a powerful predictive tool with a number of potential uses. Firstly, it will allow the past extent of surface water to be quantified and, secondly, it will enable the effects of climate change on the distribution of surface water to be explored.

1.3 OVERVIEW OF THE THESIS

This thesis consists of eight chapters. The reasons for conducting this research, as well as the aim and objectives of the study, have been described in Chapter One. The second chapter provides a background to the Eastern Shores study area, describing both the physical and human influences that have shaped the area. Chapters Three and Four locate this study within the broad body of remote sensing knowledge. In Chapter Three this is done by reviewing the theoretical concepts used in this study, while Chapter Four provides a review of the Landsat Thematic Mapper sensor, its capabilities, and how it has been used by other researchers to map water and wetlands. The fifth chapter describes the

methodologies used in this research and explains how they have been applied to the satellite images covering the study area. The results of the research are presented and analysed in Chapter Six. In Chapter Seven, these results are contrasted and compared to results from other studies and the findings arising out of this study are discussed in the light of this previous research. The water mapping protocol developed in this study is also presented in this chapter. The final chapter provides a conclusion to the study and makes recommendations for further research.

2. BACKGROUND TO THE STUDY AREA

2.1 INTRODUCTION

The Greater St Lucia Wetlands Park, declared a World Heritage Site in 1999, has long been recognised as a region of ecological importance that incorporates many areas of exceptional scenic beauty and biodiversity. The Eastern Shores is one such area. It comprises the strip of land to the east of Lake St Lucia and is often treated as a separate entity within the World Heritage Site. This study focuses on the Eastern Shores as it forms a well-defined geographical region in which hydrological inputs and outputs are well understood.

2.2 LOCATION OF THE STUDY AREA

The Eastern Shores is bounded by the Indian Ocean in the east and Lake St Lucia in the west. It stretches northwards from the town of St Lucia for a distance of 48 km and covers an area of approximately 250 km^2 (Figure 2.1). Artificial structures are confined almost exclusively to the town of St Lucia in the extreme south, although a few roads and tourist facilities can be found as far north as Lake Bhangazi. The area north of Lake Bhangazi is a Wilderness Area where access is strictly controlled. Tourist infrastructure is restricted mainly to the areas south of Lake Bhangazi and takes the form of overnight accommodation, hiking trails and game-viewing roads. Numerous access roads and tracks were created by the forestry industry that formerly operated in the region, but with the removal of the plantations these are expected to fall into disuse.

2.3 CLIMATE

The Eastern Shores study area is characterised by hot, wet summers and mild, drier winters. Mean annual precipitation exceeds 1000 mm throughout the area although a strong east-west gradient exists, with coastal areas receiving in excess of 1100 mm per year. This rainfall gradient is a noticeable feature along this section of the South African coast and is

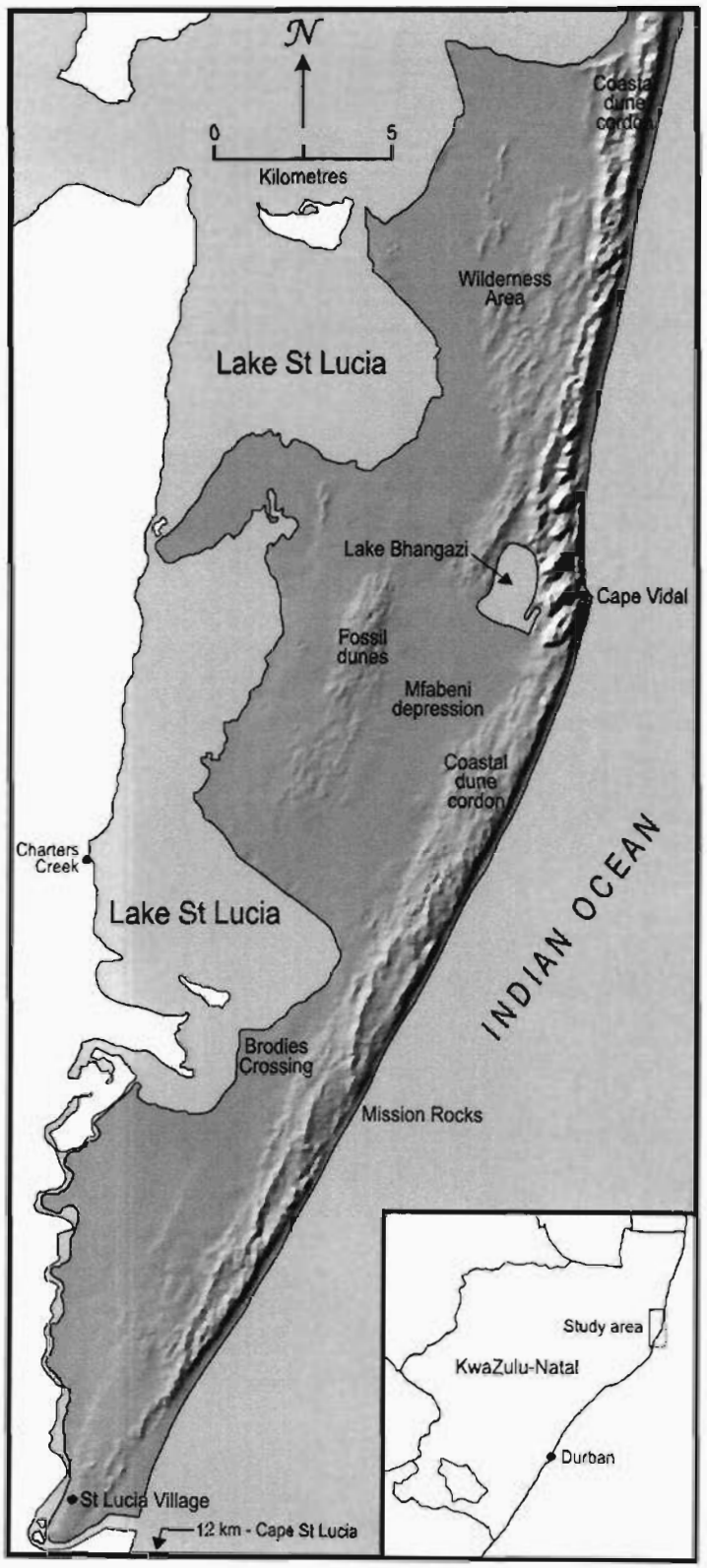

Figure 2.1: The Eastern Shores of Lake St Lucia, showing the general topography of the study area.

clearly evident in the mean monthly rainfall figures of the Cape St Lucia and Charters Creek[1] climate stations (Figure 2.2). While both stations exhibit a similar pattern of wet summers and drier winters, the Charters Creek station, located 10 km inland, experiences lower rainfall than the coastal Cape St Lucia station throughout the year. Occasional extreme rainfall events caused by cut-off low pressure cells or tropical cyclones can result in daily rainfall in excess of 300 mm. Longer term periods of above and below average rainfall can be observed from annual rainfall totals.

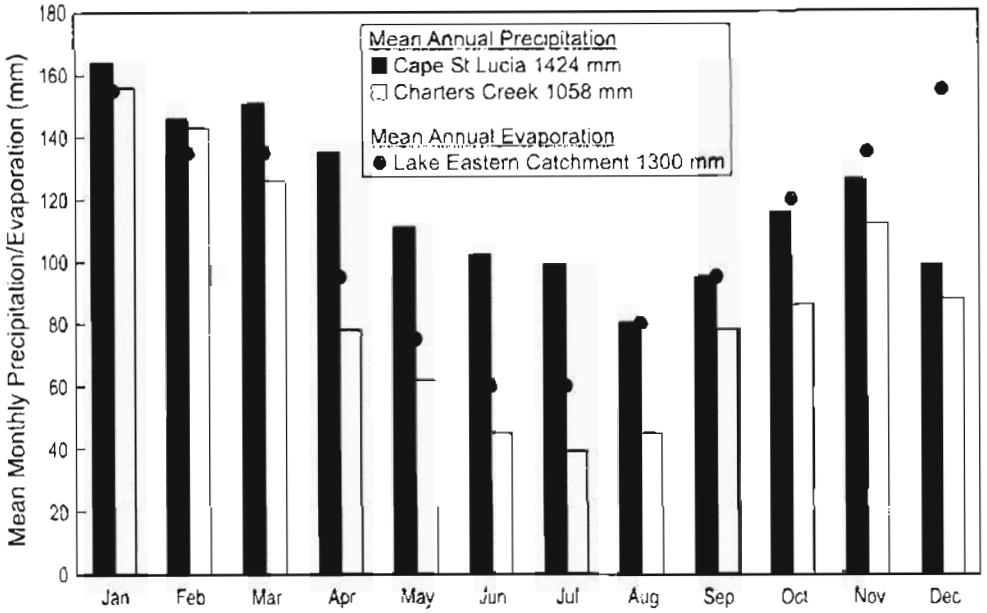

Figure 2.2: Mean monthly rainfall for the Cape St Lucia and Charters Creek climate stations. Cape St Lucia figures are averaged over the period 1961-1990 while those for Charters Creek cover the period 1964-1990 (Source: South African Weather Service). Also shown are mean monthly evaporation figures for the Eastern Shores (red circles).

Rates of evaporation on the Eastern Shores are very similar to rainfall. Mean annual evaporation is approximately 1300 mm, reaching a peak of 155 mm per month in December and January before dropping to 60 mm in June and July (Hutchison & Pitman, 1973). The evaporation is driven by the relatively high temperatures that prevail throughout the year. Average monthly maximum temperatures peak in January, reaching almost 30°C at Charters Creek and 28°C at Cape St Lucia (Figure 2.3). Average maximum temperatures remain above 21°C for both stations even in the winter months. Frost is unknown in the area, with no sub-zero temperatures ever having been recorded at either of the two stations.

1. The Charters Creek station was formerly known as the St Lucia Lake Research Centre.

Wind is another factor contributing to the high rates of evaporation, with speeds averaging over 4 m/s along the entire KwaZulu-Natal coast (Diab, 1995). The winds tend to blow parallel to the coast, being predominantly from the north-east and the south-west. Humidity levels on the Eastern Shores are generally high throughout the year, with annual averages of 84% at 08h00 and 75% at 14h00 at the Cape St Lucia climate station.

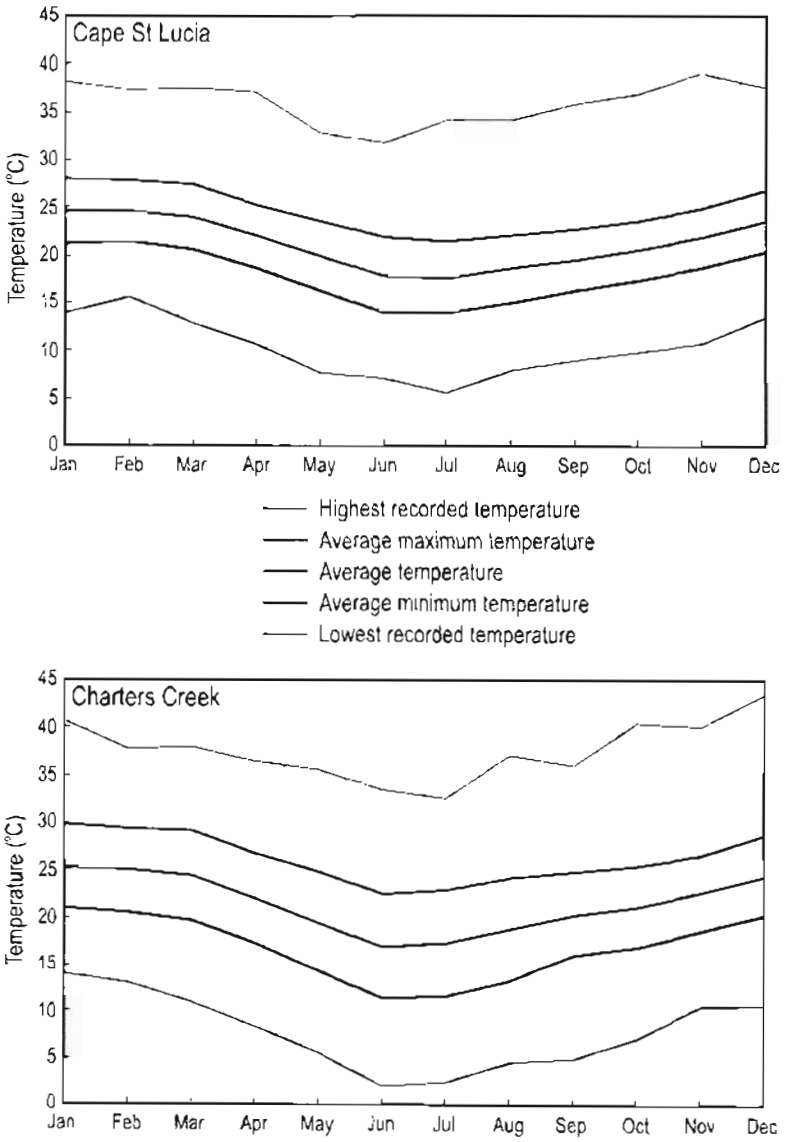

Figure 2.3: Temperature statistics for the Cape St Lucia (1961-1990) and Charters Creek (1964-1990) climate stations (Source: South African Weather Service).

2.4 BIOPHYSICAL CHARACTERISTICS

The Eastern Shores are characterised by unconsolidated dune sands, redistributed sands and alluvium (Watkeys *et al.*, 1993). This terrestrial sand cover has been reworked and redistributed since sea levels reached their current levels 6000 to 7000 years ago. A notable feature of the study area is the range of vegetated dunes forming a continuous chain along the coast, reaching heights of 160 m near Cape Vidal (Figure 2.1). Inland of these coastal dunes lies a gently undulating plain, situated for the most part below 20 m above sea level and extending all the way to the shores of Lake St Lucia in the west. In the central portion of the study area is the large Mfabeni depression. This depression usually drains southwards towards Lake St Lucia but at times drains northwards into Lake Bhangazi, the largest water body on the Eastern Shores. West of the Mfabeni depression lies a ridge of fossil dunes that reach heights of over 60 m in places.

The hydrology of the Eastern Shores is largely driven by rainfall and very little groundwater recharge from Lake St Lucia occurs (Kelbe, 2005, pers. comm.). Some rainfall is lost through evaporation and transpiration but most percolates through the permeable sands and recharges the groundwater. The numerous small lakes and wetlands so characteristic of the area form where the groundwater intersects the land surface. The size and permanence of these wetlands and lakes is driven by fluctuations in the groundwater levels, which can vary by up to three metres from year to year. Very little surface flow occurs, except during extreme rainfall events (Vrdoljak, 2004).

The coastal dunes are covered mostly in dune forest vegetation while the inland plains consist of a mosaic of grasslands, wetlands, lakes, forest patches and plantations. The vegetation on these inland plains, where not replaced by pine plantations, consists of hygrophilous grasslands, swamp forests, sedge swamps and dry grasslands (Thompson, 2002). The commercial pine plantations, planted in areas formerly occupied by hygrophilous grasslands, have altered the hydrological regime through their high rate of evapotranspiration. The resultant drying has allowed the pines to invade pans and even areas of hygrophilous grassland that would have been unsuitable for pine trees due to the high water table (Vrdoljak, 2004).

A final notable feature of the Eastern Shores is the presence of large quantities of rutile, ilmenite and zircon in the coastal dunes. These have been concentrated through wave and wind action and occur in concentrations that make mining commercially viable. Attempts by Richards Bay Minerals to mine these deposits were stopped in 1996 when the government ratified the findings of a review panel that mining should not proceed (Thompson, 2002). Thereafter the area was declared a World Heritage Site.

2.5 THE EASTERN SHORES: HUMAN IMPACTS

While the status of World Heritage Site recognises the ecological importance of the area, it should be borne in mind that the Eastern Shores is not a pristine wilderness unaffected by human impacts. These can be traced back to about 1600 years ago and include the impacts of hunter-gatherers and subsistence farmers (Thompson, 2002). While the early hunter-gatherers appear to have had little effect on the environment, the increasing use of slash-and-burn agriculture, and the keeping of livestock by iron-age subsistence farmers, started to impact the natural vegetation of the area. This has led to the suggestion that the grasslands in this region are mainly anthropogenic in nature (e.g. Thompson, 2002), although evidence from palaeobotanical, archaeological, biogeographical and ecological research indicates that these grasslands actually pre-date the arrival of iron-age peoples and are naturally maintained by fire (Ellery and Mentis, 1992). By the start of the 20th century, white traders and hunters had started impacting the area and rapidly depleted many species of game. Removal of these game species, most of them herbivores, resulted in reduced grazing and browsing of the vegetation of the region (Thompson, 2002).

From the 1950s onwards, with the arrival of commercial state forestry on the Eastern Shores, the rate of environmental change increased dramatically. Not only did this form of monoculture reduce the biodiversity of the region, it also diminished the area of grasslands by a third, reduced seepage into Lake St Lucia, and caused a dramatic lowering of groundwater levels (Thompson, 2002). As the commercial forests expanded, subsistence farmers were forcibly moved from the area and their fields and grazing lands were converted to plantations. Commercial forestry continued until a 1989 government decision to phase out the 5600 ha of plantations on the Eastern Shores (Boyes *et al.*, 2002). The drive to remove these plantations gained further impetus with the formation of the Greater

St Lucia Wetland Park, with the last of the plantations removed by 2005. The removal of these plantations is expected to have major impacts on the hydrology and vegetation of the Eastern Shores, resulting in changes to the mosaic of grasslands, wetlands, lakes and forests that characterise this region.

2.6 CONCLUSION

The Eastern Shores has been shaped over the ages by both geological and climatological forces. In recent times, however, the landscape has been altered by human activity and the present environment needs to be interpreted in the light of all three of these forces: geological, climatological and human. Understanding how these forces have shaped the landscape affords insight into the environmental conditions of the study area, thereby aiding the interpretation of the results obtained in this study.

3. THE THEORY OF IMAGE PROCESSING AND ANALYSIS

3.1 INTRODUCTION

Remote sensing can be defined as the process of acquiring information about objects using measuring devices that are not in contact with those objects. In the context of satellite-based remote sensing, this is achieved by means of sensors aboard orbiting satellites that gather data about features on the earth's surface without actually being in contact with those features. Once the data have been captured in the form of satellite images, image processing techniques are used to turn the data into information. Understanding the theory behind these image processing techniques is important for this study, as this ensures their effective application and allows informed interpretation of the information they generate. By reviewing relevant literature, this chapter will explore the theory and techniques applicable to each of the stages of image processing and analysis.

3.2 AN OVERVIEW OF IMAGE PROCESSING AND ANALYSIS

The manipulation, processing and interpretation of digital images is known as image processing. Image processing comprises a number of discrete and well-defined steps, some of which are essential, others optional. Eastman (2001), who defined digital image processing as being the application of computer analysis techniques to digital image data, recognised four image processing steps:

- Image restoration
- Image enhancement
- Image classification (including accuracy assessment)
- Image transformation

These four seemingly simple steps tend to hide the complexity of image processing. A sense of this complexity is perhaps better captured by Lillesand & Kiefer (2000) who provide a rather more detailed outline of image processing:

- Image rectification and restoration

- Image enhancement
- Image classification (including accuracy assessment)
- Data merging and GIS integration
- Hyperspectral image analysis
- Biophysical modelling
- Image transmission and compression

Both Lillesand & Kiefer (2000) and Eastman (2001) consider accuracy assessment to be part of the image classification process, whereas other authors (e.g. Sader *et al.*, 1995; Congalton & Green, 1999; Harris, 2003; McCauley & Goetz, 2004) view it as a separate step. While not explicitly stated, perhaps their rationale behind combining these two steps is that image classification and accuracy assessment should be viewed as an iterative process in which a number of iterations are performed until a suitable or optimum level of accuracy is achieved.

Lunetta (1999) described the processing of multitemporal images for use in change detection studies, a procedure which differs somewhat from one in which images are classified from a single date. Lunetta (1999) recognised six stages in this process:

1. Data acquisition and preprocessing, in which digital images are acquired and prepared for processing. This preparation includes clipping or mosaicking the images so that the complete study area is covered; masking out of unwanted areas; and the preparation of ancillary datasets.
2. Geometric and radiometric corrections, which involve registering one of the images (the reference image) to absolute geographic coordinates and then registering images from all other dates relative to this reference image. Lunetta (1999) stated that the root-mean-square (RMS) error occurring during image-to-image registration should not exceed 0.5 pixels as the images from different dates have to be compared pixel-by-pixel. In addition, radiometric corrections could be applied to compensate for the effect of the atmosphere on the transmitted radiance and also for variations in measurements occurring because of differences in sensor characteristics over time and across platforms. Lunetta (1999) called this a *first order radiometric data normalisation.*
3. Data normalisation, where one of the images is selected as the reference image and the radiometric properties of the remaining images are adjusted relative to this reference image. This *relative radiometric normalisation* further reduces differences between

images resulting from differing solar radiation incidence angles, atmospheric conditions, and sensor differences.

4. Change detection analysis is a crucial step in which differences between images are analysed. Among the analytical techniques mentioned by Lunetta (1999) are composite analysis, image differencing, and principal components analysis.
5. Accuracy assessment, an essential step in which an attempt is made to assess the accuracy of the change detection analysis.
6. Final product generation represents the final stage in the image processing methodology.

While the general steps outlined above were considered by Lunetta (1999) to be applicable to most change detection projects, the procedure followed in any particular project has to be guided by the aims, goals and required deliverables of the project.

The three image processing methodologies outlined above, while differing somewhat in detail, all contain the same broad structure of (a) image preparation, (b) image classification and (c) output image generation. This basic structure has been adopted in most remote sensing studies, although the specifics of particular studies sometimes necessitate minor variations. For instance, Eckhardt *et al.* (1990) devised a system for monitoring irrigated lands in Nevada and described their image processing as consisting of five steps, namely image acquisition, image registration, image normalisation, image transformation, and image classification. Jensen *et al.* (1995), in using change detection techniques to examine changes in the Florida Everglades, presented a three-step methodology consisting of image preprocessing (which included image rectification and image normalisation), image classification, and application of change detection techniques. Munyati (2000) also presented a change detection study, one in which changes occurring in parts of the floodplain of the Kafue River in Zambia were assessed. A five-step image processing methodology was applied to the four Landsat images used in the study:

- Geometric registration of the images
- Atmospheric correction of a selected reference image
- Normalisation of the remaining images to the reference image
- Image classification and accuracy assessment
- Change detection

Another southern African application of remote sensing was by Wannenburgh & Mabena (2002) who used Landsat-7 imagery to conduct an inventory of indigenous forest in South Africa. Once again their methodology has similarities to previously discussed studies:

- Geometric correction of the images
- Image enhancement
- Image classification
- Image interpretation
- Accuracy assessment (which the authors termed quality control)

Of the various image processing steps, perhaps the least problematic and easiest to accomplish is the geometric rectification and registration of satellite images. This is achieved by means of ground control points that are used to tie the satellite image to real world coordinates. More complicated and much harder to execute are the steps of atmospheric correction, image transformation, image classification, and accuracy assessment. These four steps, widely discussed in the literature, warrant further investigation and are discussed in more detail in the next four sections.

3.3 ATMOSPHERIC CORRECTION METHODS

Surface-reflected radiation passes through the atmosphere twice before being measured by a satellite, undergoing scattering and refraction and experiencing varying amounts of absorption. The magnitude of scattering and absorption depends not only on the state of the atmosphere, but also on the wavelength of the radiation itself (Lillesand & Kiefer, 2000).

There are three processes responsible for atmospheric scattering. Mie scattering is caused by atmospheric constituents like water vapour and dust and is particularly significant under slightly overcast conditions. This type of scattering occurs when the atmospheric particles are of a similar diameter to the radiation. Rayleigh scattering, on the other hand, is caused by atmospheric molecules that have diameters much smaller than that of the incoming radiation. This scattering is strongly wavelength dependent, with shorter wavelengths being more strongly scattered than longer wavelengths. Rayleigh scattering is responsible for the blue colour of the sky and is also the primary cause of atmospheric haze (Lillesand & Kiefer, 2000). A third type of scattering, non-selective scatter, is caused by larger

atmospheric particles (e.g. water droplets in clouds). Here visible, near- and mid-infrared radiation tends to scatter in equal amounts. The net effect of atmospheric scattering is to reflect radiation, thereby adding to the signal measured by the satellite sensor. This additional, atmosphere-reflected radiation is termed path radiance.

Whereas scattering increases the signal measured by the sensor, absorption diminishes the amount of radiation reaching the satellite (Lillesand & Kiefer, 2000). Atmospheric absorption of radiation is caused by the constituent gases in the atmosphere. These are gases like ozone, carbon dioxide and water vapour that each absorb electromagnetic energy at very specific wavelengths and are responsible for the atmospheric windows which are so crucial to satellite-based remote sensing (see Section 4.4.1 on page 51).

The effect that the atmosphere has on the signal measured by a satellite cannot be ignored, particularly for multitemporal studies that compare satellite images recorded on different dates and under varying atmospheric conditions. Teillet & Fedosejevs (1995) suggested that the main goal of atmospheric corrections should be to provide surface reflectance[2] to an accuracy of 5% or better. However, the question of how to actually remove the atmospheric effects has been, and continues to be, the subject of much research and debate. Teillet (1997) stressed that for fast and straightforward atmospheric correction, there had to be easy access to atmospheric variables describing the state of the atmosphere on the date and time the image was recorded. In an earlier study, Chavez (1996) emphasised the need for procedures to correct atmospheric effects, particularly for change detection studies. Chavez (1996) went on to say that the ideal radiometric correction procedure was one based only on the satellite image itself, needing no *in situ* field measurements.

The terminology relating to radiometric and atmospheric corrections is not always used consistently, possibly reflecting the state of flux in a field where processes are still being developed, modified and perfected. Teillet & Fedosejevs (1995) referred to radiometric correction and atmospheric correction as two different processes. They saw radiometric correction as a process whereby digital signals measured by the satellite (also known as digital numbers or DN) were converted to units of radiance, measurements that they called apparent radiance (as measured at the sensor). Atmospheric corrections went a step further,

2. Reflectance is the ratio of incident radiation to reflected radiation. Values range between 0 (no reflection) and 1 (perfect reflection). These values are sometimes expressed as percentages.

taking these measurements of apparent radiance and converting them to actual surface reflectance values. This contrasts with a number of other authors (e.g. Chavez, 1988; Hall *et al.*, 1991; Mispan & Mather, 1997; Lillesand & Kiefer, 2000) who considered atmospheric corrections to be just one part of the process of radiometric correction. While not adopting the definitions used by many other researchers, Teillet (1997) changed his terminology to refer to the two processes of *radiometric sensor calibration* and *atmospheric correction.*

Perhaps the simplest classification of atmospheric correction techniques was provided by Roberts *et al.* (1999) who mentioned only two categories, namely absolute calibration and relative reflectance retrieval (Table 3.1). Hadjimitsis & Clayton (2004) reviewed the various correction techniques described in the literature over the years and, like Roberts *et al.* (1999), found that most of them fell into two broad categories. The first category included all those methods that convert the satellite-recorded digital numbers into surface reflectance. All these methods, termed *absolute corrections* by Hadjimitsis & Clayton (2004), require atmospheric optical conditions as input. Hadjimitsis & Clayton (2004) further subdivided this first category into (a) those corrections that obtain the atmospheric optical measurement from the images themselves and (b) corrections that use independent methods of determining optical conditions. The second category comprised techniques that produce *relative corrections*. These techniques do not necessarily produce surface reflectance, but result in images being corrected relative to one another, thereby facilitating multitemporal studies.

Table 3.1: Comparison of the classification of atmospheric correction techniques used by Roberts *et al.* (1990) and Hadjimitsis & Clayton (2004).

Roberts *et al.*	**Hadjimitsis & Clayton**
Absolute calibration	Category A.1: Absolute corrections - atmospheric optical measurements are obtained from the images themselves
	Category A.2: Absolute corrections - atmospheric optical measurements are determined independently
Relative reflectance retrieval	Category B: Relative corrections

While reviewing the need for applying atmospheric corrections, Hadjimitsis & Clayton (2004) emphasise that the removal of atmospheric effects is particularly important for

studies involving water, as these effects account for most of the signal measured by the satellite over water. For multitemporal studies, they maintain that disregarding the effects of the atmosphere will lead to unreliable results. This concern was also voiced by De Haan *et al.* (1991) who asserted that the high variability of the atmosphere strongly influenced, and perhaps even hindered, multitemporal studies. Similar sentiments were expressed by Teillet & Fedosejevs (1995) who noted that the optical properties of the atmosphere are not uniform across multitemporal and multi-scene images. It is important, therefore, that atmospheric effects be reduced, particularly for multitemporal studies. Methods for doing this, both absolute and relative, are discussed in the next two sections.

3.3.1 Absolute atmospheric corrections

Absolute atmospheric correction procedures attempt to remove the effects of the atmosphere from satellite data, usually producing images in which pixel values represent surface reflectance. Many different correction methods have been described in the literature. This review will briefly mention a few of the more commonly used ones.

The most accurate means of removing atmospheric effects is to use measurements of atmospheric conditions made at the same time the satellite image was recorded. These *in situ* readings allow the exact state of the atmosphere to be determined, thereby facilitating the removal of atmospheric effects from the satellite image. In the absence of such measurements, many correction methods make use of a radiative transfer code (RTC) that models atmospheric conditions. One of the best known is the 5S method (Simulation of the Sensor Signal in the Solar Spectrum) (Tanre *et al.*, 1990) and its successor, the 6S method (Vermote *et al.*, 1997). The latter determines surface reflectance based on user-specified input parameters that define the optical characteristics of the modelled atmosphere.

Other absolute correction methods use information extracted from the satellite image to determine atmospheric conditions. Perhaps the most popular of these methods is the dark object subtraction (DOS) method that attempts to remove the effects of atmospheric haze by subtracting a haze value from each pixel. The method is based on the premise that at least some of the pixels in an image have 0% reflectance, an assumption considered reasonable due to the large number of pixels in a typical satellite image. Atmospheric

scattering, which manifests itself as haze, causes these 0% pixels to have a non-zero reading (Chavez, 1988). It is further assumed that the effect of atmospheric scattering is constant across the entire image, and that subtracting this non-zero reading from each pixel will remove the effects of haze. There are various means of determining the haze value for the DOS method. One such method is to use areas of known zero reflectance (e.g. deep water, shadows) and to assume that the non-zero readings for these areas are due to haze. Another method uses histograms to determine the zero offset of the image pixel values and assumes this offset is due to haze (Chavez, 1988). Correction methods based on haze removal are easy to implement but have a disadvantage in that they only remove the effects of atmospheric scattering. No attempt is made to compensate for absorption.

To overcome the deficiencies of DOS models, Chavez (1996) developed a model that aimed to correct the effects of atmospheric absorption. This model extended the DOS concept by incorporating a correction for the effects of absorption and Rayleigh scattering. This was achieved by using the cosine of the solar zenith angle to estimate atmospheric transmittance. Chavez (1996) called this method the COST model and found that it provided corrections comparable to models using RTC and/or *in situ* atmospheric measurements. The COST model had an advantage over RTC-based correction methods in that it was easy to use and was entirely image-based. It was also an improvement over the DOS-based methods as it included corrections for atmospheric absorption.

3.3.2 Relative atmospheric corrections

Relative correction techniques are particularly relevant to the correction of multitemporal images. These correction procedures correct multiple images relative to a selected reference image so that they appear to have been obtained under the same atmospheric conditions as the reference image.

A number of different methods of relative image normalisation have been described in the literature. One of the earlier methods was presented by Schott *et al.* (1988) who developed the procedure in order to facilitate the analysis of multidate imagery. In presenting their technique, Schott *et al.* (1988) explained that trying to compare multiple images of the same area was often problematic due to changes in illumination, atmospheric conditions

and sensor characteristics over the various image acquisition dates. Their technique required the identification of targets of constant reflectivity across the various images, targets they called *pseudoinvariant features* (PIF). These targets were typically man-made features whose reflectivity was almost constant and which were assumed to be the same across all the images. Any differences in the satellite-measured reflectivity of these targets on different dates was assumed to be due to atmospheric effects, changes in viewing geometry and/or sensor characteristics. Schott *et al.* (1988) identified pseudoinvariant targets by means of an image segmentation technique that excluded all pixels not representing urban features. The selected target pixels were then used to calculate linear transformation formulas which, when applied to the satellite images, radiometrically normalised them relative to a selected reference image. Schott *et al.* (1988) cautioned that their technique was sensitive to changes in surface moisture, and that features that were assumed to be invariant might in fact have a different reflectivity when wet.

A slightly different image normalisation technique was developed by Eckhardt *et al.* (1990). As with the Schott *et al.* (1988) method, their technique, which Eckhardt *et al.* (1990) called empirical scene normalisation, required the identification of normalisation targets. However, targets were not identified using an image segmentation approach but were selected through visual inspection of the images. Eckhardt *et al.* (1990) listed a number of criteria for potential normalisation targets:

- the targets had to be at approximately the same elevation as the features which were to be analysed on the images
- there should be little or no vegetation on the targets
- the targets needed to be relatively flat
- the patterns on the targets should be the same and should not change over time

Targets representing a wide range of brightness or reflectivity values were chosen. Typically these would include *dark* targets like deep water bodies and *bright* targets like bare soil, and were assumed to be constant reflectors. Eckhardt *et al.* (1990) reported correlation coefficients (expressed as R^2 values) of greater than 0.99 when relating target pixel values from the reference image to those from the images being normalised, verifying their assumption that the selected target areas were constant reflectors. Using the pixel values of the target areas, a series of normalisation regression equations were developed and applied to the images being normalised. Eckhardt *et al.* (1990) explained that these

regression equations, which were of the form $y = mx + c$, contained an additive component, c, which corrected for differences in path radiance between the different image dates, and a multiplicative component, m, which corrected for differences in the sensor calibration, sun angle, earth/sun distance and atmospheric attenuation.

A third method of relative radiometric normalisation was proposed by Hall *et al.* (1991). Their aim in developing the technique was to radiometrically rectify a series of images so that it would appear '..as if they were acquired with the same sensor, while observing through the atmospheric and illumination conditions of the reference image'. The authors' rationale for doing this was that it was very hard, if not impossible, to obtain measurements of atmospheric properties at the time of image acquisition. This made it extremely difficult to remove atmospheric effects across multidate images. The method proposed by Hall *et al.* (1991) was similar to the previous two methods in that target pixels were used to establish a relationship between a reference image and the images to be normalised. Where their method differed was in the method of target selection. They proposed using the extremes of a Kauth-Thomas greenness-brightness scattergram[3] to identify non-vegetated target areas. According to Hall *et al.* (1991), these non-vegetated extremes of the scattergram did not necessarily represent the same pixels across the images but instead represented non-vegetated areas of similar surface material. They identified two target areas on the scattergram, a dark radiometric control set comprising areas of deep water, and a bright control set made up of rocky outcrops and areas of concrete. Using pixels from the target areas, a series of linear transformations were generated which established a relationship between the reference image and subject images. Hall *et al.* (1991) noted that the accuracy of their technique could be compromised by (a) heterogeneity in the atmosphere across the scene, (b) non-linearity between the sensor calibrations, and (c) non-linear distortions of the scattergram due to the effects of rainfall.

A number of multitemporal studies have used relative radiometric correction in order to standardise multidate images. Jensen *et al.* (1995), in producing an inventory of cattail and sawgrass in parts of the Florida Everglades, used a slight variation of the Eckhardt *et al.* (1990) method. They selected areas of water (wet) and unvegetated bare soil (dry) as normalisation targets. Their variation resulted from the fact that the selected dry targets

3. Kauth & Thomas (1976) developed the Tasselled Cap transformation, a transformation technique that extracted brightness, greenness and wetness components from a series of multispectral Landsat images.

shifted from date to date and hence the pixels in these targets did not represent the same ground location on all the images. Apart from this, their application of the method was as outlined in Eckhardt *et al.* (1990).

Munyati (2000), in a study of changes occurring in parts of the Kafue River floodplain, also used the empirical scene normalisation method of Eckhardt *et al.* (1990). A number of target areas were identified on the images, with irrigation reservoirs representing the wet target areas and unvegetated bare soil the dry targets. Munyati (2000) reported R^2 values of above 0.99 when normalising Landsat Thematic Mapper images to the reference image (also a Landsat TM image) but obtained lower R^2 values (e.g. 0.91) when relating Landsat MSS images to the reference image. This was most likely due to differences in the spectral and spatial resolution between the multispectral and thematic mapper scanners. In another change-detection study, Roberts *et al.* (1999) used the pseudoinvariant feature technique developed by Schott *et al.* (1988). A variation they employed was to first convert the reference image to surface reflectance by using signatures from a library of reflectance spectra. An advantage of this variation was that subject images normalised relative to this reference image would then also be calibrated in terms of surface reflectance.

The various relative radiometric correction techniques described above, whether using pseudoinvariant targets, dry/wet targets or bright/dark targets all had the same aim, namely to normalise a series of target images relative to a selected reference image so that all the images appeared to have been obtained under the same atmospheric conditions and with the same sensor. These techniques have been successfully applied in a number of studies and have the advantage of being relatively easy to implement. In addition, if the reference image is converted to values of surface reflectance, then relative normalisation of the target images will convert them to surface reflectance too.

3.4 IMAGE ENHANCEMENT AND TRANSFORMATION

Image enhancement techniques are used to transform an image in order to facilitate the interpretation of features captured on the image. This is accomplished by manipulating the image data so as to enhance the features of interest. Image enhancement techniques do not create new data, they merely present existing spectral data in a different way. These

techniques are usually applied after images have been corrected for geometric and atmospheric effects but before classification is attempted (Lillesand & Kiefer, 2000).

A common image enhancement technique is to improve the visual display of satellite images by manipulating the contrast so that features on the image are accentuated. This is done by increasing the range of the image pixel values so that they are displayed using the full range of colours or shades available on the computer screen. This results in images with features that are much clearer and more easily discernible than on the original image.

Band ratioing is another common image enhancement technique in which pixel values in one band are divided by the corresponding pixels values in another band. This technique is useful for removing the effects of scene illumination and topography and also for highlighting subtle variations occurring in images (Schowengerdt, 1997; Lillesand & Kiefer, 2000). Surface features that have similar reflectances in one part of the spectrum might have different reflectances at other wavelengths. These differences are highlighted in ratioed images.

Band ratioing forms the basis of many vegetation indices, which rely on the ratio of the red to the near-infrared bands of an image. The red and near-infrared regions of the spectrum are particularly useful for vegetation studies because of the highly distinctive reflectance characteristics of vegetation in these spectral regions. Chlorophyll is a strong absorber of radiation in the red part of the spectrum, leading to low reflectance values of pixels that contain green vegetation. The opposite occurs in the near-infrared where radiation is reflected and is not absorbed by chlorophyll (Chen *et al.*, 1999; Eastman, 2001). The result is that healthy green vegetation has a low reflectance in the red part of the spectrum and high reflectance in the near-infrared. The simplest vegetation index is the Ratio Vegetation Index (RVI), which simply divides the near-infrared band by the red band. Higher values of RVI represent greater amounts of vegetation, low values represent little or no vegetation.

A problem with the RVI is that it is not linear and it is also susceptible to errors arising from division by zero (Eastman, 2001). As a result of this, numerous other vegetation indices have been developed, the most popular of which is the Normalised Difference Vegetation Index (NDVI) (Myneni & Asrar, 1994; Gao, 1996; Eastman, 2001):

$$NDVI = \frac{(NIR - RED)}{(NIR + RED)}$$

The linear scale produced by the NDVI ranges between -1 and +1, with positive values representing vegetation and values below zero showing areas with no vegetation. The NDVI is a good indicator of biomass (e.g. Gao, 1996) and is also sensitive to variations in precipitation that occur during the seasonal growth cycles of vegetation (Lunetta, 1999). Other vegetation indices include:

- the Transformed Vegetation Index (TVI), which modifies the NDVI to provide values with a normal distribution
- the Soil Adjusted Vegetation Index (SAVI), which minimises the effect of soil on the index
- the Atmospherically Resistant Vegetation Index (ARVI), which corrects for atmospheric effects

Another important class of transformation techniques performs linear rotations of the data axes in spectral space. Perhaps the best known of these transformations is the Principal Components Analysis (PCA), which produces a series of output images that are uncorrelated with one another and which contain decreasing amounts of information. Spectral data from different bands in satellite images are often highly correlated, especially in the visible regions of the spectrum. This can be seen in Figure 3.1a, which shows the high correlation between bands 1 and 2 of a Landsat image. The reasons for this correlation are many, including factors such as overlap between the sensor bands, the effects of topographic shading, and the low reflectance of vegetation throughout the visible spectrum (Schowengerdt, 1997). The PCA removes the correlation in the original spectral data by defining new axes (components) in such a way as to minimise the amount of correlation between components. The origin of these new axes is situated at the mean of the data points and, by defining each successive axis as being orthogonal to all the preceding component axes, the data along the component axes are decorrelated (Lillesand & Kiefer, 2000). This can be seen in Figure 3.1b which shows principal component axes 1 and 2 plotted against spectral data from bands 1 and 2 of a Landsat image. The data plotted along the first principal component contains the most variance, with each successive component containing a decreasing percentage of variance or information (Lunetta, 1999).

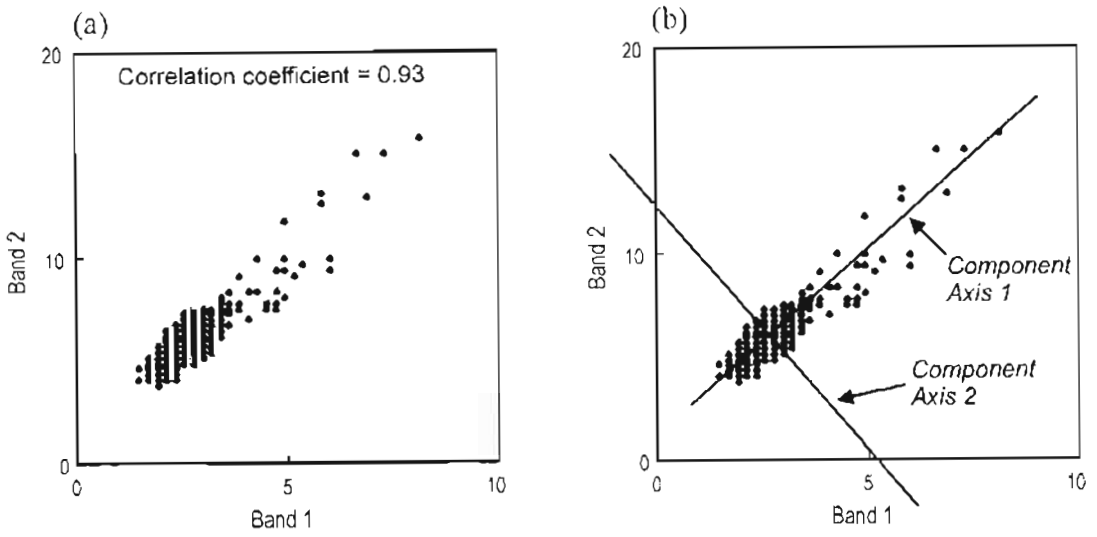

Figure 3.1: Landsat Thematic Mapper data showing (a) the high correlation between bands 1 and 2, and (b) the first two principal components for the same dataset.

Applying a PCA to a multispectral satellite image reduces data redundancy while at the same time preserving all the information present in the original image. A disadvantage of PCA is that it is a data dependent technique, meaning that principal components from different images cannot be compared directly (Schowengerdt, 1997).

3.5 IMAGE CLASSIFICATION METHODS

Lillesand & Kiefer (2000) define image classification as a procedure whereby all pixels are automatically categorised into land cover classes or themes. This is typically carried out using multispectral satellite data. An alternative definition was provided by Binaghi *et al.* (1999) who suggested that image classification was the 'transformation of relatively continuous spectral radiance measured by pixels into a finite set of thematic map classes that describe landscapes in terms of meaningful discrete categories'. Both these definitions refer to the assignment of pixels to classes, a key process in the classification of images. The underlying theory behind image classification is that each type of surface feature is presumed to have a characteristic reflectance pattern. This reflectance pattern is represented by a distinctive set of radiance measurements for each of the bands in the multispectral image. It is these radiance patterns that image classification procedures attempt to identify.

Lillesand & Kiefer (2000) discuss three different methods of pattern recognition:

- *Spectral* pattern recognition groups pixels according to distinctive patterns occurring in specific pixels across the different spectral bands in the image. Most image classification techniques fall into this group.
- *Spatial* pattern recognition techniques compare pixels with surrounding pixels, basing their classification on aspects like image texture, repetition, shape, directionality, feature size and context. These classification procedures are analogous to human pattern recognition and often require significant computing resources.
- *Temporal* pattern recognition relies on changes to reflectance patterns over time as a means of classifying features. These techniques are typically used for vegetation studies where the reflectance characteristics of plant species change according to the seasons. Crops with similar spectral reflectance patterns at one time of the year might have very different patterns later on in the season.

One of the reasons why the vast majority of classification techniques are based on spectral pattern recognition is that digital image processing is particularly well suited to analysing spectral patterns of individual pixels but not as well suited to discerning spatial patterns among different pixels (Cihlar *et al.*, 2000; Eastman., 2001). Indeed, Lillesand & Kiefer (2000) assert that spectral pattern recognition methods form the backbone of multispectral classification and may be said to represent the 'state of the art of classification procedures'.

Given the preponderance of spectral classification methods it is pertinent to explore these techniques in more detail. Spectral classification procedures are generally grouped into two broad categories, namely supervised and unsupervised classifications (San Miguel-Ayanz & Biging, 1997; Eastman, 2001), although a number of hybrid classification schemes have also been developed (Strahler, 1980; Lillesand & Kiefer, 2000) .

- With *supervised* classification, known examples of land cover classes (training sites) are identified on the image and a spectral characterisation is developed for each class. These spectral characteristics represent a spectral signature or interpretation key for each of the classes. The remaining pixels on the image are then compared to the spectral signatures for each class and an attempt is made to determine which of the spectral signatures the pixel most resembles.

- *Unsupervised* classification methods attempt to find natural groupings or clusters in the spectral characteristics of the pixels. These clusters are then examined by an analyst who tries to assign them to a land cover class.
- *Hybrid* classification schemes combine supervised and unsupervised techniques in an attempt to improve classification accuracy and efficiency.

Justice & Townshend (1982) cautioned that the term 'unsupervised classification' could be misleading as implementing these classification methods often required significant user input. In reality, all three classification schemes usually require substantial user involvement and very few are completely automated. In terms of accuracy, supervised methods generally provide superior results to unsupervised methods (San Miguel-Ayanz & Biging, 1997), with hybrid classification schemes often outperforming classifications based solely on supervised or unsupervised methods.

Alternatives to the standard supervised/unsupervised grouping of classification methods do exist. For example, Emrahoğlu *et al.* (2003), while recognising the commonly accepted supervised/unsupervised categorisation, note that classification techniques can also be divided into parametric and non-parametric algorithms. The parametric algorithms make assumptions about the statistical distributions of the elements being classified and use these assumptions in the classification process. According to Emrahoğlu *et al.* (2003) these algorithms are well suited to vegetation and crop studies and include commonly used techniques like maximum likelihood and minimum distance. Non-parametric algorithms are more suited to studying features with reasonably distinct signatures and include the nearest neighbour and artificial neural network classification methods.

3.5.1 Supervised classification

Supervised classification procedures can be classed as either hard or soft (Eastman, 2001). Hard classifiers force each pixel to be assigned to one of the land cover classes represented by the training sites, with some classifiers allowing pixels to be assigned to an unknown class. By contrast, soft classifiers produce a set of images expressing the degree of similarity, or probability of membership, that pixels have to each land cover class. A soft classifier will produce one output image for each of the land cover classes represented by

the training sites. In order for a supervised approach to produce accurate results, training sites should define all possible land cover classes present in an image. Failure to do so can result in the misclassification of pixels.

3.5.1.1 Hard classifiers

Hard classifiers make a firm decision about the identity of each pixel, either assigning it to one of the defined land cover classes or perhaps classifying it as belonging to an unknown class. A drawback with forcing a hard decision is that pixels might be allocated to classes to which they do not belong. This could happen if training sites are poorly chosen and do not adequately represent the land cover classes in question, or if the classes actually present on the image are not represented by the chosen land cover categories. Either way, classification accuracies using traditional hard classifiers are not always as high as would be hoped for (Binaghi *et al.*, 1999).

Among the supervised methods of image classification the most widely used hard classifier is the *maximum likelihood* classification procedure (Eastman, 2001; Pedroni, 2003; Emrahoğlu *et al.*, 2003). In this method, probability density functions are used to describe the distribution of reflectance values of pixels in the training sites for each land cover class. It is assumed that the distribution of reflectance values for each class is normal. Pixels outside the training sites are then compared to these probability density functions and probabilities of membership to each of the classes are calculated. Pixels are assigned to the class to which they have the highest probability of membership. Sometimes a threshold value is defined and pixels that have no membership probabilities above this value are assigned to an unknown class. This ensures that pixels are not forced to belong to a class but may remain unclassified. One of the reasons for the popularity of the maximum likelihood classifier is that it is very flexible and is easily modified (Pedroni, 2003). A common enhancement is the incorporation of prior probabilities that estimate the proportion of pixels that will fall into each class (Strahler, 1980). These prior probabilities are used to guide the maximum likelihood classification with a greater weighting given to those classes with higher prior probability values.

Other hard supervised classification methods include the *parallelepiped* classifier and the *minimum distance to means* classifier. With the minimum distance classifier, average spectral readings are calculated for training sites representing each land cover class. The spectral values of pixels being classified are compared to these mean spectral values and are assigned to the class to which they are the closest in spectral space. This classifier is mathematically easy to compute but is not very sensitive to variance in the spectral signatures of the training sites (Lillesand & Kiefer, 2000). It is thus not suitable for applications where a high degree of variance occurs among land cover types or where the presence of mixed pixels increases the spectral variance of pixels. The parallelepiped classifier, on the other hand, does accommodate spectral variance. It does this by using the range of spectral values within each training site to define regions called parallelepipeds that characterise each land cover class. A pixel is assigned to a class if its spectral value falls within the parallelepiped for that class. While this method accommodates the spectral variability of training sites it is very sensitive to outliers in the data and can also produce ambiguous results when parallelepipeds overlap (Lillesand & Kiefer, 2000; Eastman, 2001). Overlapping parallelepipeds often occur when there is covariance between data in different spectral bands, a characteristic of vegetation in the visible bands of the spectrum.

The advantages and disadvantages of the three supervised classification methods discussed above are compared in Table 3.2. Although it is sensitive to training site variability and inter-band covariance, the fact that the maximum likelihood classifier is computationally complex is becoming less and less of a drawback in these days of powerful computers.

Table 3.2: Advantages and disadvantages of three different hard classifiers widely used in supervised classification.

Classification method	*Pros*	*Cons*
Maximum likelihood	Sensitive to variance Sensitive to covariance Easy to modify	Computationally complex
Minimum distance	Mathematically simple	Not sensitive to variance
Parallelepiped	Sensitive to variance Mathematically simple	Not sensitive to covariance Sensitive to outliers Overlapping parallelepipeds cause ambiguity

High levels of hard classifier inaccuracy often occur when pixels do not resemble any of the defined signatures. This can be overcome by re-examining the training sites and redefining them where necessary. The levels of accuracy achieved using conventional hard classifiers can also be problematic in situations where the landscape is highly heterogeneous. The mixed pixels occurring in these landscapes are a major source of classification error (Foody *et al.*, 1996; Binaghi *et al.*, 1999) and attempts to improve classification accuracies have led to the development of soft classification techniques. These are described in the next section.

3.5.1.2 Soft Classifiers

Mixed pixels in satellite imagery can occur for two reasons. Firstly, the spatial resolution of the image might not be suitable for resolving the features being studied. This occurs when the target features, e.g. fields, bush clumps, etc., are smaller than the spatial resolution of the satellite sensor (Wang, 1990; Lillesand & Kiefer, 2000; Small, 2001). In these cases the reflectance of individual pixels will contain spectral information on both the target feature as well as other features present in the pixel. Another cause of mixed pixels is when seemingly homogeneous features are in fact made up of a mixture of different surface feature types (Wang, 1990). For instance, a pixel covering a maize field contains spectral information not only on the maize plants but also on the soil between the rows of maize as well as dead vegetable matter lying on the ground. These all contribute to a single reflectance reading for the pixel.

In order to analyse sub-pixel mixing, and in an attempt to achieve better classification accuracies than those obtained with traditional hard classifiers, a number of soft classification techniques have been developed. These soft classifiers generally produce one output image for each land cover class. Depending on the classification procedure being used, the pixel values in these output images can be interpreted in one of two ways. Firstly, each pixel value could represent the probability that the pixel actually belongs to the land cover class in question. Alternatively they could represent the proportions of the land cover classes present in the pixel. This provides an indication of the mixture of land cover classes in each pixel and is known as sub-pixel classification (Eastman, 2001). For example, if

training sites are provided for water, forest and grassland and a pixel is classified with values of (water: 0.7 ; forest: 0.2 ; grassland: 0.1) this could be interpreted as follows:

1. Either, there is a 70% probability that the pixel is a water pixel, 20% probability it is a forest pixel and a 10% probability it is a grassland pixel, or
2. the pixel contains a mixture of 70% water, 20% forest and 10% grassland.

It is this second interpretation that is important for mixture analysis techniques as it allows a picture to be constructed of the different proportions, or fractions, of land cover types within pixels.

The literature describes a number of different soft classification techniques based on the theories of fuzzy sets, neural networks, probability and/or spectral mixture analysis (Binaghi *et al.*, 1999; Lillesand & Kiefer, 2000; Eastman, 2001). Many of these techniques are experimental and are still undergoing development.

Fuzzy classification procedures are based on the premise that pixels may have partial membership in one or more land cover classes (Lillesand & Kiefer, 2000). As with all supervised methods, training sites are used to define areas in spectral space that describe the different land cover classes. However, these areas do not have hard boundaries but instead define fuzzy partitions of spectral space in which target pixels are allowed to have partial membership of more than one fuzzy partition (Wang, 1990). The classification procedure assigns membership grades to each target pixel that indicate how closely the pixel resembles each of the classes. Interpreting these membership grades provides a more realistic picture of class mixtures than would be obtained with traditional hard classifiers.

The use of artificial neural networks for image classification is the subject of much ongoing research (Lillesand & Kiefer, 2000). While they are generally used to perform hard classifications, they can also be adapted to produce soft classifications (Binaghi *et al.*, 1999). Artificial neural networks work in an iterative manner to generate linkages between the nodes of user-specified input and output layers. The nodes of the input layer are typically the spectral bands of a satellite image, although ancillary data (e.g. slope, aspect) may also be used. The nodes of the output layer correspond to the land cover classes being classified. In between the input and output layers are one or more hidden layers containing multiple nodes that provide linkages between the input and output layers. The network is trained by supplying the training sites as input and then performing a series of iterations in

which the linkage weights of the hidden layers are adjusted until the actual output data resembles the desired output data (the land cover classes) (Lillesand & Kiefer, 2000). Once the network is trained it can be used to classify the remaining pixels in the image. An advantage of the neural network classifier is that no assumptions are made about the statistical distribution of the input data, nor do the training sites have to contain pure spectra. A drawback of the method is that the training process can be difficult and time-consuming and no guidelines for configuring the network exist (Ardö *et al.*, 1997). Nevertheless, the use of artificial neural networks as a soft classifier shows much promise.

Eastman (2001) describes two soft classifiers that are based on probability theory, BAYCLASS and BELCLASS. BAYCLASS draws on Bayesian probability theory to determine the probability of pixels belonging to different land cover classes based on the evidence presented by training sites for the different classes. The classifier assumes that pixels must belong to one of the defined classes and cannot belong to some unknown class. In other words, the assumption is that the land cover classes are exhaustive and cover all possible classes present in the image. The BELCLASS classifier is based on a variant of Bayesian theory called Dempster-Schafer theory and does not assume that the defined land cover classes are mutually exclusive and exhaustive. It achieves this by recognising that pixels may belong to an unknown class for which training data have not been provided. This classifier also generates an uncertainty image, which provides a measure of the certainty that pixels can be assigned class membership. If, for a particular pixel, there is no class that stands out above any other class then the uncertainty value for that pixel will be high. Eastman (2001) concludes by saying that BAYCLASS is a confident classifier. Every pixel is expected to have either partial or complete membership in the defined land cover classes with no chance of belonging to an unknown class. The BELCLASS classifier, by contrast, is a reserved classifier as it recognises that unknown classes may exist for which it has no information. For this reason it can be used to check whether the chosen land cover classes truly represent all the classes actually present in the image or whether there are some unknown classes present.

As a result of the inaccuracies resulting from the hard classification of images, soft classifiers based on spectral mixture analysis have gained in popularity (e.g. Mertes *et al.*, 1993; Adams *et al.*, 1995; Roberts *et al.*, 1999; Ustin *et al.*, 1999; Small, 2001). Like the previously discussed soft classifiers, spectral mixture analysis is based on the idea that

pixels are very rarely pure and typically contain mixtures of different class types. The measurements made by the satellite for each pixel are thus made up of mixtures of reflectance signals for each of the land cover types actually present in the pixel. In order to simplify the analysis of the mixed signal, it is usually assumed that the signal from each pixel is made up of a *linear* mixture of the reflectance spectra of each of these classes (Settle & Drake, 1993; Lillesand & Kiefer, 2000; Van der Meer & De Jong, 2000). In other words, the radiation interacts with only one surface feature type before being reflected; there are no multiple reflections. The signal measured by the satellite for each pixel is then assumed to be a simple linear summation of the reflected signal from each of the surface features present in the pixel.

This is illustrated in Figure 3.2, which shows how the reflectance spectra of three different features combine to form one composite spectral signal. The aim of *linear* spectral mixture analysis, then, is to use multispectral measurements to estimate the fraction that each ground cover class occupies in each of the image pixels. This is a process known as spectral unmixing (Van der Meer & De Jong, 2000; Lillesand & Kiefer, 2000).

A key element in the unmixing process is the use of endmembers that represent the signature that each class would have if it alone occupied the pixel (Settle & Drake, 1993). Endmembers provide pure examples of each land cover class and are used to guide the unmixing process. Endmembers are usually derived either from the image itself or from reference spectra measured in a laboratory (Van der Meer & De Jong, 2000). Although in reality it is very difficult to find pure examples of class types on the image itself, image-derived endmembers have an advantage over laboratory-derived ones in that they are measured under the same atmospheric conditions as the rest of the image, conditions that reflect the state of the atmosphere when the image was recorded. The set of endmembers should be chosen so that they represent all land cover classes present in the image. Failure to identify all the land cover classes can lead to inaccuracies in the unmixing process.

One method for determining the optimum number of endmembers involves performing a Principal Components Analysis on the spectral data. The number of components accounting for the majority of the variance of the data gives an indication of how many endmembers are required to model the data (Bateson & Curtiss, 1996). Image endmembers can be selected from training sites representing pure examples of each endmember, or can

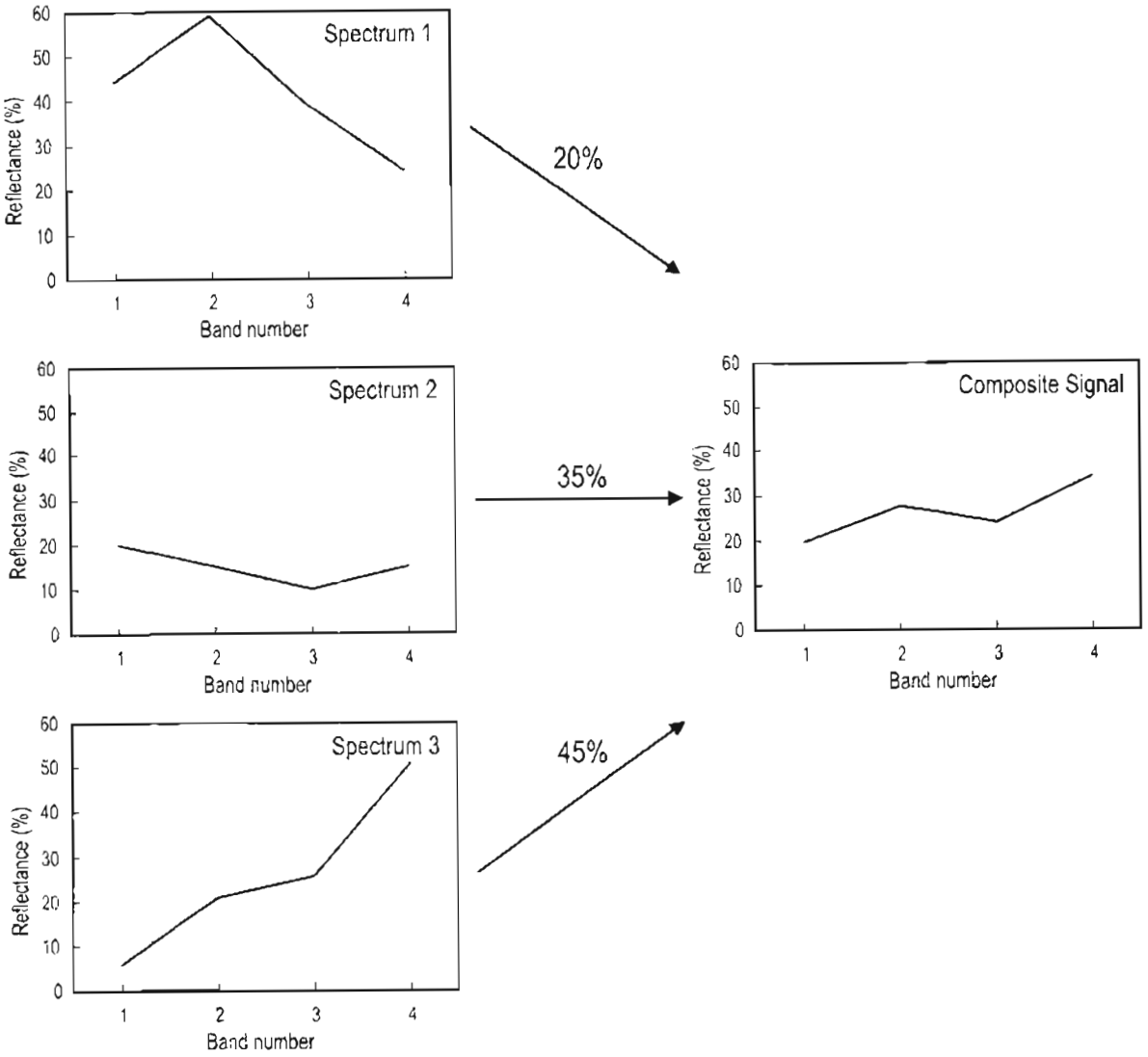

Figure 3.2: Composite spectral signal composed of a 20% mixture of spectrum 1, a 35% mixture of spectrum 2 and a 45% mixture of spectrum 3. The plots on the left represent pure spectra, or endmembers, of three different land cover types.

be selected from scattergrams depicting the image data in spectral space (e.g. Van der Meer & De Jong, 2000; Lu *et al.*, 2004; Théau & Duguay, 2004). In the scattergram approach, pure endmembers are assumed to be located at the vertices of a polygon bounding the data in spectral space. Once the endmembers have been defined, the objective of spectral unmixing is to examine the observed reflectance signal for each pixel and to estimate the fraction of each endmember spectrum that best explains this observed signal (Small, 2001).

The linear mixture model assumes that the net reflectance value of a pixel is made up of a linear combination of endmember spectra as follows (Small, 2001):

$$R_\lambda = f_1 E_{\lambda,1} + f_2 E_{\lambda,2} + \ldots + f_m E_{\lambda,m} + \varepsilon_\lambda \qquad (1)$$

where R_λ is the measured reflectance value of the pixel in band λ, $E_{\lambda,1}$, $E_{\lambda,2}$, ... , $E_{\lambda,m}$ are the reflectance values of the m endmembers with their corresponding fractions f_i, and ε_λ is the residual error term for spectral band λ. The residual error ε_λ, also called the band residual, is the difference between the actual reflectance value R_λ and the modelled reflectance value for spectral band λ. If the pixel contains only the selected endmembers then this error term should, in theory, represent noise (Van der Meer & De Jong, 2000). In addition, a constraint is often placed on the fractions, f_i, such that:

$$f_1 + f_2 + f_3 + \ldots + f_m = 1 \text{ and } 0 \leq f_i \leq 1 \qquad (2)$$

This constraint ensures that the individual endmember fractions add up to one. In imposing this constraint it is assumed that all land cover classes have been identified and are represented by their corresponding endmembers.

As there is a version of equation (1) for each of the n spectral bands and one version of equation (2), this means that there is a set of $n+1$ equations available to simultaneously solve the different endmember fractions, f_i. This has important implications for the number of endmembers that can be used in the unmixing process (Lillesand & Kiefer, 2000).

- If the number of endmembers is greater than $n+1$ then it will not be possible to produce a unique solution from the set of equations.
- If the number of endmembers is equal to $n+1$ then it is possible to produce an exact solution to the problem by solving the set of equations simultaneously. However, having $n+1$ endmembers means that no estimate of error can be produced.
- If the number of endmembers is less than $n+1$ then the fractional cover of each endmember can be calculated and so can the associated error term.

Therefore, in order to get an indication of the error involved in the unmixing process the number of endmembers cannot exceed the number of spectral bands (Lillesand & Kiefer, 2000; Eastman, 2001). Bearing in mind the constraints imposed by equation (2), it is apparent that performing unmixing on images containing many land cover classes is extremely difficult, particularly when the number of spectral bands is limited. For example, the fact that SPOT images have only four reflective bands means that it is only possible to determine fractional estimates for four endmembers along with an estimate of the error.

The accuracy of the linear mixture model can be assessed by combining the residual errors ε across all the n bands in a least-squares solution to give the root-mean-square (RMS) error:

$$\textbf{\textit{RMS error}} = \sqrt{\left(\sum_{i=1}^{n} \varepsilon_i^2 \right) / n} \qquad (3)$$

One RMS error value is calculated for each pixel and the resulting error image can be used to give an indication of the suitability of the endmembers. High RMS error values indicate a poor fit of the linear mixture model (Lu *et al.*, 2004). In this case, it could be that insufficient endmembers have been chosen or that the chosen endmembers do not adequately represent the land cover classes actually present in the image. An example of the calculation of residual errors is provided in Appendix 6.

Spectral mixture analysis is a deterministic method that makes no assumptions about the statistical distribution of the data but relies, instead, on a physical model of the spectral responses of the different land cover classes (Lillesand & Kiefer, 2000). Its main advantage over other soft classifiers is that it provides a simple, easily implementable method of decomposing the spectral signal from a mixed pixel into its constituent parts. This allows detailed sub-pixel analysis of images to be performed. Spectral mixture analysis also provides an error image that allows the accuracy of the unmixing to be assessed. This is particularly useful for examining the suitability of endmembers. The primary disadvantage of spectral mixture analysis is that the number of endmembers may not exceed the number of spectral bands (Eastman, 2001). This is particularly limiting in situations where the landscape is complex and contains many different land cover classes. Another limitation regarding endmembers is that pure examples of class types rarely exist in nature, making it difficult to find truly representative endmembers on the image itself. In addition, the linear mixture model does not take into account multiple reflections that may occur between different surface features. For instance, solar radiation might be reflected many times between leaves, branches and soil before finally being reflected into space. In this case the measured signal would not be a linear mix of the different components present in the pixel.

3.5.2 Unsupervised classification

Most unsupervised classifiers use statistical methods to identify natural clusterings that occur in spectral data. This is achieved by examining all the pixel values from the various spectral bands and attempting to classify them on the basis of their spectral similarity. These clusters of spectrally similar pixels, which are assumed to represent different features or land cover classes in the study area, can be examined by an analyst who links the different clusters to land cover classes (Schowengerdt, 1997; Lillesand & Kiefer, 2000). This can be done through expert knowledge of the study area, field visits, comparison with aerial photographs and/or previous classifications, or a combination of all these methods.

A commonly used clustering technique is based on the K-means algorithm in which the analyst specifies the number of clusters to be identified. To seed the process, each of these clusters is assigned an arbitrary mean position in the multidimensional spectral space defined by the image bands. The position of each pixel is then compared to these mean cluster positions and the pixel is assigned to the cluster whose mean position is the closest. Once all the pixels have been assigned, new mean positions are calculated for each cluster. Pixels are then compared to these new mean cluster positions and classified accordingly. This process continues in an iterative fashion until pixel assignments remain stable from one iteration to the next (Schowengerdt, 1997; Lillesand & Kiefer, 2000; Eastman, 2001).

The ISODATA method is a variant of the K-means algorithm and is the most widely used unsupervised classification method (Salvador & San-Miguel-Ayanz, 2003). This algorithm allows clusters to be merged if they are closer than a certain threshold while at the same time allowing clusters to be split if they grow above a certain size (Justice & Townshend, 1982; Schowengerdt, 1997). Further examples of unsupervised classifiers are those that use histogram peak cluster analysis or texture analysis.

Unsupervised classification requires no prior knowledge of the study area. In fact, an advantage of unsupervised classification is that this method often identifies unknown land cover classes (Schowengerdt, 1997), classes that might not have been considered had a supervised classification approach been adopted.

3.5.3 Hybrid classifiers

Hybrid classifiers combine the strengths of supervised and unsupervised classifications in order to increase classification accuracy. They can be especially useful in areas where land cover classes are complex or where the landscape is highly heterogeneous (Lillesand & Kiefer, 2000). The hybrid unsupervised/supervised classifier performs an unsupervised cluster classification on one or more heterogeneous training areas in order to identify spectral classes present in the training data. Through knowledge of the study site and by referring to aerial photos and field data, these spectral classes are analysed, identified and labelled by an analyst. During this process some spectral classes might be combined whereas others might be subdivided. The labelled classes resulting from this process are then used to perform a supervised classification of the rest of the image (Sader *et al.*, 1995; Schowengerdt, 1997; Lillesand & Kiefer, 2000).

Another example of a hybrid classifier is the ECHO (extraction and classification of homogeneous objects) classifier, which utilises both textural and spectral information from the image. The classifier first loops through subsets of the image identifying homogeneous groups of adjacent pixels. These texturally similar pixel groups are then used by a supervised maximum likelihood classifier to classify the rest of the image (Lu *et al.*, 2004).

3.6 ASSESSING THE ACCURACY OF CLASSIFIED IMAGES

Assessing the accuracy of an image classification is an important step in the processing of satellite images (Shao *et al.*, 2001). Firstly, by knowing the accuracy of a classification, some measure of confidence can be attached to the final product, thereby influencing its interpretation and subsequent use. Also, by assessing classification accuracy, analysts can iteratively modify their classification procedure in order to achieve an optimum level of accuracy. Finally, producing an accuracy assessment allows different classification techniques to be compared, allowing the analyst to choose the most accurate and appropriate technique (Congalton & Green, 1999).

While accuracy assessment is considered an essential step in image processing, it was not until the mid-1970s that attempts were made to evaluate how accurate image classifications

were. Initially a single measure of accuracy was calculated by comparing estimates of the area of ground cover with those produced by the image classification. This was later expanded to include site-specific assessments where actual site visits (known as ground truthing) were undertaken to verify classification accuracy (Congalton & Green, 1999). Ground truth data did not necessarily need be collected from site visits but could also be obtained from other sources like aerial photographs and map data (e.g. Wang *et al.*, 1998; Lunetta & Balogh, 1999). The ground truthing approach is currently still in use but has been developed into a methodology which produces an error matrix and numerous measures of accuracy.

The error matrix is most often applied to hard classifications where each pixel is assigned to only one land cover class. The matrix is used to compare reference (or ground truth) data to a sample of classified data in a way that allows the overall accuracy to be calculated while at the same time allowing errors of commission and omission to be determined (Congalton, 1991). This is illustrated in Table 3.3 which shows reference data (in columns) compared against the corresponding classified data (in rows). The values in the major diagonal represent all those pixels that have been correctly classified. Adding these and dividing by the total number of samples gives an indication of the overall classification accuracy. In this example, 68 water pixels, 45 forest pixels and 72 sand pixels have been correctly classified giving an overall accuracy of (68+45+72)/202 = 92%.

Table 3.3: Error matrix relating reference data to classified data.

		Reference Data			
		Water	Forest	Sand	Row Total
Classified Data	Water	68	6	4	78
	Forest	3	45	1	49
	Sand	1	2	72	75
Column Total		72	53	77	202

Errors of commission occur when a pixel is classified in the wrong category while errors of omission occur when a pixel is excluded from the category to which it actually belongs. These can be quantified by calculating the User's and Producer's Accuracy as shown in Table 3.4. From this table it can be seen that 68 out of the 72 water reference sites have been correctly classified as water, giving a producer's accuracy of 94%. For the producer of

the classification this means that 94% of the areas that are water have been correctly classified. However, when the user's accuracy for water pixels is calculated, it can be seen that the value is only 87%, meaning that 13% of the pixels that have been classified as water are actually not water. This can be problematic for the user of the classified data who might find forest or sand where the classification indicates water.

Table 3.4: Calculation of User's and Producer's Accuracy using data from Table 3.3.

Producer's Accuracy (omission errors)	User's Accuracy (commission errors)
Water = 68/72 = 94%	Water = 68/78 = 87%
Forest = 45/53 = 85%	Forest = 45/49 = 92%
Sand = 72/77 = 94%	Sand = 72/75 = 96%

If the error matrix is being used to evaluate a supervised classification it is important that the sites used for ground truthing are not the same as those that were used as training sites. Using the same sites both for training and accuracy assessment can result in unrealistically high accuracy values. At the same time, it should be remembered that data collected by ground truthing is often far from perfect, its quality being influenced by factors such as sampling technique and representivity (Malthus & Mumby, 2003).

The error matrix is an easily implementable and commonly used method for determining the accuracy of hard classifications. However, accuracy assessment becomes rather more difficult for studies involving soft classifications and/or historical satellite images. Assessing the accuracy of classifications performed on historical images is difficult as it is impossible to go back in time to perform traditional ground truthing (Jensen *et al.*, 1995). This is especially problematic for change detection studies that rely on differences between multidate images to identify changes in land cover (Congalton & Green, 1999). Current ground truth data would not necessarily be an accurate reflection of land cover on the date the image was captured. It is also very difficult to evaluate the accuracy of soft classifications as the traditional application of the error matrix is only applicable to hard classifications (Binaghi *et al.* 1999; Ricotta, 2004). There is thus a need to develop accuracy assessment procedures for both change detection and soft (or fuzzy) classifications. Congalton & Green (1999), Binaghi *et al.* (1999) and Ricotta (2004) discussed methods for doing this but in all cases relied on the availability of accurate and

contemporary ground truth data to test their classifications. In addition, Congalton & Green (1999) observed that even though a few procedures for assessing change detection accuracies had been proposed, there was still no standard technique available and very little work had been done on comparing the relative merits of those techniques.

An alternative method of accuracy assessment was utilised by Vicente-Serrano *et al.* (2004) in their recent study using Landsat ETM+ and NOAA AVHRR images to map soil moisture in the Ebro River valley in Spain. They used meteorological records from the area to calculate a Standardised Precipitation Index (SPI) which was then used to verify their soil moisture map. They called this method an 'indirect climate approach' and found a clear relationship between the SPI and the soil moisture maps produced by their image classification. In calculating the SPI they did not use meteorological data taken at the time of image acquisition but used an aggregation of data from the preceding 15 days.

In another alternative to the error matrix approach, studies based on linear mixture analysis are able to use the band residuals and root-mean-square (RMS) error values to give some indication of classification accuracy (e.g. Adams *et al.*, 1995). Low values of band residuals and/or RMS error indicate that the overall fit of the mixture model is good while high values indicate the possible presence of additional land cover classes that have not been included as endmembers.

In conclusion, it can be seen that although classification accuracy assessment is fairly straightforward for studies involving single images and hard classifications, problems occur when soft classifications are performed and/or no ground truth data are available. While some methods have been proposed for assessing accuracies in these situations, much development is still needed in this area.

3.7 CONCLUSION

The term 'image processing and analysis' describes a broad range of methodologies and techniques that are used to prepare, process and analyse digital satellite images. While some of these techniques are mature and not currently undergoing much development (e.g. geometric rectification), others are still experimental and the subject of much debate.

Ongoing developments are taking place in the areas of atmospheric correction and especially in the field of soft classification. Soft classifiers are being developed, modified and assessed as scientists try to extract as much information as possible out of each image. Many studies are now using spectral unmixing in order to determine sub-pixel classifications, thereby extracting information at scales smaller then the spatial resolution of the satellite image. Of the soft classifiers, spectral mixture analysis is gaining in popularity as researchers become more familiar with its application and interpretation of its outputs. In the area of accuracy assessment, methods are well developed for hard classifiers but are often poorly developed, or lacking entirely, for soft classifications. Much study is needed to develop assessment methods for soft classifiers, particularly for studies using classification of historical images for which no *in situ* ground truthing is available.

This chapter has provided an extensive review of the theory and processes involved in image processing. The understanding of image processing that this has afforded will be invaluable in guiding the development of a water mapping protocol in this study. Firstly, though, the next chapter outlines the development of satellite-based remote sensing with particular emphasis being placed on Landsat and its use in the mapping of water and wetlands.

4. REMOTE SENSING AND ITS APPLICATION

4.1 INTRODUCTION

The development and application of remote sensing technologies has been an area of much research over the last few decades. Understanding these technologies is important as this will guide the image processing phase of this project. This chapter traces the development of these remote sensing technologies, starting with early satellite-based remote sensing in the 1960s and 1970s, progressing through to present day studies that have the benefit not only of powerful computers, but also of data with superior spatial, temporal and spectral resolutions. The Landsat Thematic Mapper programme will be examined, along with a review of studies that have used Landsat data to map wetlands and their surface waters. Descriptions of the reflectance characteristics of surface features relevant to this study are also included. The chapter concludes with an investigation into the application of spectral mixture analysis to Landsat data.

4.2 EARLY SATELLITE-BASED REMOTE SENSING

Satellite-based remote sensing became possible with the launch of the first satellites in the late 1950s. Although many early satellites were designed for meteorological applications, scientists analysing data returned by these satellites soon realised that remote sensing could be used for more than just meteorology (e.g. Greenwood *et al.* 1969a, 1969b). An important milestone in the early development of remote sensing was the initiation of the Earth Resources Technology Satellite (ERTS) programme in 1967. This programme, later renamed the Landsat programme, commenced with the launch of its first satellite, ERTS-1, in July 1972. This was the first satellite designed to systematically and repetitively measure data on the earth's resources.

Early results from the ERTS-1 satellite (later renamed Landsat-1) were promising, allowing geological, hydrogeomorphic, anthropogenic and vegetative features to be identified (Kondratyev *et al.*, 1973). However, the 79-metre resolution of the images limited their usefulness for identifying small surface features. The images were also distorted, but the

distortions were found to be highly systematic and could be corrected by means of ground control points (Wong, 1975).

The development of image classification techniques gained momentum in the late 1960s and into the 1970s. While most early attempts at classification were in the fields of meteorology and oceanography, the development of techniques for mapping vegetation and hydrology soon followed. Examples of these include the following studies:

- Aldrich *et al.* (1971) used images from the ESSA and Nimbus meteorological satellites to map the forest-tundra boundary in northern Canada.
- Anuta & MacDonald (1971) applied pattern recognition techniques to multiband photographs taken during the Apollo 9 mission, finding that bare soil, water and salt flats were easily recognised but that different crops types were not as easy to discriminate.
- Klemas *et al.* (1973) and Brooks (1975) used ERTS-1 images to map suspended sediments in water bodies.
- Gausman *et al.* (1975) were able to use Multispectral Scanner (MSS) imagery from ERTS-1 to distinguish between normal and iron-deficient grain sorghum.
- Lawrence & Herzog (1975) performed a classification of ERTS imagery that enabled the mapping of geology and forestry in Oregon. These classifications, supplemented by photo-interpretation, also detected areas of water and snow.

The regular and reliable images being returned by the first generation of ERTS (Landsat) satellites soon allowed scientists to perform multitemporal studies. For example, Ashley & Rea (1975) used ERTS-1 MSS images from 1972 and 1973 to examine seasonal differences in vegetation while Masry *et al.* (1975) developed a change detection routine that made it possible to compare different images of the same scene.

4.3 CONTEMPORARY SATELLITES AND REMOTE SENSING SYSTEMS

With satellite-based remote sensing now in its fifth decade, the current generation of satellite-based sensors are much more sophisticated than their predecessors, not only in terms of spatial, spectral and temporal resolution but also in terms of the accuracy of measurements made from space. This increasing technological sophistication has been

mirrored by the continuous development and refinement of image classification techniques. However, Teillet (1997) notes that even while technologies for remote sensing continue to develop, earth observation techniques are struggling to mature. This, he suggests, is because earth observation technology is expensive and complex and not yet able to provide products that are easily accessible, accurate, and of consistent quality.

Similar sentiments are expressed by Malthus & Mumby (2003) who feel that there are a number of areas in which image processing techniques need further investigation and development. For instance, they argue that standardized and consistent atmospheric correction techniques need to be developed as these are crucial to the success of multitemporal studies. Malthus & Mumby (2003) also draw attention to the fact that the inadequate spatial resolution of sensors often leads to classification problems, especially where sub-pixel mixing occurs.

In terms of contemporary satellite-based systems, Glackin (1998) notes that there was a proliferation of remote sensing missions during the 1980s and 1990s and that this was expected to continue in the 21st century. While only seven countries had built and launched space-based remote sensing systems by 1995, Glackin (1998) predicted that more than 20 nations would be operating such systems by 2001. At the same time, remote sensing was becoming more commercialised and there had been a move away from government and military missions. Some of the new-generation systems would have sub-metre resolutions while others would be capable of capturing over 100 spectral bands at a time.

Of the currently operating remote sensing satellites, the Multispectral Scanner (MSS) and Thematic Mapper sensors of the Landsat programme continue to provide valuable data for scientific and commercial applications. The continuity of the Landsat programme has proved attractive as it provides an unbroken record going back to the launch of ERTS-1 (Landsat-1) in 1982 (Lillesand & Kiefer, 2000). Other moderate and high resolution satellite systems include the *Système Pour l'Observation de la Terre* (SPOT) programme, the Russian RESURS-01 satellites, the Indian Remote Sensing (IRS) programme and the Japanese Advanced Earth Observing Satellite (ADEOS) (Lillesand & Kiefer, 2000). These moderate resolution systems have all been designed to record data in the visible and infrared parts of the spectrum with ground resolutions ranging from tens to hundreds of metres. Among the high resolution systems are Quickbird, IKONOS-2, Orbview-3 and

EROS. All these high resolution sensors are able to record spectral data to a resolution of about one metre (Lillesand & Kiefer, 2000).

Two important instruments were launched aboard the Terra satellite in 1999. MODIS (MODerate resolution Imaging Spectrometer) is a high spectral, low spatial resolution sensor designed to provide global-scale measurements of oceanographic and terrestrial ecosystems. ASTER (Advanced Spectrographic and Thermal Emission Radiometer) provides both high spatial and high spectral resolution data in the visible, shortwave and thermal infrared wavelengths (Donoghue, 2000).

In terms of the mapping capability of contemporary systems, Shoshany (2000) found that Landsat Thematic data have been widely used in vegetation studies. This is because they incorporate the frequencies of chlorophyll absorption and mesophyll reflection and are particularly useful for mapping vegetation. Shoshany (2000) also noted wide use of Landsat MSS, SPOT, AVHRR, ERS SAR and RADARSAT products as they are able to provide information valuable for broad-scale vegetation monitoring. The Landsat Thematic Mapper, Landsat MSS, SPOT and AVHRR all make measurements in the visible and infrared portions of the spectrum while ERS SAR and RADARSAT use the radar wavelengths. Shoshany (2000) found that the spatial resolution of satellite sensors (e.g. 30 m on Landsat-7, 20 m on SPOT-4) is often inadequate to allow measurements of relatively small vegetation features, prompting the development of unmixing techniques that quantify the fractions of different vegetation types present in a pixel.

As this review of literature on contemporary satellite systems has shown, there are now satellite-based sensors that have the ability to provide images with a higher spatial and/or spectral resolution than Landsat Thematic Mapper. What continues to make Thematic Mapper products so attractive, however, is that they provide continuous, global-scale measurements dating back to 1982, a time-span unmatched by any other system. Indeed, if MSS products are included, then the Landsat programme is able to provide multispectral measurements going all the way back to 1972. It is this long record of measurement, coupled with the relatively low cost of the data, that has resulted in Landsat Thematic Mapper data being so widely used.

4.4 REMOTE SENSING USING LANDSAT

Three different types of sensor that have been carried aboard the various Landsat satellites, namely the three-channel Return Beam Vidicon (RBV) system aboard Landsats 1-3, the four-channel Multispectral Scanner (MSS) aboard Landsats 1-5, and the Thematic Mapper aboard Landsats 4-7. The Thematic Mapper offers increased spectral and spatial resolution over the MSS. It is able to acquire seven bands of data in the visible, mid-infrared and thermal portions of the electromagnetic spectrum (Lillesand & Kiefer, 2000) while the spatial resolution has been improved to 30 metres (from approximately 80 m for MSS).

Landsat Thematic Mapper (TM) products are widely used because they provide continuous, global-scale measurements dating back to 1982, while at the same time being relatively cheap and easily accessible. In addition, the latest generation of the Thematic Mapper, the Enhanced Thematic Mapper (ETM+) aboard Landsat-7, produces data of a higher radiometric quality than previous satellites in the Landsat programme (Markham *et al.*, 1997). This has been achieved primarily by adding two solar calibrators to the satellite that use solar radiation to provide calibration data for the sensors. Furthermore, a ground-based Image Assessment System has been implemented that not only assesses the performance of the system but also provides updated calibration data to the scientific community (Markham *et al.*, 1997).

To date there have been seven Landsat missions, starting with Landsat-1 (formerly called ERTS-1) in 1972 and continuing with the launch of Landsat-7 in 1999 (Table 4.1). All the satellites were launched into sun-synchronous orbits, ensuring that satellite overpasses at particular locations always occur at the same time (Lillesand & Kiefer, 2000).

The main sensor aboard Landsat missions 4-7 has been the Thematic Mapper. This sensor images three channels in the visible part of the spectrum, one in the near-infrared, two in the mid-infrared and one in the thermal infrared. The specifications of each of these bands are shown in Table 4.2 while their positions in the electromagnetic spectrum are illustrated in Figure 4.1. The Enhanced Thematic Mapper Plus (ETM+) aboard Landsat-7 has an extra panchromatic band that images the same spectral region covered by bands 2, 3 and 4 but does so at a spatial resolution of 15 metres (Markham *et al.*, 1997).

Table 4.1: Characteristics of the Landsat missions.

Satellite	*Launched*	*Orbit*	*Status*
Landsat-1	July 1972	18 days / 900 km	Decommissioned, 1978
Landsat-2	January 1975	18 days / 900 km	Decommissioned, 1982
Landsat-3	March 1978	18 days / 900 km	Decommissioned. 1983
Landsat-4	July 1982	16 days / 705 km	
Landsat-5	March 1984	16 days / 705 km	Operational
Landsat-6	October 1993	16 days / 705 km	Failed at launch
Landsat-7	April 1999	16 days / 705 km	Operational

Table 4.2: Band characteristics of Landsat TM and Landsat ETM+.

Band	*Bandwidth (μm)*	*Resolution (m)*	*Spectral Region*
1	0.45 – 0.52	30	Blue
2	0.52 – 0.60	30	Green
3	0.63 – 0.69	30	Red
4	0.76 – 0.90	30	Near-Infrared
5	1.55 – 1.75	30	Mid-Infrared
6	10.40 – 12.50	60	Thermal Infrared
7	2.08 – 2.35	30	Mid Infrared
8*	0.50 – 0.90	15	Panchromatic

* Panchromatic band 8 appears only on Landsat-7

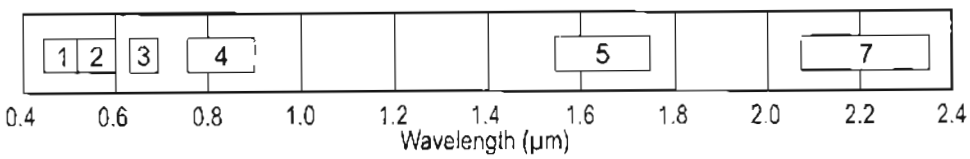

Figure 4.1: Wavelength ranges of Landsat TM bands 1-5 and 7 in relation to the electromagnetic spectrum. These are known as the reflective bands.

Though Landsat images are widely used, a number of studies have highlighted problems associated with the data. Foremost among these is the temporal resolution of 16 days, which is often considered too long for studies of transient or rapidly changing surface features (e.g. Tassan & Ribera d'Alcalá, 1993; Wang *et al.*, 1998; Malthus & Mumby, 2003). For example, monitoring the duration of flooding after rainfall events is not possible given Landsat's revisit frequency of 16 days (Lunetta & Balogh, 1999). Malthus & Mumby

(2003) also note that the spectral ranges covered by the image bands do not necessarily capture distinctive patterns present in the reflectance patterns of surface features. As can be seen in Figure 4.1, there are a number of gaps in the spectral coverage provided by the six reflective bands. This hinders the identification of surface features that might have distinctive reflectance patterns occurring in these gaps. Furthermore, the spatial resolution of 30 m limits attempts to study small features and also causes problems when different land cover types are present in the same pixel, resulting in a mixed spectral reflectance being measured (Small, 2001; Malthus & Mumby, 2003).

In mentioning the limitations of Landsat TM and ETM+ data it should be remembered that these spatial, temporal and spectral constraints are widely acknowledged and well understood, and most remote sensing studies are able to accommodate them. Landsat data continues to be widely used and it is therefore not surprising that the literature abounds with studies based on this data. Some of these will be reviewed in the next few sections, starting with an examination of the reflectance characteristics of surface features detectable with Thematic Mapper, followed by a look at studies aimed at water and wetland mapping, and concluding with an examination of the application of spectral mixture analysis.

4.4.1 Reflectance characteristics of surface features

It is important to understand the reflectance characteristics of different surface features as this allows the most suitable bands to be chosen for image classification. For this study, the most important surface features are those associated with vegetation, wetlands and water. Understanding how these surface features are measured by the Landsat Thematic Mapper will ensure that the most appropriate bands are used for classification.

The design and choice of Landsat TM bands has been largely influenced by two factors, namely, (a) the presence of atmospheric windows, and (b) the reflectance characteristics of the earth's surface features. Atmospheric windows are spectral regions in which the atmosphere is relatively transparent and where solar radiation can pass through the atmosphere without being absorbed (Schowengerdt, 1997). The location of these windows is determined by the absorption characteristics of the different atmospheric constituents

(e.g. oxygen, water vapour, ozone). The spectral bands of Landsat TM were designed to take advantage of these windows.

The reflectance characteristics of surface features have also been an important consideration in sensor design. For example, locating band 3 in the 0.63 – 0.69 μm region allows the chlorophyll absorption of plants to be determined. while band 4 (0.76 - 0.90 μm) covers an area where water is a strong absorber and is therefore useful for delineating water bodies (Wang *et al.*, 1998). Numerous studies have reported on the reflectance characteristics of different surface features and how these relate to the different TM bands.

(a) Vegetation

Many applications of vegetation mapping and monitoring have been described in the literature. Shoshany (2000) found that TM bands 3, 4. 5 and 7 are most suitable for differentiating between vegetation types because of the chlorophyll absorption and mesophyll reflections that occurs at these wavelengths. These reflections are most noticeable in the near-infrared band (TM4), which shows high reflectance values for riparian woodlands (Ringrose *et al.*, 2003), forests (Eastman, 2001) and green vegetation (Lillesand & Kiefer, 2000). Most green vegetation shows a pattern of low reflectance in the blue (TM1), slightly higher in the green (TM2), lower again in the red (TM3) and very high in the near-infrared (TM4) (Eastman, 2001). Dead vegetation, on the other hand, shows high reflectance in both the red (TM3) and near-infrared (TM4) and can therefore be distinguished from living vegetation (Jensen *et al.*, 1984). The near-infrared region, in addition to having high reflectance values for vegetation, is also a region where there is a large variation in reflectance by different vegetation types (Eastman, 2001). These variations are very useful for discriminating between different types of vegetation.

(b) Water

Water has a spectral reflectance pattern that is not often confused with other land cover types (Wickware *et al.*, 1991). Reflectance by water is low in all TM bands, with the lowest values occurring at the longer wavelengths (TM4, TM5 and TM7) (Eastman, 2001; Braga *et al.*, 2003). Indeed, in the infrared bands water has such a low reflectance that it appears to be almost black (De Haan *et al.*, 1991). This property of water allows for the relatively easy delineation of water bodies using bands TM4 or TM5 (e.g. Wickware *et al.*, 1991; Frazier *et al.*, 2003). Water does show some reflectance, albeit low, in the visible part of

the spectrum with highest values in the blue (TM1) and successively lower values occurring in the green (TM2) and red (TM3). This property has been used to study features in shallow waters (e.g. Braga *et al.*, 2003; Shaghude *et al.*, 2003).

(c) Wetlands and mires

The spectral reflectance patterns of wetlands and mires are generally rather complex due to the varying proportions of water and vegetation that occur. Wickware *et al.* (1991) used TM bands 3, 4 and 5 for classifying wetlands while Edgley & Werstak (1998) found that a combination of these same bands was useful for contrasting emergent vegetation with open water. Of these three TM bands, band 5 has been found to be the most useful in wetland detection (e.g. Lunetta & Balogh, 1999; Munyati, 2000; Boresjö Bronge & Näslund-Landenmark, 2002).

(d) Urban areas

Urban areas show varied reflectance patterns due to the different types of surfaces that occur in these areas. Non-vegetative features like buildings and concrete structures tend to have high reflectance across all the TM bands while gardens, trees and parks exhibit the reflectance patterns characteristic of vegetation (Eastman, 2001). In addition, the spatial heterogeneity of urban areas in relation to the 30-metre spatial resolution of Landsat TM means that many pixel reflectance values actually comprise a mixture of reflectances from different surface features (Small, 2001).

(e) Bare soils

Exposed sandy soil has high reflectance values across all the Landsat TM bands (Ringrose *et al.*, 2003). This allows for relatively easy separation of bare sand from vegetation and water during image classification, but can cause some confusion with artificial structures that have similar reflectance characteristics. Organic soils and soils saturated with water show different reflectance patterns to dry sandy soil. Lunetta & Balogh (1999) reported that Landsat TM band 5 is useful for studying soil moisture content while bands 2 and 3 can be used to distinguish saturated surfaces from organic soils.

(f) Burnt areas

Newly burnt areas can have very low reflectance values in the visible and near-infrared bands. This can lead to classification confusion with open water, which has a similar

reflectance pattern (Munyati, 2000). This problem can be averted by visual inspection of the image or by comparison with images from another date.

4.4.2 Mapping surface water

Clear, open water has a spectral signature that is quite distinct from other surface features (Wickware *et al.*, 1991). This characteristic of water is borne out by numerous studies described in the literature. For instance, Frazier & Page (2000) found that Landsat TM bands 4, 5 and 7, which fall in the near- to mid-infrared region of the spectrum, are very useful for mapping water bodies, with band 5 producing the highest classification accuracies. The only confusion occurs in the case of shadows, waterlogged soil and burnt areas, which can sometimes exhibit similar reflectance patterns to open water. More recently, Braga *et al.* (2003) showed that the spectral reflectance patterns of water are influenced not only by the water depth and the characteristics of the bottom type, but also by dissolved and suspended materials in the water. This is particularly so in the visible part of the spectrum.

Mapping of surface water becomes more complicated when attempts are made to quantify flooding and inundation. In these situations there are often large amounts of suspended sediment and emergent vegetation in the water, both of which change the reflectance characteristics of the water. Nevertheless, Frazier *et al.* (2003) found that the Landsat TM mid-infrared band 5 provides enough information to map areas of floodplain and wetland inundation. They maintain that this bestows an advantage on satellite-based remote sensing, as alternative methods of modelling wetland and floodplain inundation often require the use of sub-metre accuracy Digital Elevation Models (DEMs) that rarely exist.

4.4.3 Mapping wetlands

Wetland mapping using satellite imagery is rather more difficult than mapping open water. This is because the wetland environment is a complex one in which the reflected signal is complicated by the presence of varying amounts of emergent vegetation in the water, and also by the presence of wetland vegetation through which no water is visible. Jensen *et al.* (1984) demonstrated this while mapping non-tidal wetlands in South Carolina, USA,

finding that the spectral reflectance characteristics represented a continuum from open water to increased vegetation cover. Nevertheless, in spite of their complex spectral signatures, the use of remote sensing for mapping wetlands has gained in popularity, particularly as the difficulties of traversing and navigating wetlands makes it hard to map these areas using traditional methods.

The difficulty of acquiring good wetland data from field visits is reflected in many studies. Jensen *et al.* (1984) cited this as one of the reasons why alternative techniques like aerial photography and satellite remote sensing are used to map wetlands. Landsat TM, for instance, is suited for mapping wetlands as it contains bands that cover both the chlorophyll absorption (band 3) and water absorption (band 4) regions of the spectrum (Wang *et al.*, 1998). Band 3 can be used for vegetation discrimination while band 4 is useful for distinguishing between water/wetlands and dry land. Nevertheless, findings from a study by Wickware *et al.* (1991) illustrate the difficulties of mapping wetlands from satellite data. While they found it relatively easy to map water, unsatisfactory results were obtained when mapping wetlands using a supervised maximum likelihood approach. This is perhaps the main reason why many subsequent studies have used hybrid classification methods.

A case in point is the study by Jensen *et al.* (1995), which used a number of Landsat MSS and SPOT images to map changes in aquatic vegetation in the Florida Everglades. Using five images covering the period 1973 and 1991, Jensen *et al.* (1995) first performed a relative image normalisation using the 1991 image as a reference image. Clusters from an unsupervised cluster analysis of the reference image were checked against ground cover data collected from 129 reference sites. The data from the 129 reference sites were then used to seed a supervised maximum likelihood classification. Jensen *et al.* (1995) found that the hybrid supervised/unsupervised classification technique provided a suitable means of monitoring and mapping changes in aquatic vegetation in the Everglades.

In another wetland mapping exercise, Wang *et al.* (1998) made use of Landsat-5 TM and ERS-1 radar data to map and classify wetlands in the Great Lakes region of the USA. Using TM bands 3, 4 and 5 as input into a supervised maximum likelihood classifier, they mapped agricultural land, forest, open water and wetlands. The results were verified against ground truth data obtained from site visits, aerial photographs, topographic maps

and a Landsat TM colour composite image. The authors quoted wetland mapping accuracies of 96% and 84% for classifications of Landsat TM images from June 1992 and August 1992 respectively. They also found that the Landsat TM images yielded higher classification accuracies than those obtained from the ERS-1 radar data (55%), an advantage which arose because of the multispectral characteristics of the TM images.

The use of multidate imagery to increase classification accuracy of wetlands is demonstrated by Lunetta & Balogh (1999). Noting that wetlands are dynamic systems, they hypothesised that classification accuracies of wetlands from single-date images could be significantly increased when combined with data extracted from an additional image. Their study mapped vegetation using a late spring image, and merged the results with a second image that was used to delineate wet and dry areas. This second image was an early spring image chosen to coincide with the annual inundation. The study employed a hybrid classification scheme, starting with an unsupervised cluster analysis of the late spring image to identify spectral patterns and then using this information as input into a supervised maximum likelihood classification. The classification of this late spring image was then combined with the wet and dry areas delineated from the early spring image. In choosing to use Landsat TM bands 2, 3, 4 and 5 for the classification, Lunetta & Balogh (1999) cited the following reasons:

- Bands 2 and 3 allowed the differentiation of saturated surfaces from very dark features like organic soil and asphalt
- Band 4 was used because of its sensitivity to leaf structure
- Band 5 was found useful in differentiating soil moisture

Lunetta & Balogh (1999) found that the classification accuracy for the combined data (88%) was much higher than that of the single-date image (69%).

A southern African study using a hybrid classification scheme was described by Munyati (2000), who investigated changes along parts of the Kafue River floodplain in Zambia. In this study, green, red and near-infrared bands from Landsat MSS and TM images were used to map open water, emergent vegetation in shallow water, and fringe vegetation consisting of reeds. The results of an initial cluster analysis were used as input into a maximum likelihood classification. The results revealed that confusion occurred between burnt areas and areas of open water, implying that these surface feature types could not be easily separated using spectral information from the green, red and near-infrared part of the

spectrum. In contrast to this, fringe vegetation could be easily identified as it contrasted well with other land cover types.

Pillay (2001) tested the effectiveness of both the maximum likelihood and the cluster classifiers for wetland mapping in the Midmar sub-catchment in KwaZulu-Natal, South Africa. Results showed that (dry) winter images were difficult to classify due to confusion between the spectral characteristics of wetlands and other land cover types such as shadows, fire breaks and burnt areas. While classification accuracies for both the supervised and unsupervised classifications were higher for images captured during the wet summer season, these accuracies never exceeded 71%.

A novel approach to wetland mapping was adopted by Boresjö Bronge & Näslund-Landenmark (2002) who used a stepwise approach to map different classes of mire in Sweden. Their study found that Landsat TM bands 4 and 5, as well as ratios between bands 2 and 3 (TM2/TM3) and bands 4 and 5 (TM4/TM5), are most useful for mapping and discriminating between different mire types. They also found considerable spectral variation both within and between the different mire types they mapped. An examination of this variation revealed that it was caused by differences in (a) the amount of green biomass present in the mire, (b) the degree of wetness of the mire, and (c) the characteristics of the bottom layer of the mire. The stepwise technique employed in this study used threshold values, derived from the different bands and from ratios between the bands, to eliminate non-mire areas and to classify the remaining areas into different mire types.

The usefulness of integrating ancillary datasets with spectral datasets was investigated by Sader *et al.* (1995), who were attempting to map forest wetlands in Maine, USA. In this study, ancillary datasets were combined with the spectral data by means of decision rules that guided the classification of each pixel (Table 4.3). The study showed that incorporating ancillary data into the classification process yielded better classification results than traditional classification techniques based solely on spectral information. Part of the reason for this is that the spectral characteristics of wetland forests are very similar to those of other forests. Using ancillary datasets like slope and soil helped eliminate those areas in which forest wetlands could not occur, thereby removing possible sources of confusion between wetland and non-wetland forests.

Table 4.3: Rules used by Sader *et al.* (1995) to map forest wetlands in Maine, USA.

Rule	*Dataset Used*
Is pixel a forest pixel?	Unsupervised cluster classification of TM bands 3, 4 and 5
Is pixel in a wetland?	US Fish and Wildlife Service National Wetland Inventory
Pixels contains hydric soil?	US Soil Conservation Service soil data
Is slope < 5%?	USGS DEM
Pixel close to a river or pond?	USGS Hydrography

Another example of a technique incorporating ancillary data to map wetlands is provided by Thompson *et al.* (2002) who developed a methodology using satellite-based remote sensing to map South African wetlands. The hybrid technique they proposed makes use of both derived and ancillary datasets and consists of three steps:

- **Step 1: Determine wetland potential areas by masking out all areas in which wetlands cannot occur.** This is achieved by means of an iterative unsupervised cluster analysis of spectral data in which non-wetland areas are successively removed until only potential wetland areas remain. Inputs into this stage are components from a Principal Components Analysis of the NDVI and the six TM reflective bands.
- **Step 2: Perform an unsupervised spectral classification of the data within the wetland potential areas.** This step uses the NDVI for the wetland potential areas (identified in step 1) along with the Tasselled Cap greenness and wetness components of these same areas.
- **Step 3: Use a terrain-derived topographic model to modify the spectrally defined wetland boundaries.** Areas of Landscape Wetness Potential are derived from a DEM. This terrain-derived topographic model is then combined with the spectrally defined wetland areas (from step 2) to produce a final wetland delineation and classification.

Thompson *et al.* (2002) found that an unsupervised classification is most suitable for the first two steps as this technique performs well in the complex landscapes associated with wetlands. In addition, the final step is critical in identifying confusion between wetlands and non-wetland areas that have similar spectral characteristics. This is achieved by locating and eliminating areas topographically unsuitable for wetland formation.

This brief review of wetland mapping has shown that the complex spectral characteristics of these environments makes classification difficult. Nevertheless, some success has been achieved. An analysis of the spectral bands used to map wetlands reveals that all the reviewed studies used TM bands 3 and 4, and all used at least three bands (Table 4.4). The mid-infrared band 5 was used by most studies, with some also using band 2. Only one study used all 6 reflective bands. Improved classification accuracies were obtained by using hybrid classifications techniques (e.g. Jensen *et al.*, 1995; Lunetta & Balogh, 1999; Munyati, 2000; Thompson *et al.*, 2002) and by incorporating ancillary datasets (e.g. Sader *et al.*, 1995; Thompson *et al.*, 2002; Ringrose *et al.*, 2003).

Table 4.4: A list of wetland studies showing the Landsat TM bands used to delineate wetlands and/or water.

Study	*TM1*	*TM2*	*TM3*	*TM4*	*TM5*	*TM7*
Wickware *et al.*(1991)			x	x	x	
Sader *et al.* (1995)			x	x	x	
Wang *et al.* (1998)			x	x	x	
Lunetta & Balogh (1999)		x	x	x	x	
Munyati (2000)		x	x	x		
Boresjö Bronge & Näslund-Landenmark (2002)		x	x	x	x	
Thompson *et al.* (2002)	x	x	x	x	x	x
Ringrose *et al.* (2003)			x	x	x	

4.4.4 Mixture analysis

As will be seen in subsequent chapters, the application of spectral mixture analysis plays an important role in this study. It is pertinent, therefore, to review previous applications of mixture analysis, particularly those that have used this technique to map water, vegetation and/or wetlands.

A review of studies employing spectral mixture analysis reveals the ongoing development of this technique as a usable and accurate means of sub-pixel classification. Numerous studies of linear unmixing have been described in which Landsat data are used to investigate water sediment concentrations and vegetation heterogeneity. Also present in the literature are comparisons between classifications obtained via spectral unmixing and those

obtained through traditional hard classification methods. Comparisons like these allow the accuracy of the unmixing technique to be compared against more traditional classifiers.

Two such comparative studies are presented by Binaghi *et al.* (1999) and Lu *et al.* (2004). Binaghi *et al.* (1999) investigated sub-pixel land cover of a lagoon environment near Venice, Italy, using three different methods: a neural network classifier, a fuzzy-statistical classifier and a linear mixture model. Binaghi *et al.* (1999) felt that using traditional hard classification methods would have produced unreliable results due to the presence of varying mixtures of water and wetland in the lagoon. Analysis was performed using water and wetland endmembers obtained from aerial photographs of the lagoon. The fractions of water and wetland produced by the three different methods were then compared against test data taken from the aerial photographs. Findings from the study showed that the neural network model and the linear mixture model produced comparable results, while the fuzzy-statistical classifier produced outputs that were less accurate. Binaghi *et al.* (1999) also stressed the importance of classification accuracy assessment but conceded that in the case of sub-pixel analysis, this could sometimes only be achieved though complimentary techniques and not by direct ground truthing.

Lu *et al.* (2004) also conducted a comparative study, one in which results from a linear spectral mixture analysis were compared against those obtained from a minimum distance supervised classification, a maximum likelihood supervised classification and an ECHO hybrid classification. Using a June 1998 Landsat TM covering Rondônia State in Brazil, they attempted to map 11 different land cover classes using the four different classification techniques. Prior to classification, a principal components analysis was carried out on the TM data in order to remove redundancy. Only the first four principal components were used in subsequent mixture analysis. Three endmembers were used for the unmixing process, namely shade, soil and green vegetation. The three fraction images obtained from the mixture analysis were then classified by means of a decision tree using class threshold values derived from the training data. Of the four different classification methods, linear spectral mixture analysis produced the highest accuracies (86%). This was particularly apparent in areas of vegetation heterogeneity where spectral unmixing was able to tease out the fractional abundances of different land cover classes within pixels. The other classification methods were not able to do this.

Applications of spectral mixture analysis to studies of water sediment concentrations in rivers and river floodplains are described in a series of articles by Mertes *et al.* (1993), Mertes *et al.* (1995) and Mertes (1997). The first of these papers describes how mixture analysis of Landsat data was used to examine suspended sediment concentrations in the waters of the Amazon River wetlands. Processing was carried out in two steps. First, the image was corrected for radiometric and atmospheric effects by using endmembers of soil, shade and vegetation to relate satellite-measured reflectance to laboratory-derived readings. These endmember features were assumed to have constant reflectance characteristics from year to year. The second step saw linear spectral mixture analysis applied to the images using laboratory-derived reference endmembers of water/sediment mixtures. Interpretation of the results showed that sediment concentrations were highest near the main river channel and decreased with distance into the floodplain. Furthermore, results indicated that vegetation in the water could be readily detected if a vegetation endmember was included in the unmixing process.

In a follow-up paper, Mertes *et al.* (1995) used spectral mixture analysis to investigate water sediment concentrations along sections of the Amazon River and also to examine the spatial distribution of vegetation and floodplain features. The three Landsat images analysed covered periods of high water levels and floodplain inundation. Three different endmembers were selected, each representing pure examples of shade, sediment-laden water and vegetation respectively. The shade endmember was selected from pixels of dark, clear water and hence provided information on both water and shade. Spectral mixture analysis was performed using the three endmembers and the six reflective bands from the Landsat images (i.e. bands 1 to 5 and band 7). The fraction images were classified into five different water classes (each with a different sediment concentration), two forest classes and three macrophyte classes. The macrophyte classes ranged from a class with high water/low vegetation fractions through to a class with low water/high vegetation fractions. An analysis of the results showed a high diversity of vegetation along floodplain drainage channels with more homogeneous conditions on the floodplain itself. It was also possible to identify a high diversity of water types, as well as different floodplain landforms like bars, swales, drainage channels and deltas.

In the third of these studies looking at sediment concentrations, Mertes (1997) examined the mixing of river water and locally-derived floodplain water on inundated river

floodplains by unmixing spectral data from Landsat-5 TM images. The study demonstrates the usefulness of Landsat data for investigating water characteristics. Endmembers were derived either from laboratory-based spectral measurements or were extracted from the Landsat images themselves. The endmembers were chosen to include both muddy and clear water. For one of the rivers, selection of an additional vegetation endmember allowed the relative proportions of vegetation in the different water types to be investigated. In this case, interpretation of the resulting fraction images clearly showed areas of mixed vegetation and muddy water contrasting with clear water.

Spectral mixture analysis has also been used to quantify land cover change. Adams *et al.* (1995) described a classification scheme based on fraction images that allowed changes in land cover to be determined from a series of four Landsat TM images from consecutive years. Simultaneous field observations were used to generate reference endmember spectra. The study area, located in northern Brazil, was dominated by forest but also contained areas cleared for cultivation and pasture. Prior to unmixing, the 1989 image was calibrated to reflectance values, followed by a relative radiometric normalisation of the remaining images using the method developed by Hall *et al.* (1991). Spectral unmixing was applied to all four images using endmembers of green vegetation, non-photosynthetic vegetation, soil and shade. An examination of the output showed that changes in land cover were reflected as changes in fractions in the fraction images, allowing patterns of land cover change to be traced over the four year period. In assessing the accuracy of the results, possible sources of error were ascribed to cases where different surface features had similar reflectance spectra (called mimicking by the authors) as well as situations where reflectance characteristics of surface features straddled class boundaries, leading to classification uncertainty.

Another methodology aimed at identifying land cover change by using spectral mixture analysis was proposed by Roberts *et al.* (1999). They tested their technique by applying it to an area in South America undergoing rapid land cover change. Land cover in the region included areas of water, bare soil, pristine and regenerating forest, as well as plantation and pastures. Five Landsat TM images covering the period 1984 to 1994 were used in the study. One of the images was selected as a reference image and was converted to apparent reflectance through the use of reference endmembers. The remaining images were then radiometrically normalised relative to the reference image using a series of invariant targets. Spectral mixture analysis was performed on all the images using endmembers of

shade, soil, green vegetation and non-photosynthetic vegetation. Fraction images from the spectral mixture analysis for each date were classified into six land cover types by means of a decision tree, the rules for which had been developed based on data obtained from training sites. An analysis of the classification revealed a pattern of dynamic changes in land cover. The first eight years of the study period were characterised by deforestation, slowly increasing regeneration and pasture maintenance, whereas the last two years revealed faster rates of deforestation and regeneration. In interpreting their results, Roberts *et al.* (1999) asserted that the technique they had developed provided a direct measure of the type and magnitude of land cover change.

The use of spectral mixture analysis is not only restricted to rural or natural landscapes. An urban application of linear unmixing was described by Small (2001) who used the technique to estimate the abundance of vegetation in New York and New Jersey. The rationale for using mixture analysis was that traditional hard classification methods are not suited to the spectral and spatial heterogeneity of the urban environment. There had also been very few applications of remote sensing to urban studies as the spatial resolutions of Landsat and SPOT imagery were deemed inadequate for the task. The three endmembers used for the unmixing process defined areas of high albedo, low albedo and vegetation. Fraction images produced by the mixture analysis were verified against ground truth data derived from aerial photographs. This verification revealed a strong correspondence between vegetation fractions obtained from Landsat and those obtained from the aerial photography. Small (2001) showed that fraction images produced by the spectral unmixing were easy to interpret and seemed to provide reasonable estimates of vegetation cover.

This review of applications of spectral mixture analysis has shown that a number of studies have used this technique to map water, vegetation and/or wetlands. However, endmembers need to be selected carefully if the process of spectral unmixing is to be accurate. The chosen endmembers should represent pure examples of surface features and should also cover all the different feature types present in the image. As can be seen in Table 4.5, most of the studies used three or four endmembers and almost all of them included a shade endmember. In addition, interpretation of the fraction images is made easier by classifying the fractions into a number of discrete classes.

Table 4.5: Endmembers used in the reviewed spectral mixture analysis studies.

Study	*Endmembers selected*
Mertes *et al.* (1993)	Soil, shade, vegetation, various water/sediment mixtures
Mertes *et al.* (1995)	Vegetation, shade (also representing clear water), sediment-laden water
Adams *et al.* (1995)	Green vegetation, non-photosynthetic vegetation, soil, shade
Mertes (1997)	Clear water, muddy water, vegetation
Roberts *et al.* (1999)	Green vegetation, non-photosynthetic vegetation, soil, shade
Binaghi *et al.* (1999)	Water, wetland
Small (2001)	High albedo, low albedo, vegetation
Lu *et al.* (2004)	Shade, soil, green vegetation

4.5 CONCLUSION

One of the most important benefits of satellite-based remote sensing is that these technologies have allowed global-scale measurements to be made in a regular and systematic manner. This is especially true for the Landsat Thematic Mapper programme, which has been extensively used for many different applications. Thematic Mapper data is fairly cheap and readily available, has a long coverage going back to the early 1980s, and provides spectral measurements in the visible and infrared that facilitate the mapping of many of the earth's features. The spectral and spatial resolution of TM data also allows vegetation, water bodies and wetlands to be mapped at scales that permit long term changes in land cover to be assessed. TM bands 3, 4 and 5 are particularly useful for mapping wetlands, while open water is easily mapped using near- or mid-infrared bands. Incorporating ancillary datasets into the classification process has also proved beneficial, often leading to significant increases in classification accuracy.

Recent years have seen an increase in the use of soft classification techniques, particularly spectral mixture analysis, as researchers attempt to extract land cover information at sub-pixel levels. Studies have shown that spectral mixture analysis is able to identify mixtures of water and vegetation although it is difficult to assess the accuracy of these classifications in the absence of ground truth data. Of particular importance in mixture analysis studies is the accurate identification of endmembers. These can be selected from laboratory-derived

spectra although endmembers selected from the images have the advantage of being measured under the same atmospheric conditions as the rest of the image.

This review of the Landsat programme, the reflectance characteristics of surface features and the mapping of water and wetlands has provided an indication of how satellite-based remote sensing may be used to accomplish the aims of this study. In addition, the review has provided an understanding of the application of spectral mixture analysis, an understanding that is especially important for this project, as will be shown in the following chapters.

5. METHODOLOGY

5.1 INTRODUCTION

Image processing follows well-defined procedures for manipulating and interpreting images, procedures that have been applied throughout this study. This chapter outlines how the image processing framework was used and how it allowed the spatial and temporal extent of surface water on the Eastern Shores of Lake St Lucia to be investigated. The chapter commences with a description of the satellite imagery used in the study, followed by an outline of the rectification and atmospheric correction techniques used to prepare these images for classification. The preparation of ancillary and secondary datasets will be discussed, along with an outline of how these were used to prepare image masks. The application of a number of hard and soft classification techniques will then be described, with particular emphasis being placed on the selection of image endmembers and the application of spectral mixture analysis. The chapter concludes with an outline of the methods used to assess the accuracy of the final classified images.

5.2 IMAGE ACQUISITION

The first step in any remote sensing study is choosing which satellite imagery to work with. For this study the imagery needed to be suitable not only in terms of cost and availability, but also in terms of the spatial, spectral and temporal resolution of the data. Another important factor was the length of the available historical record, as a long record would allow changes over time to be examined. Most important for the current study, though, was the ability to map water and vegetation at a resolution detailed enough for the landforms found on the Eastern Shores. A review of currently operating earth observation platforms quickly revealed that only two suitable candidates existed, namely Landsat Thematic Mapper and SPOT. Of the two, Landsat TM data was deemed more suitable even though it had a slightly poorer spatial resolution (~30 metres for Landsat vs. ~20 metres for SPOT). This suitability was not only because of the presence of a continuous record going back to 1982, but also because the measurement of reflectance in seven spectral bands allowed for greater scope in the investigation of surface water distribution in the study area. In addition,

the larger footprint of Landsat TM meant that fewer images were needed to cover the study area, resulting in significant cost savings.

Having chosen Landsat as the preferred sensor platform, the next step was to conduct a survey of the available data and to select a set of cloud-free images covering a full seasonal cycle. Given that one of the key aims of the study was to examine the distribution of surface water on the Eastern Shores, it was important to obtain a series of images that included both the wet summer and dry winter seasons. Finding cloud-free images during the summer months proved to be a serious constraint, however, particularly as Landsat overpasses occurred only once every 16 days. A survey of the available images from 2000, 2001 and 2002 revealed no cloud-free images of the study area during the months November through to February. This was not surprising given that these months fell within the height of the rainy season. As a result of the absence of cloud-free images during the summer months it was decided to select images from both 2001 and 2002 which, when seen in terms of the month they were recorded, covered a complete seasonal cycle as can be seen in Figure 5.1. The dates of these images are shown in Table 5.1. In addition to the six Landsat-7 ETM+ images from 2001 and 2002, a single Landsat-5 TM image from 1991 was ordered so that results obtained from this sensor could be compared against those obtained using Landsat-7 ETM+. All the images were supplied by the Satellite Applications Centre (SAC).

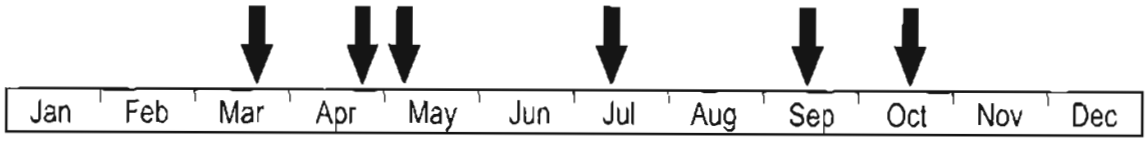

Figure 5.1: The months during which the images were recorded.

5.3 IMAGE PREPARATION

All data processing for this project was done using Idrisi 32 Release Two and ArcGIS 9 software. Idrisi is a raster-based GIS program which is well suited for processing satellite imagery. It provides methods for developing signatures and endmembers and also contains numerous hard and soft classification algorithms. ArcGIS is primarily a vector-based GIS, although current versions of this software provide significant support for raster datasets

(like satellite images). The satellite images acquired from the SAC were received on CD-ROM and converted into Idrisi format using Idrisi's PARE module. Each spectral band was stored as a separate image resulting in a total of 61 images for the entire dataset. The pixel values for each band were recorded as digital numbers (DN), ranging between 0 and 255, and which were proportional to the reflected radiation from each pixel.

Table 5.1: The dates of the satellite images acquired for this study, showing the spectral bands recorded for each image.

Date	*Spectral Bands**	*Satellite, Sensor*
1991/07/23	1, 2, 3, 4, 5, 6, 7	Landsat-5 TM
2001/03/20	1, 2, 3, 4, 5, 6L, 6H, 7, 8	Landsat-7 ETM+
2001/05/07	1, 2, 3, 4, 5, 6L, 6H, 7, 8	Landsat-7 ETM+
2002/04/24	1, 2, 3, 4, 5, 6L, 6H, 7, 8	Landsat-7 ETM+
2002/07/13	1, 2, 3, 4, 5, 6L, 6H, 7, 8	Landsat-7 ETM+
2002/09/15	1, 2, 3, 4, 5, 6L, 6H, 7, 8	Landsat-7 ETM+
2002/10/17	1, 2, 3, 4, 5, 6L, 6H, 7, 8	Landsat-7 ETM+

* ETM+ recorded both low gain and high gain measurements for band 6, the thermal band

The next two stages in the image preparation process, namely image rectification and image normalisation, required the use of a reference image. The image from 7 May 2001 was chosen for this purpose as an inspection of weather records revealed that an active cold front, associated with a lot of rain, had passed through the area two days previously, resulting in very clear atmospheric conditions on the day the image was recorded. Not only did these clear conditions facilitate the identification of ground control points for use during image rectification, they also meant that atmospheric effects on this date were less pronounced than on the other dates, resulting in a more accurate atmospheric correction process for this date.

5.3.1 Image rectification

A series of 12 widely-spread ground control points (GCP) were located on the reference image as well as on 1:50000 topographic maps. The coordinates of the GCPs from the unrectified reference image were recorded in terms of row and column numbers while the

corresponding latitude and longitude coordinates were digitised from the 1:50000 maps and reprojected to the South African LO33 coordinate system[4]. The GCP coordinates were then used to construct a set of polynomial equations which were used to rectify the image data. All the bands of the reference image were rectified using a quadratic resampling process and a nearest neighbour interpolation technique[5]. The rectified image had a spatial resolution of 30 metres (i.e. a cell size of 30 metres by 30 metres) and was clipped to the study area as shown by the red box in Figure 5.2.

The images for the remaining dates (the target images) were then rectified relative to the reference image using ground control points located on the reference image and the target images. This relative rectification was also performed using quadratic resampling and nearest neighbour interpolation.

5.3.2 Radiometric correction and image normalisation

Once the images had been rectified and georeferenced, the next step was to remove the effects of the atmosphere while at the same time converting the digital numbers (DN) into values of reflectance. In calculating these reflectance values, corrections were also made for sensor calibration, seasonality and the viewing geometry of the satellite. Calibrating all the images to reflectance was particularly important in this multitemporal study as it facilitated the comparison of images across different dates. The thermal and panchromatic bands (i.e. bands 6 and 8) were left uncorrected as they were not used in the image classification stages of this project. As with geometric rectification, the process of radiometric correction was carried out in two steps:

1. An absolute correction of the reference image (7 May 2001) was performed using Chavez's COST method.
2. Relative corrections were performed on the remaining images (the target images) by normalising them to the reference image.

4. The LO33 system is a metres-based system which uses a Gauss-Kruger projection, the Hartebeesthoek datum and longitude 33° East as the central meridian. The x-coordinates in this system represent the distance in metres from the central meridian while the y-coordinates indicate the distance from the equator.
5. Guidelines for quadratic resampling recommend a minimum of 6 control points, a criterion easily met by the 12 GCPs used in this study. Nearest neighbour interpolation ensured that the pixel values from the original images were transferred to the rectified images without being modified.

Figure 5.2: Rectified image from 7 May 2001 showing the 12 ground control points used in the rectification process. The red box shows the Eastern Shores study area.

The COST model required a number of input parameters, some of which were obtained from the bands of the reference image themselves and some from the accompanying metadata. These can be seen in Figure 5.3, which shows the input parameters used for running the COST model on band 2 of the reference image. The haze value for each band (DN haze) was determined by examining the histogram of the band in question and selecting the lowest DN with a frequency > 100. The values for the sensor offset and gain, satellite viewing angle and sun elevation were obtained from the metadata received from the SAC when the satellite images were purchased. The spectral solar irradiance (E_0, the solar radiance as measured at the top of the atmosphere) was based on the central wavelength of the band and image acquisition date and was calculated by the software once

the required date and wavelength parameters had been entered. Once all the reflective bands of the reference image had been radiometrically corrected they were multiplied by 100 to scale the reflectance to values between 0% and 100% with 0% representing no reflectance and 100% implying total reflectance of all the incoming solar radiation.

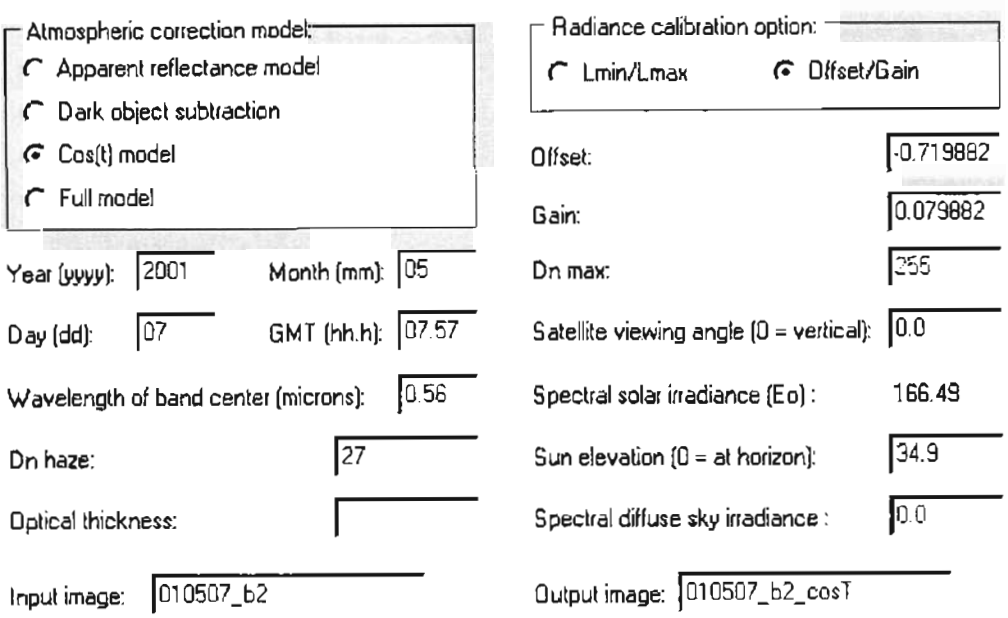

Figure 5.3: Input parameters used when applying the COST atmospheric correction model to band 2 of the reference image.

The next phase of the image normalisation process was the radiometric normalisation of the target images relative to the reference image. This was done using the method developed by Eckhardt *et al.* (1990) and made use of a number of *dark* and *bright* normalisation targets located on both the reference and target images (Figure 5.4). These target areas were assumed to be constant reflectors and were used to define a series of regression equations which, when applied to the target images, would convert them to the same units as the reference image. In addition, as the reference image had already been radiometrically corrected, normalising the target images to the reference image would effectively also perform a radiometric correction on the target images. Selection of the normalisation targets followed the guidelines laid down by Eckhardt *et al.* (1990) in that they were flat, unvegetated areas that did not contain patterns that changed over time. Three areas of open water were used as dark normalisation targets while two large patches of exposed beach sand north of Cape Vidal were selected as bright targets. From the details of the target areas shown in Table 5.2 it can be seen that the size and position of the two

bright targets differed slightly from image to image. This was due mainly to the differing state of the tides on these beach targets, with some images having smaller areas of exposed beach sand than others.

Table 5.2: Details of the invariant targets used to generate regression formulas for the image normalisation process.

Target	*Name*	*Target Description*	*Size (pixels)*
1	Dark Target #1	Open sea	484
2	Dark Target #2	Lake Bhangazi	484
3	Dark Target #3	Northern part of Lake St Lucia	506
4	Bright Target #1	Beach south	175-198
5	Bright Target #2	Beach north	228-275

Only one of the dark targets was used for the final normalisation of each band. This ensured that the number of pixels from the bright targets was approximately the same as the number of dark target pixels. The dark targets were selected by examining the impact of each one on the R^2 values obtained when comparing normalisation target pixels from the target images against those from the reference image. Dark Target #2 was found most suitable for normalising band 1, Dark Target #1 was used for bands 2, 3 and 4 while Dark Target #3 was used to normalise bands 5 and 7. Mean pixel values for the selected normalisation target areas on both the reference and target images were calculated and used to generate regression (normalisation) equations. One equation was generated for each of the six reflective bands of the six target images, giving a total of 36 equations (see Appendix 1). Each of the image bands was then transformed using the relevant normalisation equation, resulting in all the target images being normalised relative to the reference image from 7 May 2001.

5.4 IMAGE TRANSFORMATION

Image transformation techniques were applied in this study with two different aims in mind. Firstly, a Principal Components Analysis (PCA) was carried out in order to reduce the inherent redundancy of the data, thereby producing a set of uncorrelated images for each date. These uncorrelated images would be used during the image classification stage

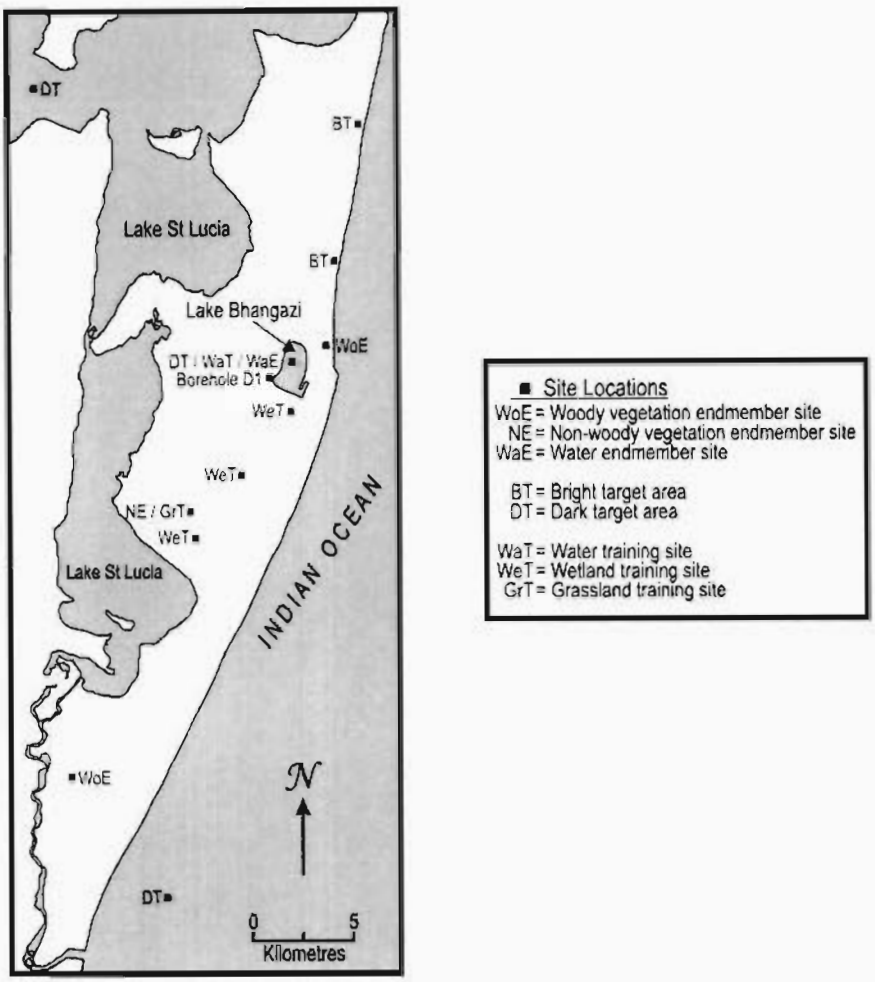

Figure 5.4: Location of bright and dark target areas, training sites used in the supervised classification, and training sites used to define endmembers.

to investigate whether they improved classification accuracy. Secondly, a set of exclusion masks were used to exclude areas on the Eastern Shores that would not be analysed in the study. This not only reduced the volume of data to be processed but also eliminated areas in which surface water would not be found. The following areas were excluded:

1. Areas of land and water surrounding the study area were excluded from further processing. These areas comprised Lake St Lucia and the ocean as well as parts of the Western Shores of Lake St Lucia.
2. All forested areas were excluded. Most of the forest on the Eastern Shores was quite dense and it would not be possible to view surface water through the canopy.
3. Areas with slopes exceeding 5% were excluded as surface water was unlikely to collect in areas as steep as this.
4. All areas of bare sand. Most of these areas were beach sand.

5.4.1 Principal components analysis (PCA)

A principal components analysis was carried out before image masking took place, thereby ensuring that all the spectral data was included in the covariance matrix calculations of the PCA. Producing a covariance matrix based on the masked data would have resulted in unrealistically high covariances due to the fact that the zero values of the masked areas would have caused inter-band correlations to appear higher than they actually were. All six reflective bands were used in the analysis (i.e. bands 1-5 and 7) and those bands with a greater variance were given a greater weighting in the analysis. Six components were extracted for each image with components being offset, where necessary, to fit within the range 0-255. This was done in order to facilitate further processing by the Idrisi software. Table 5.3 shows how virtually all of the variance present in the original spectral data was contained in the first three components. Together, these three components explained over 99% of the variance for each of the study dates. The remaining three components contained mostly noise and were not used during the image classification stage of this study. From here onwards, the PCA dataset will be referred to as the component data while the original, untransformed spectral dataset will be referred to as the spectral data.

Table 5.3: Percentage of variance explained by the first three components of the PCA.

	Variance explained by each component (%)			
Date	*Comp 1*	*Comp 2*	*Comp 3*	*Total (%)*
1991/07/23	81.6	11.8	5.8	99.1
2001/03/20	81.6	11.1	6.7	99.4
2001/05/07	81.4	11.2	6.6	99.3
2002/04/24	83.5	10.8	5.0	99.3
2002/07/13	85.1	10.7	3.5	99.3
2002/09/15	80.8	12.2	6.2	99.2
2002/10/17	85.1	9.5	5.0	99.7

5.4.2 Preparation of exclusion masks

Four sets of exclusion masks were created: a study area mask, a forest mask, a slope mask and a sand mask. These masks were prepared as binary images in which areas to be excluded were given a value of zero while areas to be retained were assigned values of one.

5.4.2.1 Study area mask

On-screen digitising was used to delineate an outline of Lake St Lucia and the sea shore so that the areas of water surrounding the study area could be excluded from further processing. A 43-metre buffer generated inland of these shorelines was used to define the study area mask. There were two reasons for using this buffer. In the first place it was used to account for fluctuations in the position of the water's edge, which varied according to the state of the tides and the level of the water in the lake. Secondly, it was used to compensate for possible misregistration of the images during the rectification process. A distance of 43 metres represented the diagonal distance across one pixel meaning that a 43-metre buffer defined a buffer zone of at least one pixel around the whole study area.

5.4.2.2 Forest mask

Coastal dune forests, swamp forests and pine plantations represent the main types of forest found on the Eastern Shores. These were mapped using the normalised difference vegetation index (NDVI), which, as an indicator of biomass, was used to distinguish forested from non-forested areas. One NDVI image was created for each of the seven study dates. A large patch of dune forest and another of plantation forest were identified on these NDVI images by means of visual inspection. Minimum NDVI values within these two patches for each of the study dates were then used as threshold values to delineate all forested areas for each of the images. The seven delineated forest areas were merged into a single image, producing a forest mask showing all areas that had been forested at some time during the study period. This compensated for the effects of afforestation and deforestation while at the same time ensuring that the size of the area being analysed was the same across all seven dates.

5.4.2.3 Slope mask

An ancillary data set was required in order to exclude steep slopes. This took the form of a digital elevation model (DEM) that was generated from spot heights and height contours obtained from 1:50000 topographical maps. The DEM was constructed with a 30-metre resolution which matched the spatial specifications of the Landsat images. Using the DEM,

a map of slope steepness was created for the whole study area. From this steepness map, all areas with slopes steeper than 5% were identified and combined into a single slope mask.

5.4.2.4 Sand mask

The sand mask was used to exclude areas of sand from further processing. Sand is characterised by high reflectance values in all six of the Landsat reflective bands and was thus fairly easy to delineate. This was in contrast to soil which contains varying amounts of organic material and has a very different spectral signature to that of sand. This was particularly apparent in the visible bands of the electromagnetic spectrum where soil reflectance values tended to be lower than those of sand. Spectral band 3 was used to delineate areas of sand for each date and these were combined into a single sand exclusion mask.

5.4.3 Application of the exclusion mask

The study area, forest, slope and sand masks were combined into a single exclusion mask in which all areas to be excluded from further study were assigned a value of zero. All other areas were given a value of one. In a series of overlay operations the exclusion mask was multiplied with each of the bands from the seven study dates resulting in all the masked areas being set to zero in the image data. The exclusion mask was also applied to all the component images resulting from the principal components analysis.

5.5 IMAGE CLASSIFICATION

Three different classification methods were used to map the surface water in the study area. Two of these, an unsupervised cluster analysis and a supervised maximum likelihood classification, were hard classifications while the third method, a spectral mixture analysis, performed a soft classification of the data. The outputs from these three different classifications were assessed to see which method was best able to map surface water. The results of this assessment are presented in the next chapter. Classifications were performed on the untransformed spectral data as well as on the first three PCA components.

5.5.1 Cluster analysis

Cluster analysis was performed using the Idrisi software's ISOCLUST routine. This is a hybrid clustering routine that uses the output from a standard cluster analysis to seed an iterative cluster analysis based on the ISODATA clustering method. Three bands of data were required to seed the routine. Once seeded, the routine was set to run for three iterations and 15 clusters were extracted for each of the study dates. The total of 15 clusters was chosen following an inspection of cluster frequency histograms produced by the seeding cluster analyses of the various study dates. The majority of these histograms revealed the presence of a discontinuity in frequencies at approximately 15 clusters.

(a) Cluster analysis of the untransformed spectral data

Seeding was performed using data from bands 3, 4 and 5. These bands were chosen following a review of the literature which revealed that these were the bands most often used in studies of water and wetlands (see Table 4.4 on page 59). Once the seeding was complete, all six reflective bands were used in the iterative cluster classification.

(b) Cluster analysis of the principal components dataset

The first three principal components were used to seed the process and were also used in the subsequent iterative cluster analysis. The 4^{th}, 5^{th} and 6^{th} components were not included in the analysis as they contained mostly noise.

The 15 clusters extracted for each date were examined and assigned to classes. This was done through a process of examining colour composite images and aerial photographs and by using knowledge gained through field visits. In most cases, clusters representing similar land cover classes were combined into a single class.

5.5.2 Maximum likelihood classification

Performing a supervised classification required the identification of training sites from which the spectral characteristics of land cover types in the study area could be defined. The main land cover types found on the Eastern Shores are grasslands, wetlands and water

along with a few artificial structures like roads and buildings. Forests and sandy areas were not considered as these had been excluded in the image transformation stage. Training sites identified during field visits to the study area were located on colour composite images of the Eastern Shores. These were then digitised and spectral signatures were developed for each of the land cover types represented by the training sites. Details of all the training sites are shown in Table 5.4 and Figure 5.4.

Table 5.4: Details of training sites used in the supervised classification.

Land cover class	*Locations of training sites*	*No. of pixels*
Open water	Lake Bhangazi	711
Grassland	West of the southern end of the Mfabeni swamp	102
Wetland	Central section of the Mfabeni swamp and two small areas at the northern and southern ends of the swamp	91

Using signatures developed from the training sites, a maximum likelihood classification was performed on both the spectral and the component data for all seven study dates. Only bands 2, 3, 4 and 5 were used to classify the spectral data as these were found to be most suitable for identifying water and wetlands (see Sections 4.4.2 and 4.4.3 on page 54 and Table 4.4 on page 59). No prior probabilities of occurrence were specified for any of the signatures, implying that all pixels had an equal probability of belonging to each of the three land cover classes. Pixels were assigned to the class to which their probability of membership was the highest. An exception was those pixels which had the least likelihood of belonging to any of the three classes; these pixels were left unclassified.

5.5.3 Spectral mixture analysis

The only large water body on the Eastern Shores is Lake Bhangazi. This lake comprises mostly open water with narrow fringes of reeds on the western, northern and eastern shores. Aside from Lake Bhangazi, most of the remaining surface water on the Eastern Shores occurs in conjunction with emergent vegetation (Figure 5.5). This mixing of water and vegetation is problematic for hard classifiers as these techniques assume that pixel values comprise radiation reflected from only one land cover type. Spectral mixture analysis was therefore applied in order to determine whether surface water could be

mapped by identifying pixels containing mixtures of water and vegetation. The assumption was that spectral unmixing would reveal the presence of pixels containing varying fractions of water and vegetation, ranging from pixels with only water and no vegetation through to pixels containing only vegetation and no water. It was also assumed that mixing was linear and that there were no multiple reflections of radiation by the vegetation in the pixels.

5.5.3.1 Endmember selection

Due to the fact that no laboratory-measured reference spectra were available, endmembers had to be derived from the image datasets themselves. Two different methods of selecting endmembers were used: a scattergram approach for the component data and a method based on training sites for the spectral data. Both these methods involved the identification of water and vegetation endmembers, thereby facilitating modelling of the water/vegetation mixtures within the study area.

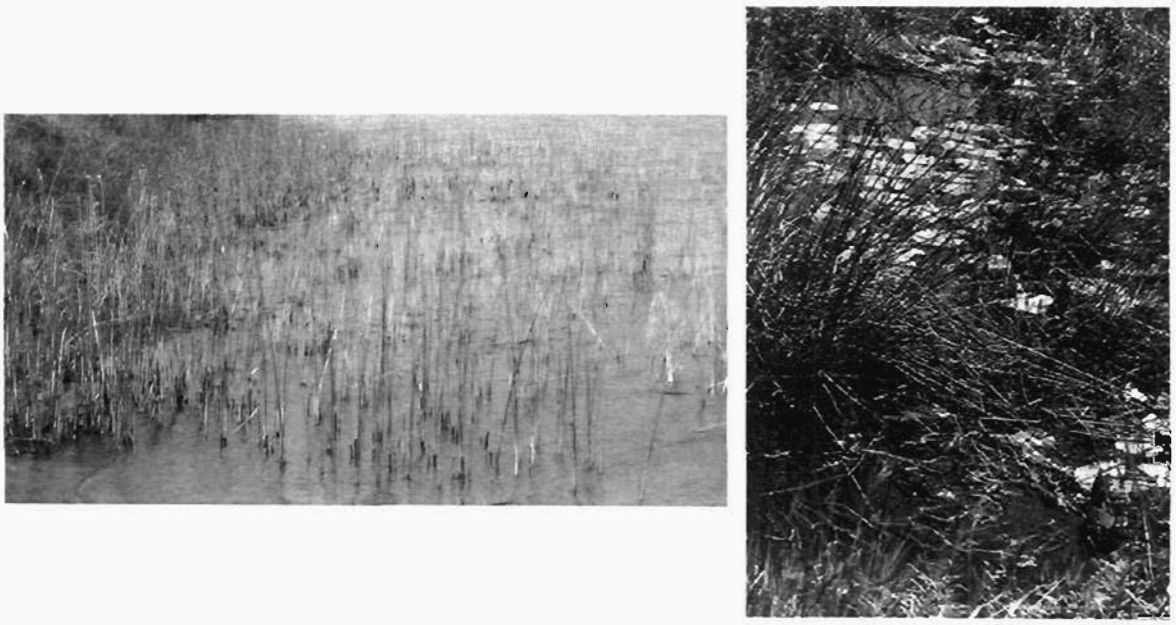

Figure 5.5: Examples of the mixing of vegetation and water in the study area.

(a) Component data endmembers

Endmembers for the principal component datasets were chosen from scattergrams of the first three components. These three components can be conceptualised as forming a three-dimensional feature space within which the image pixels were located. Each pixel was located within this space according to its component

values, with the first component value located on the x-axis, the second component value on the y-axis and the third component value on the z-axis of the scattergram. Scattergrams of the first two components (Figure 5.6) for each study date revealed a triangular spread of pixels, indicating that most pixels in the study area were made up of mixtures of three basic features. These basic features defined the triangular area within which most of the mixed pixels were located. Pixels comprising relatively pure examples of one of these features were located close to the relevant vertex of the triangle while pixels exhibiting a high degree of mixing occupied the space near the centre of the triangle. In the case of the Eastern Shores study area, the three features represented pure examples of water, woody vegetation and non-woody vegetation. Those few pixels located outside the mixing triangle usually contained spectral information from features other than the three basic ones (e.g. soil, buildings, burnt vegetation) or else indicated the presence of sensor noise.

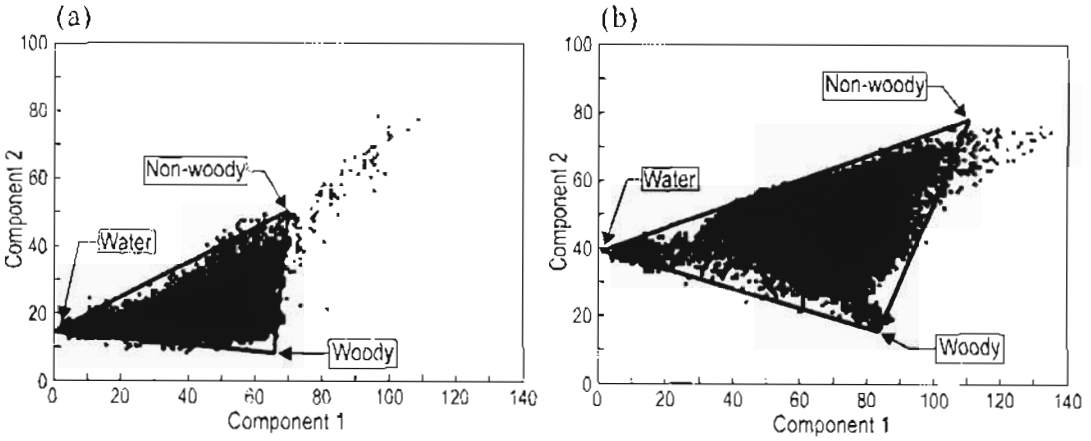

Figure 5.6: Scattergrams showing the distribution of pixels of the first two principal components for (a) 7 May 2001 and (b) 17 October 2002. Mixing triangles are shown in red and endmembers are indicated by the arrows.

Although the mixing triangles were located within a three-dimensional feature space, the locations of the triangles within this space were governed largely by the first principal component, which contained over 80% of the variance for each of the study dates. The mixing triangles for each date were first located on scattergrams which plotted component one values against those of the second principal component (as shown in Figure 5.6). These triangles were then transferred to scattergrams of the first and third components and the values of the triangle vertices along the third component axis were recorded.

Each endmember thus had three values, or coordinates, corresponding to their location in the three-dimensional feature space. The endmembers for the different study dates were not strictly comparable due to the fact that each dataset had undergone a different coordinate transformation during the PCA process. However, each set of endmembers was used for unmixing only those image bands from which they were selected, producing fraction images that were comparable across dates.

(b) Spectral data endmembers

Locating pure water pixels was relatively uncomplicated as water has a distinctively low reflectance in all Landsat bands, especially bands 4, 5 and 7. A training site from Lake Bhangazi was used to define the water endmember, with the *lowest* pixel values for each band being selected as endmembers (Figure 5.4). Choosing the lowest reflectance values ensured that only the purest water pixels were used to define the endmembers. The water endmember could also, in theory, be used to represent shade although the presence of shade was considered to be very small as forests and steeply sloping terrain had been excluded from the analysis.

Locating pure vegetation endmembers was more problematic, especially given the mosaic of vegetation types on the Eastern Shores. Although forested areas (woody vegetation) had been removed through the application of a forest exclusion mask, these excluded areas consisted only of pixels with a (largely) pure forest signature (as defined by the NDVI threshold value). Mixed pixels containing trees, shrubs or small forest patches still remained in the unmasked portion of the study area. This is evident from the scattergrams of the PCA (Figure 5.6), which indicate the presence of three basic features, namely water, woody vegetation and non-woody vegetation. To allow for this, a woody vegetation endmember was included as one of the vegetation endmembers. The same two sites used to define the NDVI thresholds for the forest mask were used for this purpose, although in this case only the *highest* NDVI values for each date were used. This ensured that woody vegetation endmembers were defined from the purest examples of forest pixels available for each study date. These pure forest pixels were then used to extract the corresponding pixel reflectance values for each of the spectral bands from the seven study dates.

Woody vegetation aside, the remaining vegetation in the study area consisted of non-woody vegetation found in grasslands and wetlands. Using known wetland pixels to define a non-woody vegetation endmember would have been problematic due to the high probability of water being present in these pixels. This would have resulted in an endmember with a mixed water/vegetation signal, thereby causing unreliable results in the linear mixture analysis. To rule out the possibility of water contaminating the endmember spectra, endmembers from a grassland site were used to represent all non-woody vegetation. In making this decision it was assumed that, given the relatively broad bandwidths of the Landsat TM bands, the spectral reflectance characteristics of the various types of non-woody vegetation (e.g. reeds, sedges, grasses) were similar, and that a grassland endmember was an adequate surrogate for a non-woody vegetation endmember. This assumption needs to be verified. The same grassland training site used for the supervised classification was used to define the non-woody endmembers. Frequency distribution histograms for the grassland training site were plotted for each date and the modal reflectance values for each spectral band were selected as endmember values. Choosing the modal value ensured that the most representative grassland pixels were used to define the endmember, avoiding contamination caused by the possible presence of other land cover types within the training sites. During a visit to the grassland training site undertaken in 2003 it was established that the area was indeed free of other land cover types although there was no way of verifying whether this was also true for the study dates in 1991, 2001 and 2002.

In defining the woody and non-woody vegetation endmembers for spectral mixture analysis, it should be noted that they represented two fundamental vegetation classes. The woody endmember represented forest while the non-woody endmember represented vegetation dominated by grasses (including reeds) and/or sedges. Taken together, these two endmembers defined an all-encompassing vegetation class for the study area, and would allow the mixing of water and vegetation to be examined.

The outcome of endmember selection was the identification of three endmembers representing the main land cover classes present in the unmasked portion of the study areas. For ease of reference, these endmembers were named Water, Woody and Non-

woody, although Table 5.5 shows how each of them represented varieties of classes with similar reflectance characteristics. The endmember values for both the spectral and component datasets were entered into Idrisi in preparation for the unmixing phase of the spectral mixture analysis.

Table 5.5: Details of the image endmembers used in the spectral mixture analysis.

Endmember	*Representing*
Water	Open water, shade
Woody	Plantations, dune forests, bush clumps and other dark green vegetation
Non-woody	Grassland and wetland vegetation

5.5.3.2 Linear spectral unmixing

Linear spectral unmixing was carried out with the UNMIX module in Idrisi and was performed on bands 2, 3, 4, and 5 of the spectral data and on the first three components of the component data. Using the values of the three endmember signatures, the spectral reflectance signal from each pixel was unmixed and the percentage cover of each of the endmember land cover classes was calculated. The output from the spectral unmixing was a series of fraction images, one for each endmember, which indicated the percentage cover of the endmember land cover class within each pixel. A residual image showing pixel residual values was created by summing the absolute values of each of the band residuals[6]. High residual values implied a poor fit between the modelled and actual pixel values.

5.6 ACCURACY ASSESSMENT

Assessing the accuracy of surface water mapping in the study area posed a major problem, due not only to the ephemeral nature of much of the surface water, but also to the fact that no ground truth measurements were available from the time the images had been recorded. Traditional methods of accuracy assessment were, therefore, not possible in this study as

6. Residuals calculated for each band are called *band residuals*. Band residuals represent the differences between the actual pixel values for each band and the modelled values determined by the spectral mixture analysis (see Appendix 6).

these rely primarily on ground truth measurements. This prompted the investigation of alternative methods of assessing the accuracy of the image classifications. To this end, daily rainfall records and water table depths from a number of stations in and around the study area were obtained and their suitability for verifying the accuracy of the image classifications was assessed.

In investigating the use of ground water table levels it was noted that there was a close link between groundwater and the amount of surface water in the study area (Figure 5.7). Depth to groundwater readings covering periods close to the study dates were obtained from a borehole located at the south-western edge of Lake Bhangazi (Borehole D1, 28°07'49"S; 32°31'37"E, 8.01m asl). This was the only borehole in the study area from which readings covering the entire study period were available. Water table heights calculated from these borehole readings are shown in Table 5.6.

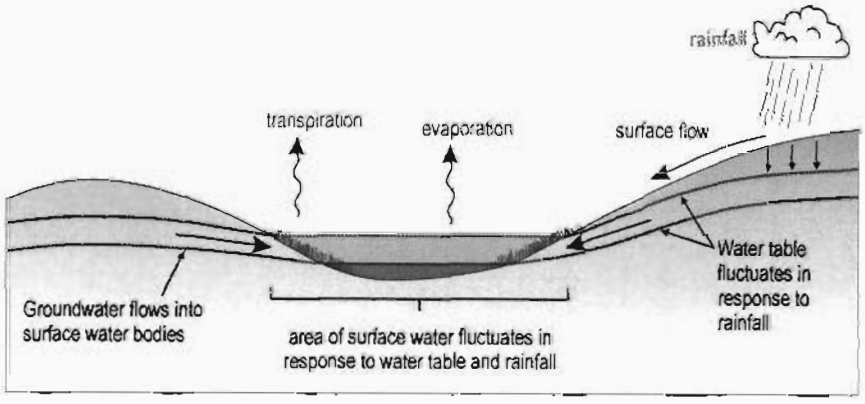

Figure 5.7: Conceptual model showing factors controlling surface water on the Eastern Shores.

From Table 5.6 it can be seen that borehole readings had been made at irregular intervals before and after the study dates. In some cases the gap between study date and borehole reading was two months, in others, three weeks. There was only one instance of a borehole reading coinciding with a study date. This situation made the use of borehole data as a verification tool extremely difficult as it was impossible to determine the influence of rain that fell between the study dates and the dates of the borehole readings. For this reason, the use of borehole data for accuracy assessment was not considered a viable option.

Table 5.6: Water table heights in metres above mean sea level for borehole D1. The nearest study dates are indicated with arrows while the figures in brackets show the number of days between each study date and the nearest water table measurement.

Date	*Water Table Height (m)*
1991/07/06	7.93
2001/01/05	7.98
2001/03/01	7.47
2001/07/20	7.69
2001/08/21	7.75
2001/10/01	7.72
2001/11/21	7.67
2001/12/14	8.03
2002/04/24	7.01
2002/05/29	6.83
2002/06/21	6.81
2002/08/26	6.89

Study Date
1991/07/23 (-17)
2001/03/20 (-19)
2001/05/07 (-67)
2002/04/24 (0)
2002/07/13 (-22)
2002/09/15 (-20)
2002/10/17 (-52)

The assumption behind using rainfall data for accuracy assessment is based on the nature of hydrological inputs and outputs on the Eastern Shores. For the study area as a whole, surface and subsurface hydrological inputs and outputs are limited as there are no rivers flowing into the area. Ground and surface water inputs occur entirely though the addition of rainfall, with virtually no groundwater recharge occurring from the nearby Lake St Lucia (Kelbe, 2005, pers. comm.). For individual water bodies on the Eastern Shores, inputs are also controlled by rainfall. This occurs either directly through rain falling onto the water bodies themselves, or indirectly via groundwater flow and surface run-off of rainfall (Figure 5.7). Losses occur only through evaporation and transpiration, with no loss of surface water into the groundwater (Ellery, 2006b, pers. comm.). Rainfall is therefore the main factor driving surface water levels on the Eastern Shores. Given this close relationship between water levels (the dependent variable) and rainfall (the independent variable), comparing the outputs of the spectral mixture analysis against rainfall measurements provides an important means of validating the accuracy of the water mapping. If, through regression analysis, it is found that mapped water extents fluctuate in tandem with variations in rainfall, this would serve to verify the accuracy of the spectral unmixing process.

Daily rainfall records covering the entire study period as well as the months preceding the study dates were obtained for the Cape St Lucia Lighthouse and Charters Creek recording stations. The Cape St Lucia station is located 12 km south of the study area while Charters Creek is situated on the Western Shores, 3 km to the west of the study area. Cumulative rainfall totals for various periods prior to the study dates were computed for both stations and correlated against the amounts of surface water obtained through the image classification. These comparisons of rainfall against surface water were used to assess the accuracy of the image classification. The borehole data was not used.

5.7 CONCLUSION

This chapter has shown how the theories and techniques of image processing have guided the methodologies applied in this study. The image preparation phase saw the application of geometric and radiometric correction processes, which allowed inter-comparison of the multitemporal images. This was a crucial step in this multidate study and ensured that all the images were accurately georegistered and calibrated to units of reflectance. The important image transformation stage saw the elimination of areas unsuitable for analysis as well as the reorganisation of the unmasked spectral data into uncorrelated principal components. Both these steps resulted in a reduction of the data but did so without any significant loss of information. The reduction of data had important implications for the subsequent classification and interpretation phases of this study. Three different types of image classification were performed on the datasets with particular attention being paid to spectral mixture analysis. This technique, which relied heavily on the accurate identification of endmembers, held the most promise for unravelling the complex mosaic of land cover types in the study area.

6. RESULTS

6.1 INTRODUCTION

The image processing framework around which this project has been structured defines a series of steps that guided the image manipulation process from the initial acquisition and preparation of satellite imagery through to the final assessment and interpretation of the classified images. The results obtained from each step were important as they were used to guide subsequent phases of the image processing, thereby ensuring that the objectives of the study were met. It was crucial, therefore, that the results were accurate and of high quality as they provided the foundation upon which the success of the whole image classification process rested. This chapter commences with a look at the results of the image preparation and transformation phases of the project, from the rectification of the raw images through to the masking of zones of the study area that were not of interest. This will be followed by a detailed presentation of the results from the image classification stage, with particular emphasis being placed on the results from the spectral mixture analysis. Based on the outcomes of the classification stage, the most suitable classification method will be selected and the accuracy of the results from this method will be assessed. Finally, by referring to the outputs from the chosen classification method, the temporal and spatial distribution of surface water in the study area will be described.

6.2 IMAGE PREPARATION

The main aim of the image preparation stage was to prepare a set of geometrically and radiometrically corrected images. This was a crucial first step in this multitemporal study as it allowed the accurate inter-comparison of images from different dates. This section describes the results of this process and highlights the levels of accuracy that were achieved in both the geometric rectification and the radiometric correction of the images from the seven study dates.

6.2.1 Image rectification

The image rectification process transformed the image data from a raw coordinate system based on row and column numbers to a geographic system using metres-based coordinates. This was achieved via a series of ground control points (GCP), which established links between identifiable features on the raw images and their true, real-world coordinates in geographic space (see Table 6.1). A comparison of the GCP coordinates from the unrectified reference image and the 1:50000 maps revealed a root-mean-square (RMS) error of 0.80 pixels or 24 metres, an acceptable figure bearing in mind the 30-metre pixel size of the unrectified images. Also calculated were residual values, which provided an indication of how much each control point deviated from the polynomial equation. Appendix 2 shows the complete transformation data for the reference image.

Table 6.1: Details of the ground control points used to rectify the 7 May 2001 reference image.

GCP Description	*Raw coordinates*		*Geographic coordinates*		*Residual*
	X	*Y*	*X*	*Y*	
N2 road bridge over the Mfolozi rover	2527	1677	-83532	-3149384	1.29
N2 road bridge over the Mkuze River	1558	4745	-97679	-3053799	0.03
Point on the southern shore of Lake Mgobezeleni	3608	5318	-34226	-3046586	0.16
Weir on the Mzinene River	2864	3902	-63004	-3084965	1.25
Kink in the old Lower Mkuze Road	2849	4670	-59840	-3062179	0.67
Junction of old Lower Mkuze Road and Kleinspan farm boundary	2768	4553	-62806	-3065225	0.50
Tip of southern breakwater of Richards Bay harbour	2587	347	-88087	-3189035	0.24
Intersection of the N2 and the southern access road to Mtubatuba	2559	1834	-81879	-3144832	1.00
Prominent bend in the Mtubatuba-Hluhluwe Road	2192	2246	-90764	-3130886	1.05
Centre of the Hluhluwe dam wall	2427	2914	-80643	-3112262	1.26
Road bridge over the Lake St Lucia narrows	3324	2134	-57778	-3139557	0.09
Intersection of Monzi and St Lucia roads	3029	2039	-66972	-3140966	0.23

All the RMS error values for the relative rectification of the target images were less than 0.5 pixels (15 metres) (Table 6.2). This was achieved by selecting only those GCPs that were well defined and easily identifiable on both the reference image and the relevant target image. This ensured that the spatial error, or offset, of each of the target images was no more than 15 metres relative to the reference image.

Table 6.2: Details of ground control points and RMS errors for the target images.

Date	*No. of GCPs used*	*RMS Error*
1991/07/23	19	0.49
2001/03/20	19	0.49
2002/04/24	21	0.48
2002/07/13	22	0.48
2002/09/15	21	0.46
2002/10/17	22	0.46

The final output from the image rectification process was a series of geographically rectified images, with each of the target images having spatial offsets of no more than 15 metres from the reference image. In addition, all the images were clipped to a 19.4 by 47.2 km region covering the Eastern Shores of Lake St Lucia (see Figure 5.2 on page 70). The size of this area was approximately 915 km^2.

6.2.2 Radiometric correction and image normalisation

The absolute atmospheric correction of the reference image attempted to remove the effects of atmospheric scattering and absorption. The frequency histograms in Figure 6.1 show how the pixel values of the uncorrected data (left) have been converted from digital numbers ranging from 0 to 255, to values of reflectance (right) ranging from 0% to 100%. The effects of atmospheric scattering can clearly be seen in the uncorrected data. Scattering manifests itself as an additive effect and results in an offset of all the data readings from zero. This offset was particularly noticeable at shorter wavelengths, i.e. bands 1, 2 and 3, where there were no readings close to zero, and decreased with increasing wavelength. From the histograms of the corrected data it can be seen that this additive effect of atmospheric scattering has been largely removed by the atmospheric correction.

Also noticeable in the histograms is the strongly bimodal distribution of bands 4 and 5, which both had pronounced peaks close to zero, and smaller, secondary peaks at higher reflectance values. The sharp peaks close to zero reflectance in these bands are due to the high absorbance of electromagnetic radiation by water in the near- and mid-infrared. The secondary peaks represent the reflectances of other surface materials like grasslands and forests. The fact that these secondary peaks are spread out over a wide reflectance range

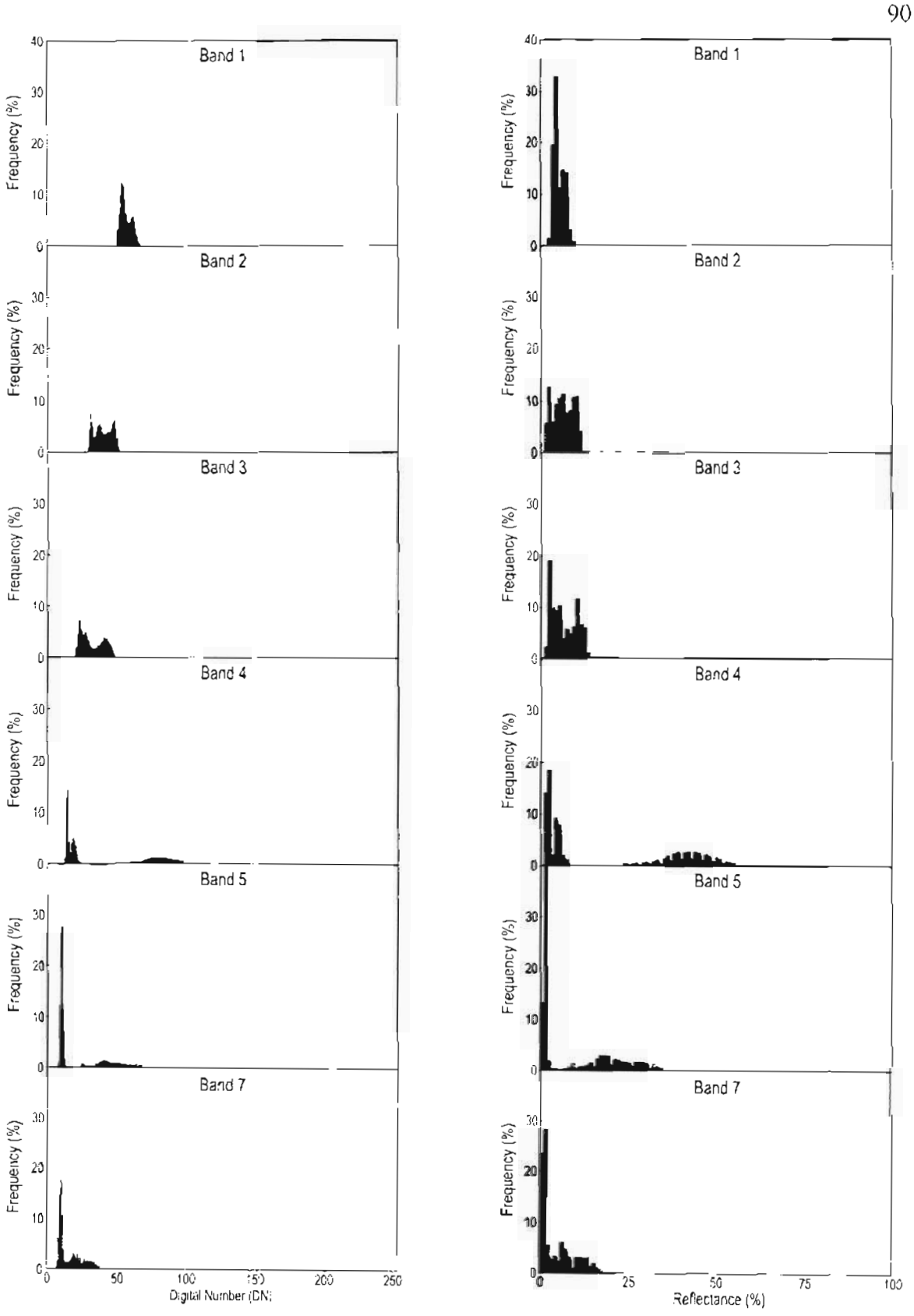

Figure 6.1: Frequency histograms for the uncorrected data (left) and the corrected data (right) for the bands of the reference image, 7 May 2001.

indicates variability of the reflectance characteristics of these features. This is in stark contrast to the much smaller reflectance range covered by the water peaks.

Relative normalisation of the target images relied on invariant dark and bright targets being located on both the reference image and the target images. A linear regression between the bright and dark targets from each image and the equivalent targets from the reference image produced very high R^2 values in all cases (Table 6.3). This suggested that the dark and bright targets were indeed invariant and were thus suitable for performing the relative normalisation of the target images. The high R^2 values could also be ascribed to the fact that only three values were used to generate each regression equation. However, when the number of targets was increased to six (three bright and three dark) the worst R^2 value was still as high as 0.968, confirming once again the invariant nature of the selected target areas.

Table 6.3: R^2 values obtained when regressing the mean pixel values from the bright and dark invariant targets of the target images against the mean target values from the reference image.

Date	*Band 1*	*Band 2*	*Band 3*	*Band 4*	*Band 5*	*Band 6*
1991/07/23	1.000	1.000	1.000	1.000	1.000	1.000
2001/03/20	1.000	1.000	0.999	0.999	0.998	0.999
2002/04/24	1.000	0.999	1.000	0.999	1.000	1.000
2002/07/13	1.000	1.000	1.000	1.000	1.000	1.000
2002/09/15	1.000	1.000	1.000	1.000	1.000	1.000
2002/10/17	1.000	1.000	1.000	1.000	1.000	1.000

Figure 6.2 illustrates the effects of normalisation on bands 3 and 4 of the 20 March 2001 study date. These two bands were normalised via application of the following two regression formulas:

```
band3_normalised = 0.392 * [band3] - 8.548
band4_normalised = 0.866 * [band4] - 7.817
```

From the left-hand scattergrams the additive effect of atmospheric scattering on the uncorrected data is noticeable as an offset from zero on the x-axis. This effect has been removed in the normalised data as shown in the right-hand scattergrams. Also noticeable from these scattergrams is the fairly linear relationship between pixel values from the target

image and the reference image. Deviations from this linear relationship were due to factors like seasonal changes in vegetation, fluctuations in the size of ephemeral water bodies, and the effect of wind on water surfaces. It is important to note that the inter-date linearity shown in these scattergrams was not affected by the normalisation techniques applied in this study. This is because the regression formulas are linear equations that scaled the target image bands without changing the inherently linear relationship that existed between these bands and the reference image bands. This was confirmed by correlation coefficients

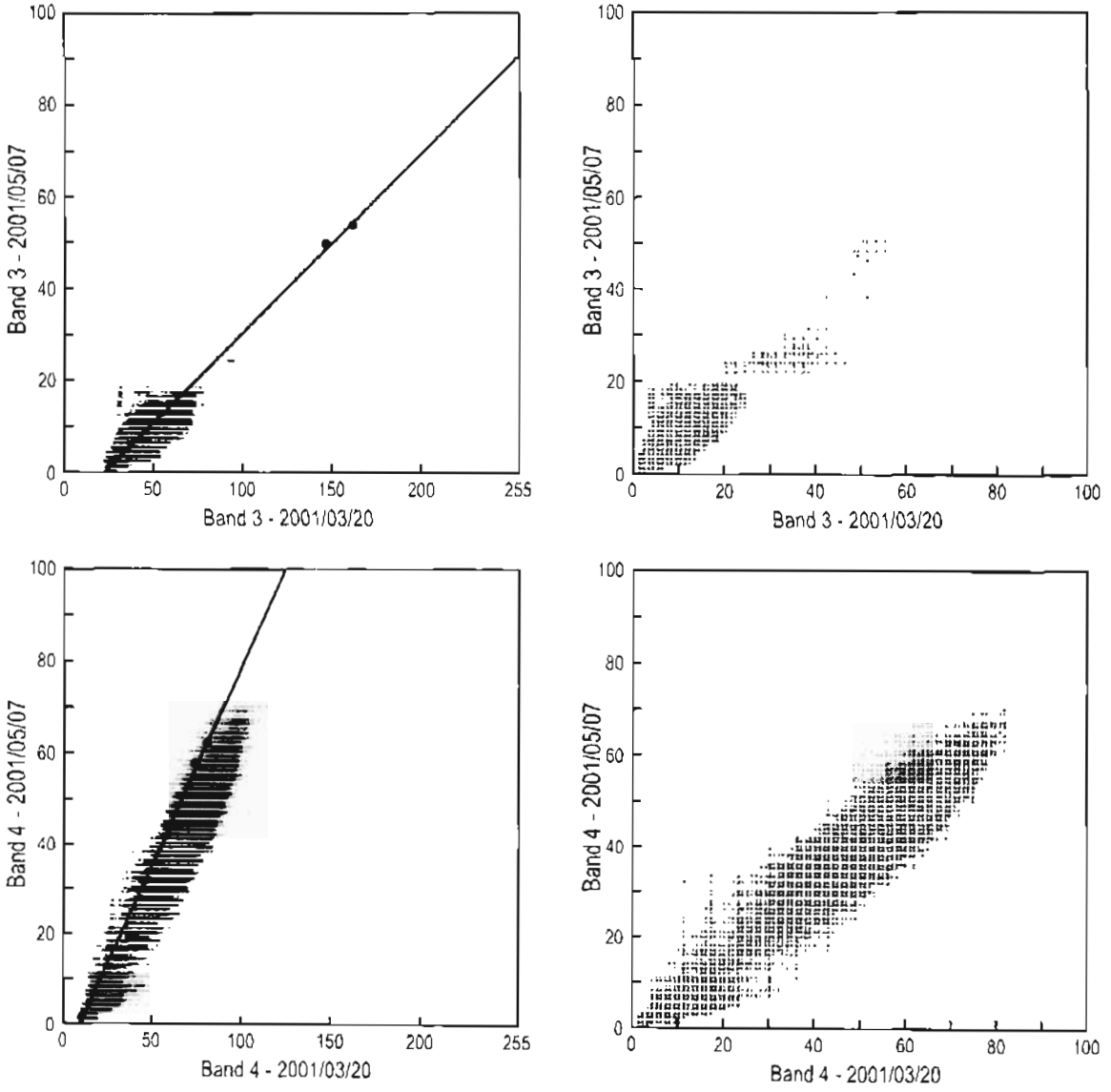

Figure 6.2: Scattergrams showing the results of relative radiometric normalisation on bands 3 (top) and 4 (bottom) of the 3 March 2001 study date. The scattergrams on the left show the unnormalised data while the normalised data are depicted in the scattergrams on the right. The invariant targets are shown with red dots and the regression lines are shown in blue.

calculated both before and after normalisation (0.855 for band 3, 0.982 for band 4), which are identical to within four decimal places. The slight differences in correlation before and after normalisation are due to rounding-off errors during application of the normalisation equations. Also shown on the left-hand scattergrams are the bright and dark targets (red dots) as well as the lines defined by the normalisation formulas.

6.3 IMAGE TRANSFORMATION

Images in this study were transformed in two ways: a principal components analysis (PCA) was used to reduce data redundancy while exclusion masks were used to exclude areas that would not be classified during image classification.

6.3.1 Principal Components Analysis

Performing a Principal Components Analysis on the spectral data from each study date produced a set of uncorrelated images, or components. This can be seen in Table 6.4, which shows correlation matrices for the October 2002 study date. From the correlation matrix of the untransformed spectral data it can be seen that a high degree of correlation existed between many of the bands (e.g. 0.998 between bands 5 and 7). Examination of the correlation matrix for the transformed dataset shows how the PCA effectively decorrelated the spectral data, with almost all the inter-component correlation coefficients being close to zero. This was true for all the study dates as can be seen from the correlation matrices shown in Appendix 3.

Further insight into the effects of the Principal Components Analysis can be gained by examining the eigenvalues for each component. The eigenvalue associated with each component indicates the amount of variance explained by that component. An examination of these values shows that the first three components explain most of the variance in the data and can be classed as primary components as they summarise virtually all the information in the dataset (Tables 6.5 and 6.6). By contrast, the secondary components (components 4, 5 and 6) account for less than 1% of the variance in the datasets and represent mostly noise introduced by the satellite sensors during measurement. For this reason only the primary components were used for the remainder of this study.

Table 6.4: Correlation matrices for 17 October 2002 for (a) the untransformed spectral data and (b) the transformed PCA data. Highest correlation coefficients are shown in red and the lowest in blue.

(a)	*Band 1*	*Band 2*	*Band 3*	*Band 4*	*Band 5*	*Band 7*
Band 1	**1.000**					
Band 2	0.768	**1.000**				
Band 3	0.703	0.954	**1.000**			
Band 4	-0.359	0.194	0.186	**1.000**		
Band 5	-0.164	0.272	0.329	0.799	**1.000**	
Band 7	-0.168	0.269	0.326	0.801	0.998	**1.000**

(b)	*Comp 1*	*Comp 2*	*Comp 3*	*Comp 4*	*Comp 5*	*Comp 6*
Comp 1	**1.000**					
Comp 2	-0.001	**1.000**				
Comp 3	0.001	0.003	**1.000**			
Comp 4	0.013	0.009	0.044	**1.000**		
Comp 5	0.000	0.065	-0.018	0.493	**1.000**	
Comp 6	0.101	-0.027	0.018	-0.002	-0.026	**1.000**

Table 6.5: Eigenvalues for each of the PCA components. The primary components are shown in blue, the secondary components in red.

Date	*Comp 1*	*Comp 2*	*Comp 3*	*Comp 4*	*Comp 5*	*Comp 6*
1991/07/23	510.22	73.79	35.94	3.68	1.19	0.66
2001/03/20	787.28	107.13	64.41	2.71	2.37	0.70
2001/05/07	540.62	74.55	43.95	2.08	1.93	0.76
2002/04/24	674.41	87.48	40.32	2.84	2.44	0.48
2002/07/13	541.77	68.05	22.16	2.45	1.22	0.85
2002/09/15	642.76	97.09	49.20	3.07	2.57	0.45
2002/10/17	920.76	103.21	54.35	1.79	0.85	0.71

6.3.2 Exclusion Masks

A number of areas were excluded from further processing through application of a series of exclusion masks (Figure 6.3). The first of these was the study area mask, which resulted in the exclusion of all areas outside of the Eastern Shores study area. This left an area of

250 km^2 on which subsequent processing could be performed. The forest, slope and sand mask were used to mask out areas within this 250 km^2 zone that would also be excluded from subsequent processing. The sizes of these three areas are shown in Table 6.7.

Table 6.6: Percentage of variance explained by each of the PCA components. The primary components are shown in blue, the secondary components in red.

Date	*Comp 1*	*Comp 2*	*Comp 3*	*Comp 4*	*Comp 5*	*Comp 6*
1991/07/23	81.6	11.8	5.8	0.6	0.2	0.1
2001/03/20	81.6	11.1	6.7	0.3	0.3	0.1
2001/05/07	81.4	11.2	6.6	0.3	0.3	0.1
2002/04/24	83.5	10.8	5.0	0.4	0.3	0.1
2002/07/13	85.1	10.7	3.5	0.4	0.2	0.1
2002/09/15	80.8	12.2	6.2	0.4	0.3	0.1
2002/10/17	85.1	9.5	5.0	0.2	0.1	0.1

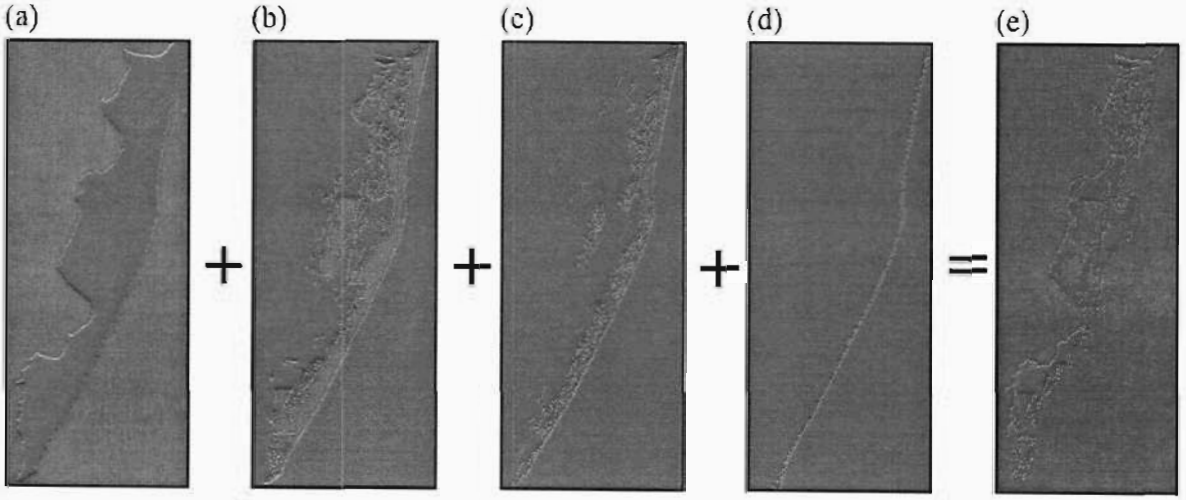

Figure 6.3: Construction of an exclusion mask showing, in red, areas excluded by (a) the study area mask, (b) the forest mask, (c) the slope mask, (d) the sand mask, and (e) the final exclusion mask. Only areas shown in green in the final exclusion mask were used for image classification.

The forest, slope and sand masks were not mutually exclusive, as many areas classed as steep slopes also fell within the forest or sand masks. This is readily apparent in Figures 6.3b and 6.3c where many afforested areas and steep slopes can be seen to coincide. The four exclusion masks were combined into a final exclusion mask that was applied to both the spectral and component datasets. After application of the exclusion

mask a total of 114165 pixels, representing an area of almost 103 km^2, remained for use in the image classification stage of the study.

Table 6.7: Sizes of areas in the Eastern Shores study area excluded by the forest, slope and sand masks.

Mask	*Pixels*	*Area (km^2)*
Forest	152428	137.2
Slope	83900	75.5
Sand	15191	13.

6.4 IMAGE CLASSIFICATION

The unsupervised cluster analysis, supervised maximum likelihood classifier and spectral mixture analysis produced a series of classified images, the interpretation and appraisal of which allowed the most accurate method of mapping surface water to be selected.

6.4.1 Cluster analysis

The unsupervised cluster analysis produced 15 clusters for each study date for both the spectral and component datasets (see Appendix 4). The first cluster in all cases represented the masked area, leaving 14 clusters to be classified into water, wetland and grassland categories. However, many of these clusters were found to comprise both wetland and grassland, and were therefore assigned to a grassland/wetland class.

Lake Bhangazi, the largest water body in the study area, was used to identify clusters representing open water. For each of the study dates, it was found that the cluster classification had grouped the waters of Lake Bhangazi into one or two clusters (Table 6.8). These water clusters were combined into a single water class, the areas of which are shown in Table 6.8.

Table 6.8: Details of the clusters found to represent open water.

	Component Data		*Spectral Data*	
Date	*Clusters*	*Size (Ha)*	*Clusters*	*Size (Ha)*
1991/07/23	9	300	10	297
2001/03/20	7, 12	292	8, 11	287
2001/05/07	9	312	9, 13	304
2002/04/24	7, 11	297	7, 8	285
2002/07/13	9	284	8, 10	274
2002/09/15	10	481	11	289
2002/10/17	12, 15	311	10, 12	304

As expected, Lake Bhangazi accounted for virtually all the open water in the study area. An exception to this appeared in the cluster classification of the component dataset from September 2002. This is shown in Figure 6.4 where a large increase in the area of water is recorded on this date, an increase not reflected in the spectral dataset.

This apparent increase in the amount of surface water appeared to be related to a large fire scar to the north of Lake Bhangazi (Figure 6.5). It can clearly be seen from Figure 6.5c how parts of the burnt area have been assigned to the water class. This could either have been due to water becoming visible through the removal of covering vegetation by the fire, or because the spectral characteristics of the burnt area in the component dataset were very similar to those of water. The former explanation seems unlikely as the spectral

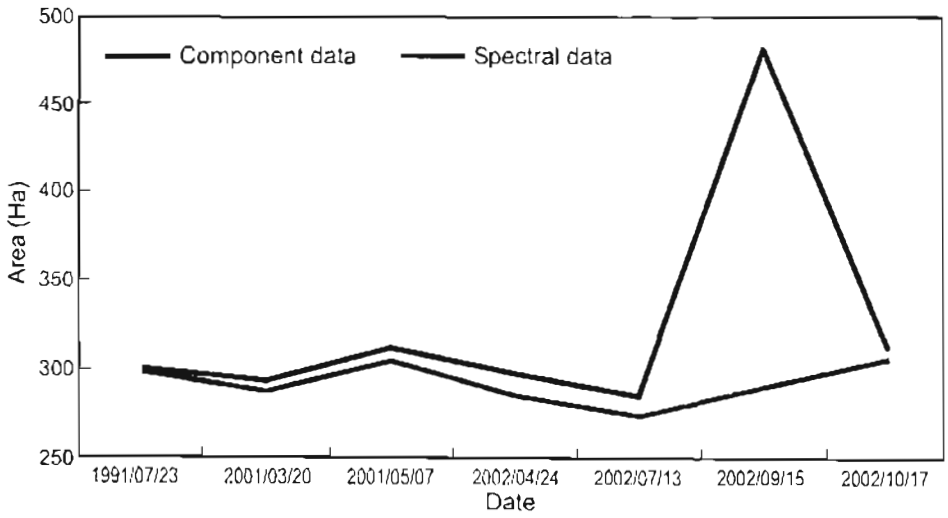

Figure 6.4: Results from the cluster classification showing the size of the area covered by open water.

characteristics of water are quite distinctive and if water was actually present in the burnt areas, it would also have been detected in the cluster analysis of the spectral dataset. The effects of fire scars are discussed in more detail in Section 6.5.2.

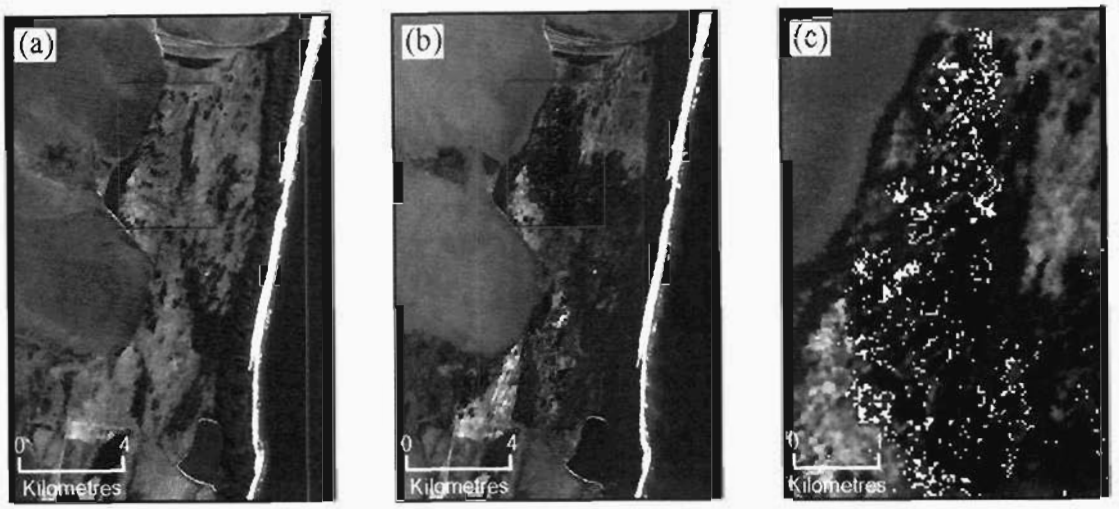

Figure 6.5: Colour composite images of the area north of Lake Bhangazi showing (a) the 13 July 2002 image without a fire scar, (b) the fire scar visible on the 15 September 2002 image, and (c) the areas of the fire scar within the red outline that were mapped as open water by the cluster classification of the component data.

The allocation of clusters to the grassland and wetland classes was guided by ground truth measurements made during field visits to the study area. In many cases it was found that the same clusters were present in both grassland and wetland areas. This confusion, which was present in both the spectral and component datasets, appeared to be due to the spectral similarity of wetland and grassland vegetation in dry periods. The three study dates in 1991 and 2001 fell within periods of higher rainfall and appeared to have much more distinctive spectral signatures for wetland and grassland classes. This is shown in Table 6.9, where it can be seen from the overlapping clusters that there was much less confusion between grassland and wetland classes in both the component and spectral datasets for these dates. It is also readily apparent from Table 6.9 that wetland environments were a lot more complex than grassland environments, with up to six different clusters being represented in the wetland ground truth areas. Grasslands tended to have a more homogeneous structure, being represented by only three clusters in most cases.

Table 6.9: Details of cluster allocations determined through ground truthing for (a) the component dataset and (b) the spectral dataset. Clusters present in both wetland and grassland areas are noted in red.

(a) Component Dataset

Date	*Wetland Clusters*	*Grassland Clusters*	*Overlapping Clusters*
1991/07/23	5, 6, 8, 11, 12	2, 3, 4	None
2001/03/20	2, 5, 6, 8, 15	3, 4, 5	5
2001/05/07	4, 6, 8, 10, 12, 13	2, 3, 5, 7	None
2002/04/24	2, 4, 8, 9	2, 3, 8	2, 8
2002/07/13	2, 3, 4, 5, 8, 14	2, 3, 5, 6, 7	2, 3, 5
2002/09/15	4, 5, 6, 8, 11, 14	3, 4, 14	4, 14
2002/10/17	2, 5, 8, 11	2, 4, 6, 8	2, 8

(b) Spectral Dataset

Date	*Wetland Clusters*	*Grassland Clusters*	*Overlapping Clusters*
1991/07/23	5, 6, 7, 11, 14, 15	2, 3, 9	None
2001/03/20	4, 7, 9, 14	2, 3	None
2001/05/07	2, 4, 7, 8, 10, 15	2, 3, 6	2
2002/04/24	2, 4, 5, 9, 14, 15	2, 3, 4	2, 4
2002/07/13	2, 4, 7, 13	2, 3, 4	2, 4
2002/09/15	3, 4, 7, 10	2, 4, 7	4, 7
2002/10/17	3, 6, 7, 15	2, 3, 4	3

While it is possible that the different clusters produced by the cluster classification represented various ratios of water and vegetation, interpreting and classifying these clusters into meaningful classes proved extremely difficult. Even a simple classification into three classes yielded large areas for which it was not possible to make an allocation. Given the confusion caused by the large numbers of overlapping clusters, it was not possible to adequately map surface water in the study area using cluster analysis.

6.4.2 Maximum likelihood classification

The maximum likelihood classification resulted in the assignment of pixels to three classes, namely water, grassland and wetland. Although the maximum likelihood classifier is a hard classifier, it bases the classification of pixels on a probability function, with pixels

being assigned to the class to which their probability of membership is the greatest. In performing this classification, those pixels which had a low probability of belonging to any of the classes were left unclassified. As shown in Table 6.10, the number of unclassified pixels ranged from 34% in July 2002 to 77% in September 2002. That so many pixels were left unclassified could have been due to a number of factors. Firstly, the training sites might have been poorly chosen and, hence, did not adequately represent the intended land cover classes. Secondly, the water, wetlands and grasslands in the study area are possibly a lot more complex than could be captured with just three types of training site. This landscape complexity was also reflected in the results of the cluster and mixture analyses discussed elsewhere in this chapter. In addition, the fact that the numbers of unclassified pixels varied so greatly from date to date suggests the presence of seasonal and other effects (e.g. fire) on the Eastern Shores landscape.

Table 6.10: Percentage pixels left unclassified by the maximum likelihood classifier.

Date	*Component Data*	*Spectral Data*
1991/07/23	55	55
2001/03/20	73	70
2001/05/07	59	57
2002/04/24	51	49
2002/07/13	37	34
2002/09/15	77	75
2002/10/17	58	61

As with the unsupervised cluster classification, virtually all the pixels classified as water were found in Lake Bhangazi (See Appendix 5). These water areas ranged from a maximum of 290 ha in July 1991 to a minimum of 227 ha in October 2002, with the lower value being 78% of the size of the larger area (Figure 6.6). While these values are similar to the values obtained by the unsupervised cluster analysis, they tend to be slightly lower for each of the study dates. When compared to the wetland and grassland classes, the range in size of the open water class is rather small, with the smallest grassland and wetland sizes being only 18% and 20% respectively of their largest areas. Once again, this could be due to the training sites not adequately capturing the heterogeneity and/or seasonality of the landscape. Of particular interest in both Figures 6.6(a) and 6.6(b) is that the variation in the

sizes of the wetland and grassland classes appears to be negatively correlated with the number of unclassified pixels. This is borne out by regression analysis, which shows a correlation of -0.995 between the number of unclassified pixels and the combined totals of the wetland and grassland classes. Given that the sizes of the water classes are very similar to those obtained by the cluster classification, it would appear that most of the unclassified pixels are either grassland or wetland pixels and not water.

A cross-tabulation of the spectral data classification against that of the component data provides an indication of how closely the classifications of the spectral and component datasets match. Table 6.11 shows how in July 1991, pixels classified as water, grassland or wetland using the component data were either given the same classification using the spectral data or were left unclassified. This contrasts with the cross-tabulation of the July 2002 data where it can be seen that some degree of confusion exists between wetland and grassland classes. The figures highlighted in bold in Table 6.11(b) show pixels that,

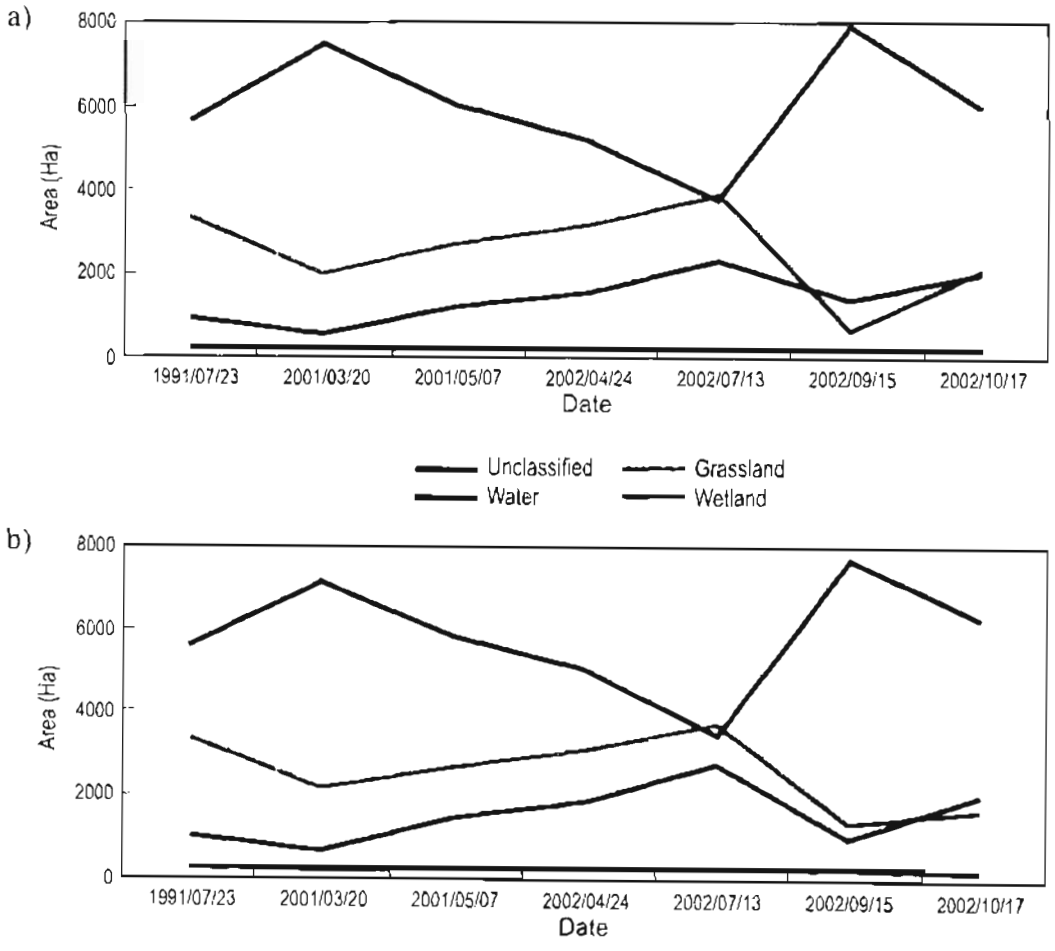

Figure 6.6: Results of the maximum likelihood classification for (a) the component data and (b) the spectral data. Areas for each land cover class are shown in hectares.

when classified as being either grassland or wetland using the spectral data, were classified as wetland or grassland respectively using the component dataset. This 'cross-classification' of grassland and wetland occurred in all four of the 2002 study dates but not at all in 1991 and 2001. Water pixels, by contrast, when classed as water using one of the datasets, were always given the same classification using the other dataset, or where left unclassified. This was true for each of the study dates.

Table 6.11: Cross tabulation of maximum likelihood classification results of the component data against the spectral data for (a) July 1991 and (b) July 2002.

(a)

Spectral Data \ *Component Data*	*Unclassified*	*Water*	*Grassland*	*Wetland*
Unclassified	58304	65	2585	1323
Water	30	3152	0	0
Grassland	2364	0	35033	0
Wetland	1999	0	0	9310

(b)

Spectral Data \ *Component Data*	*Unclassified*	*Water*	*Grassland*	*Wetland*
Unclassified	33725	174	2713	2303
Water	28	2794	0	0
Grassland	2974	0	37674	**1194**
Wetland	5347	0	**2892**	22347

The large numbers of unclassified pixels and the cross-classifications that occurred between grassland and wetland pixels from the two different datasets, made it difficult to interpret the results with any degree of confidence. The fact that so many pixels had been left unclassified made it impossible to map seasonal and spatial variations in water and wetlands with any certainty.

6.4.3 Spectral mixture analysis

The endmember spectra for the spectral data exhibit clear differences (Figure 6.7). Values for the water endmember are low for all bands, barely exceeding 4% reflectance in band 3. The woody vegetation endmember is also low in the visible bands but shows a pronounced peak in the near-infrared before decreasing in the mid-infrared bands. The non-woody

vegetation endmember has higher values than both the water and woody endmembers in the visible bands. Like the woody endmember, it also peaks in the near-infrared but maintains these high values in band 5 before dropping somewhat in band 7. The bars in Figure 6.7 indicate the range of endmember values across the seven study dates. These ranges are low in all three visible bands but are much higher for the woody and non-woody vegetation spectra in the infrared bands. The fact that the three endmembers show such clear differences greatly improves the likelihood of a successful mixture analysis. Spectrally similar endmembers would have led to confusion in the unmixing process, thereby compromising the accuracy of the results.

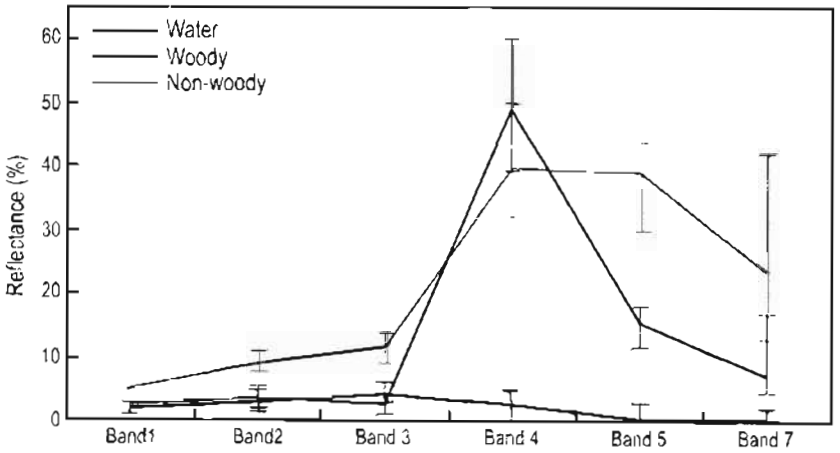

Figure 6.7: Average endmember spectra for the spectral dataset. These spectra are averages of the endmembers of the seven study dates. The bars indicate the maximum and minimum endmember values for each band.

The endmembers of the spectral dataset were all measured in terms of reflectance and could be compared against one another. This was not the case for the component data endmembers as these were selected from datasets that had each undergone a different transformation during the PCA process (Table 6.12). This made it difficult to assess these endmembers for similarities.

Table 6.12: Endmember values for the component dataset.

Date	*Endmember*	*comp 1*	*comp 2*	*comp 3*
1991/07/23	Water	0	32	26
	Non-woody	73	62	2
	Woody	62	8	41
2001/03/20	Water	0	14	92
	Non-woody	79	54	130
	Woody	81	11	80
2001/05/07	Water	0	14	98
	Non-woody	70	51	129
	Woody	66	8	86
2002/04/24	Water	0	30	52
	Non-woody	83	63	35
	Woody	76	16	64
2002/07/13	Water	0	30	14
	Non-woody	80	66	0
	Woody	63	15	20
2002/09/15	Water	0	32	11
	Non-woody	101	89	19
	Woody	64	16	0
2002/10/17	Water	1	54	12
	Non-woody	111	15	6
	Woody	84	78	28

The spectral mixture analysis resulted in three fraction images and one residual image for each study date (see Appendix 6 for an explanation of residual image calculation). The fraction images show the modelled amounts of water, woody vegetation and non-woody vegetation for each image while the residual images provide an indication of how well these modelled amounts match the actual pixel values measured by the satellite. High residual values indicate poor agreement between the modelled and actual values and are likely to occur when materials other than water or vegetation (e.g. sand, buildings) are present. An examination of the frequency distribution histograms of the residual images (Figure 6.8) showed that most of the residual values tended to cluster in the 0 to 15 range, with frequencies decreasing sharply towards higher values. Poorly modelled pixels were eliminated from further processing by excluding the 5% of pixels that had the highest residual values. In doing so it was assumed that these poorly modelled pixels contained features such as bare sand or buildings that contributed to the poor agreement between the modelled and actual values. The mixture modelling of the remaining 95% of the pixels was

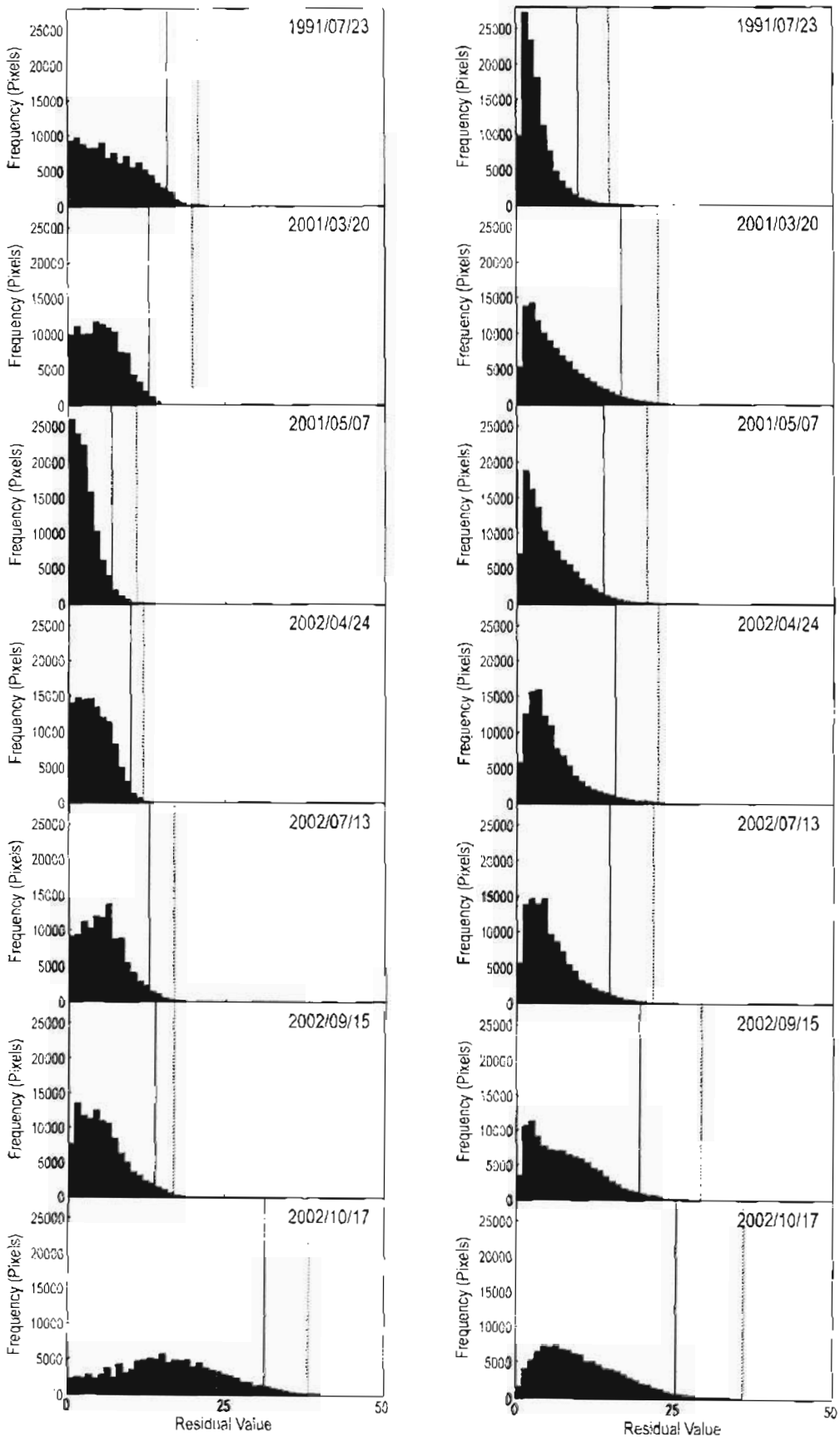

Figure 6.8: Frequency histograms of the residual images for the component data (left) and spectral data (right). The 95% thresholds are indicated with solid red lines while the 99% thresholds are indicated with dashed red lines.

therefore deemed accurate enough for this study. The significance of the 95% threshold value can be interpreted by way of an example:

> *The 95% threshold value for the residual image of the July 1991 spectral dataset was 16. As four bands had been used in the mixture analysis, this meant that for 95% of the pixels the residual averaged out at a reflectance value of 4% or less per band. In reality, though, the band residuals in most cases were much less than this.*

Excluding 5% of the pixels reduced the size of the area being evaluated by 5 km^2. For purposes of comparison, Figure 6.8 shows both the 95% (solid red lines) and 99% thresholds (dashed red lines).

In order to facilitate interpretation of the water fraction images, values were grouped into ten different classes as shown in Table 6.13. These classes represent a continuum of increasing water / decreasing vegetation, with class 1 (0 to 10%) representing areas with only vegetation and class 10 (91 to 100%) areas of pure water. Although class 1 represents amounts of up to 10% water, it is thought that much of this value was actually shade, which, while small, was not negligible at this end of the continuum. Shade occurs in nature as a result of shadows cast by leaves, grass, trees and topography. As forests and steep slopes had already been excluded from the study area, any small amounts of shade remaining in the reflected signal would be due to shadowing by grass. This small amount of shade becomes increasingly irrelevant in higher classes where the water signal dominates.

Table 6.13: Class ranges for the water fraction images.

Class	*Range*	
1	0 to 10%	No water
2	11 to 20%	
3	21 to 30%	
4	31 to 40%	
5	41 to 50%	
6	51 to 60%	
7	61 to 70%	
8	71 to 80%	
9	81 to 90%	
10	91 to 100%	Only water

The results of the spectral mixtures analysis are presented in Figures 6.9 and 6.10. These figures show the fraction of water present in each pixel according to the classes laid out in Table 6.13 (excluding the 5% of pixels with high residual values). The most noticeable feature on all of these figures is Lake Bhangazi, which was mapped as class 10 for all the study dates. This is not surprising given the unique spectral characteristics of pure water. The large Mfabeni swamp to the south of Lake Bhangazi is well picked out on the images

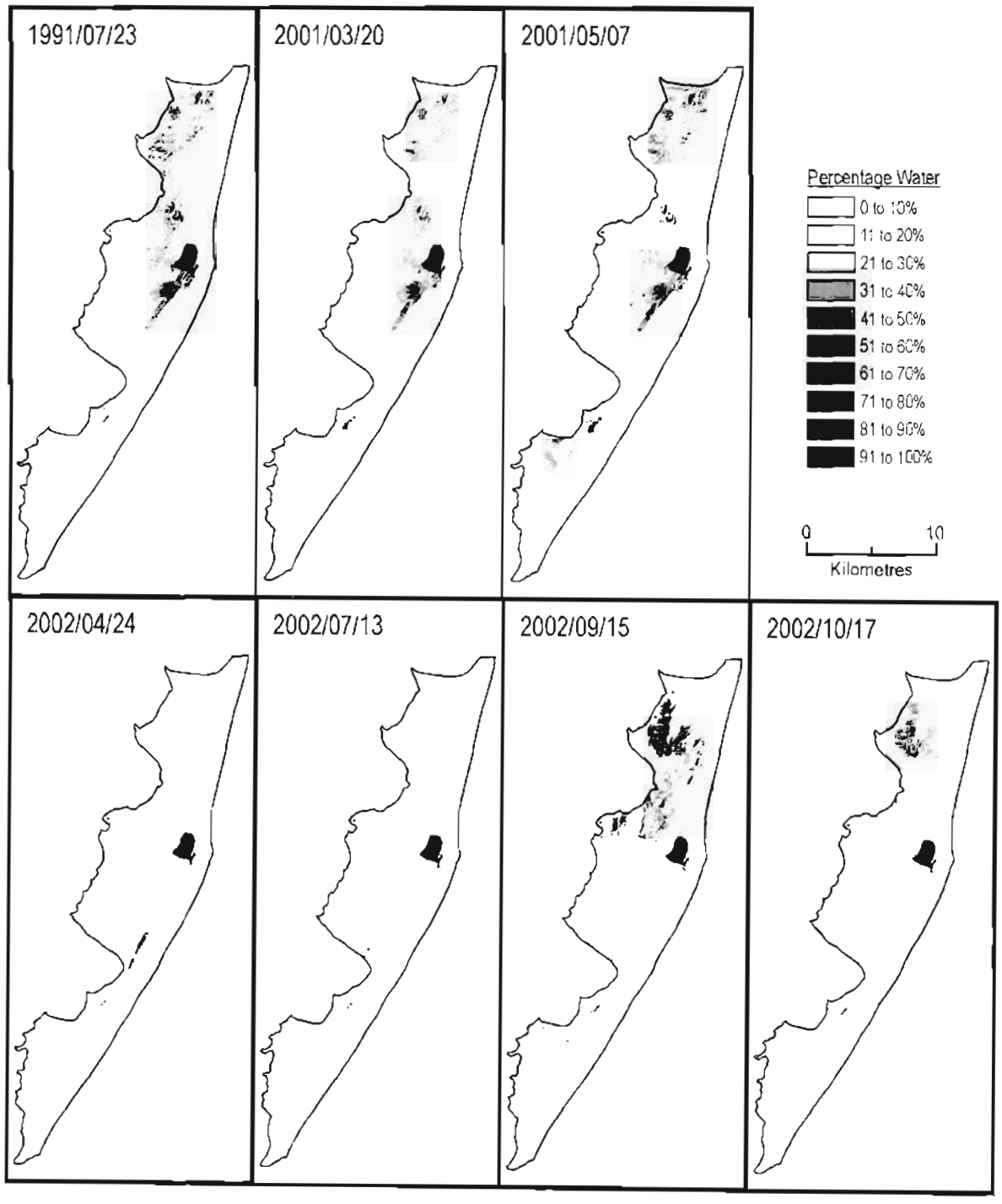

Figure 6.9: Water fraction images for the spectral data.

from 1991 and 2001 but is much less noticeable in the 2002 images. This is most likely due to the lower rainfall in 2002 resulting in lower surface water levels. Another feature clearly evident in Figure 6.10 (and also reflected in Figure 6.11a) is the widespread distribution of water classes 2, 3 and 4 in the fraction images produced with the component data. Water class 1 (0 to 10%) is very poorly represented in this dataset. This contrasts strongly with the results from the spectral data where class 1 dominated and classes 2, 3 and 4 were found

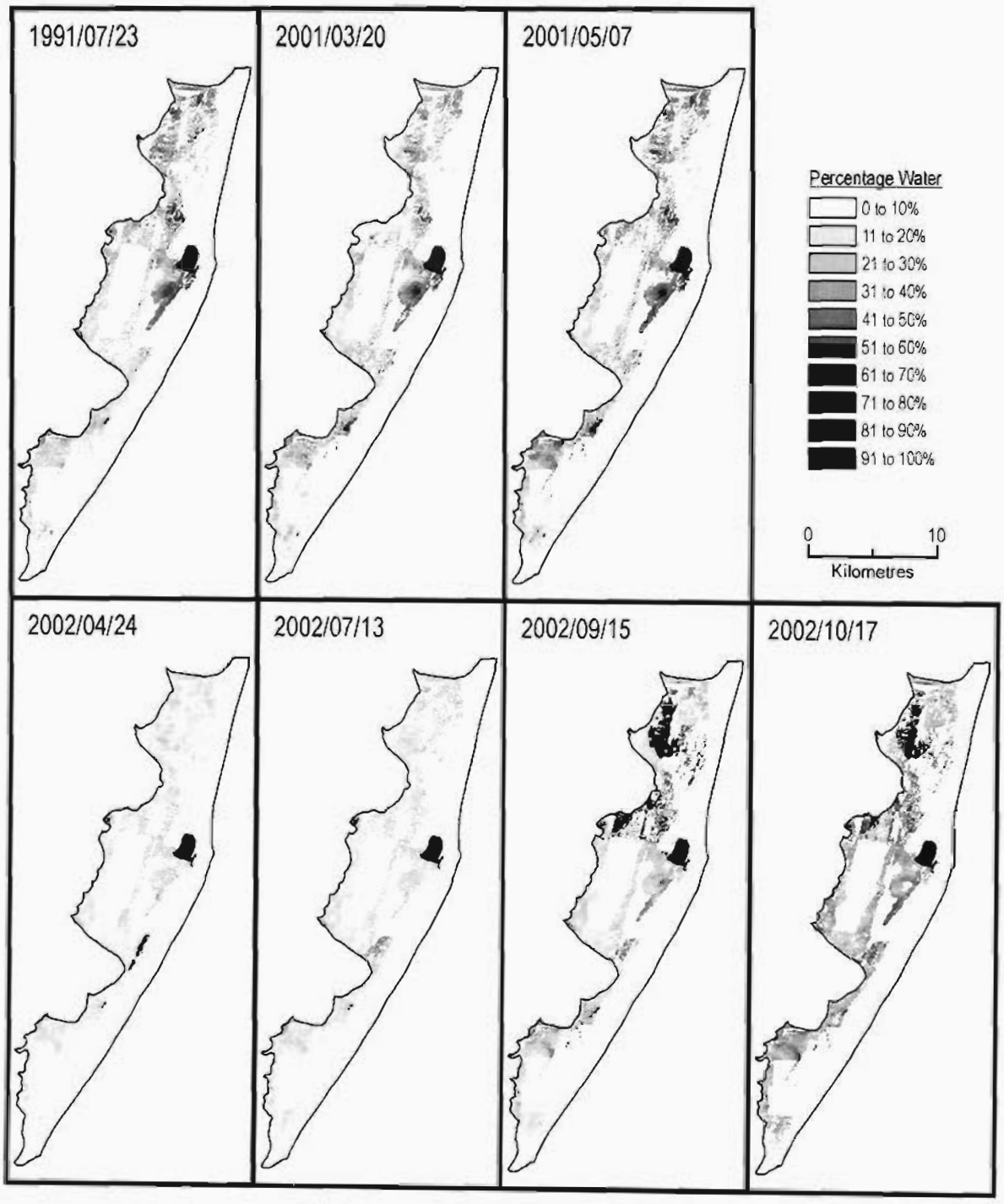

Figure 6.10: Water fraction images for the component data.

mostly in the northern part of the study area and around the Mfabeni swamp. This widespread presence of water in the 11 to 40% range as mapped by the component data was not verified by inspections conducted during field surveys, indicating a significant over-estimate of the amount of surface water in these classes. This could be due to the scattergram approach used to select endmembers for the component data or as a result of the principal components analysis used to prepare this dataset. Either way, the results from the component dataset appear to be unrealistic for classes 1 to 4.

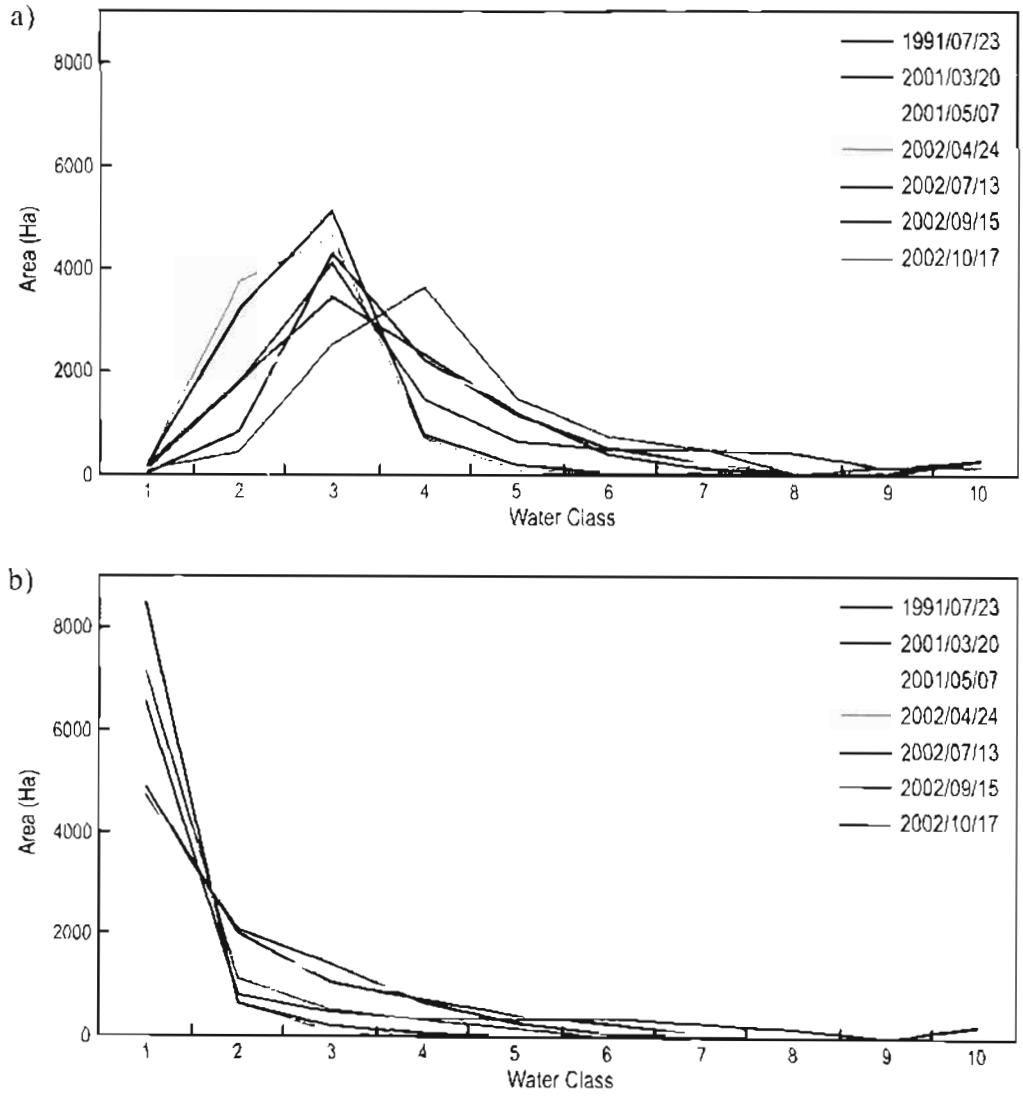

Figure 6.11: Results of the spectral mixture analysis for (a) the component data and (b) the spectral data. Areas for each of the 10 water classes are shown in hectares.

The two fire scars in the study area are reflected in the results as apparent increases in surface water. The April 2002 fire scar to the south of the Mfabeni shows up clearly in both datasets as an enhancement of classes 6, 7 and 8 (51 to 80%). For the other study dates this

region is classed as being 0 to 50% water for the spectral data and 11 to 60% water for the component data. The September 2002 fire scar also shows up in both datasets, this time as an enhancement to classes 7, 8 and 9 (61 to 90%). By October 2002 the effects of this fire scar were reduced but still visible, particularly in the component data. In the October spectral data, the amounts of surface water in the fire scar seem to be similar to those recorded in 1991 and 2001. This apparent increase in surface water in the fire scars will be discussed further in the Accuracy Assessment section of this chapter (Section 6.5.2 on page 114).

The areas represented by each of the water classes are presented in Figure 6.11, which shows large differences in the distribution of surface water obtained from the two datasets. The spectral data shows a clear maximum for class 1, implying that large parts of the study area were dry. Contrast this with the results from the component data in which class 3 is the most common class. This result from the component data is clearly unrealistic, particularly in the drier period of 2002 when very little surface water was visible in the study area. Figure 6.12 shows how the size of the 'no water' class is more realistic for the spectral data, ranging from 49% in the wetter years of 1991 and 2001, to 87% in 2002.

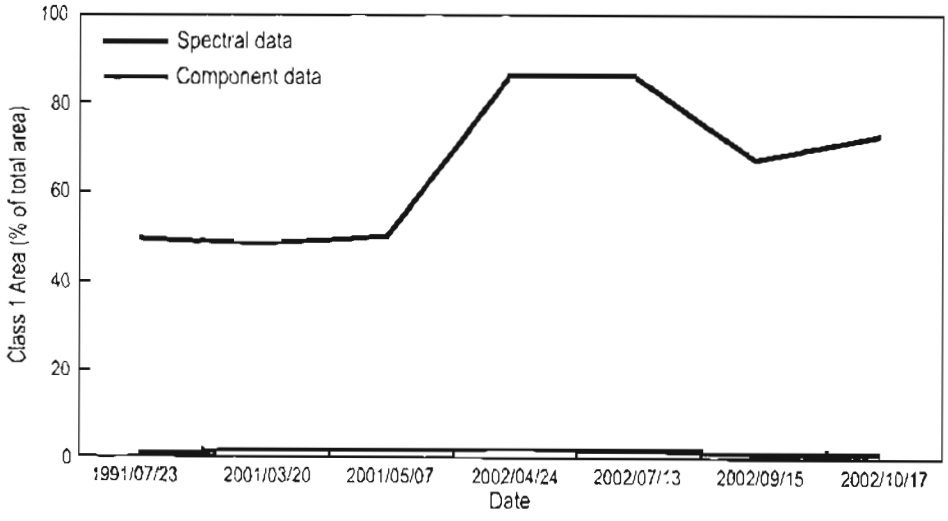

Figure 6.12: Area of class 1 (no water) relative to the size of the study area.

The reasons for the anomalous results in classes 1 to 4 for the component data are not fully understood and require further study. Using a scattergram approach to select endmembers could have been part of the problem. In the first place, the assumption that the vertices of the triangles in the scattergrams represented pure examples of water, woody and non-woody vegetation might have been incorrect. Secondly, the process of selecting the mixing

triangle vertices was clearly subjective and might not have been the most suitable means of determining endmember values. The selection of the endmembers was further complicated by the fact that the vertices were located in a three-dimensional feature space but were selected using two-dimensional scattergrams. The transfer of the vertices into the third dimension, represented by component 3, was a subjective process with potential for error.

6.4.4 Appraisal of image classification techniques

The results from both the cluster analysis and maximum likelihood classifications showed that these techniques were unsuited for mapping the fluctuations of surface water in the study area. Many of the clusters generated by the cluster analysis seemed to occur in both wetland and grassland areas, leading to uncertainty in their classification. This led to a large number of pixels being assigned to a wetland/grassland class which was extremely difficult to interpret. The maximum likelihood classification produced large numbers of unclassified pixels as well as cross-classifications between the results from the spectral and components datasets. This compromised the mapping of surface water, making it impossible to determine if there were any spatial and/or temporal trends in water distribution.

The results from the spectral mixture analysis were much more promising in that they produced maps indicating the actual percentage of water in each pixel. This allowed for a more intuitive interpretation of the results than was possible for the two hard classifiers. The outputs from the mixture analysis of the component dataset appeared to produce unrealistically low numbers of 'no water' pixels, casting some doubt on the accuracy of these results. On the other hand, the results from the spectral dataset appeared more realistic and matched observations made during field surveys.

Given the unrealistic results obtained with the component dataset, as well as the unsuitable outcomes of the unsupervised cluster analysis and the supervised maximum likelihood classification, it was decided to continue this study using only the results from the mixture analysis of the spectral data. The method of applying spectral mixture analysis to the spectral data using image derived endmembers produced the most realistic results, as will be shown in the next section of this chapter where the accuracy of the results is tested.

6.5 ACCURACY ASSESSMENT

Traditional methods of accuracy assessment require extensive use of ground truthing to verify the results of image classification. This was a problem in this study, where the intention was to measure bodies of water that in many cases were ephemeral. Given also the difficulty of accessing large wetlands, and the inaccessibility of the wilderness area to the north of Lake Bhangazi, it was decided to use rainfall as a surrogate to assess the accuracy of the image classification. The impacts of fire scars on classification accuracy also had to be investigated as these clearly had an affect on the overall results.

6.5.1 Assessment using cumulative rainfall

The first stage in the assessment process compared cumulative rainfall totals measured at Cape St Lucia and Charters Creek against the surface area of water in Lake Bhangazi. Lake Bhangazi was chosen for this initial assessment as it was well defined and the surrounding vegetation had not been affected by fire. The sum of water classes 9 and 10 was used to determine the area of the lake; class 10 because it was the pure water class and class 9 as it captured the mixture of water and reeds on the western, northern and eastern fringes of the lake. Cumulative rainfall totals, calculated in 30-day increments, were correlated against the area of the lake and are presented in Figure 6.13.

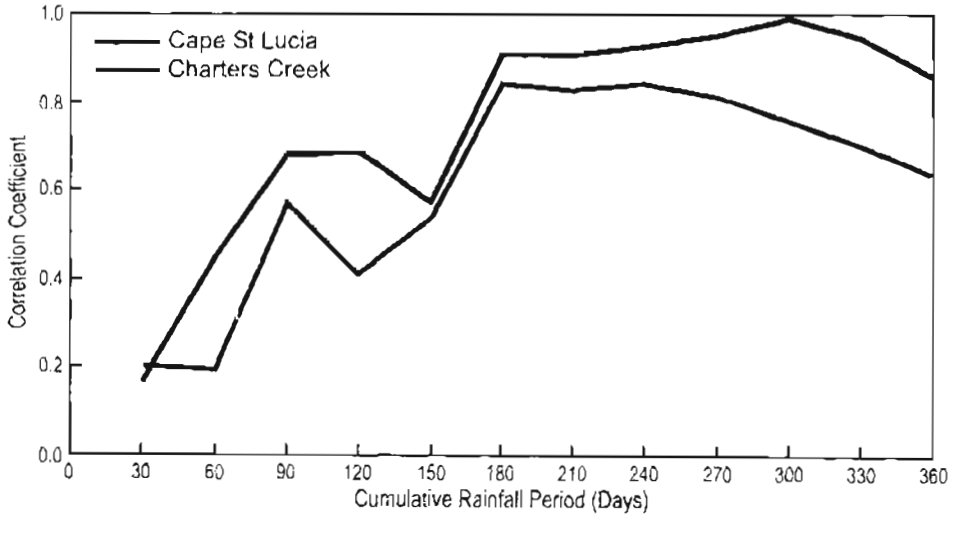

Figure 6.13: Correlation coefficients between the area of Lake Bhangazi and cumulative rainfall.

Correlation coefficients are initially low but increase steadily, eventually reaching values of 0.9 after six months (180 days). Thereafter values stay high and slowly tail off after eight to nine months. A secondary peak is also present at 90 days. The values for Cape St Lucia are higher throughout, indicating that rainfall figures measured at this coastal station are more representative of the study area than those figures measured further inland at Charters Creek. The correlation coefficients are always positive, reflecting a direct link between rainfall and surface water extent.

The high correlation between six-month rainfall and Lake Bhangazi indicates a strong relationship between cumulative rainfall and the area of the lake. That this also applies to other classes in the rest of the study area is demonstrated in Figure 6.14 which compares the sizes of classes 6, 7 and 8 against cumulative rainfall. This figure excludes data from September 2002 as these results were skewed by the presence of a large fire scar (see Section 6.5.2). Classes 1 to 5 were also not considered in this calculation as they were vegetation-dominated.

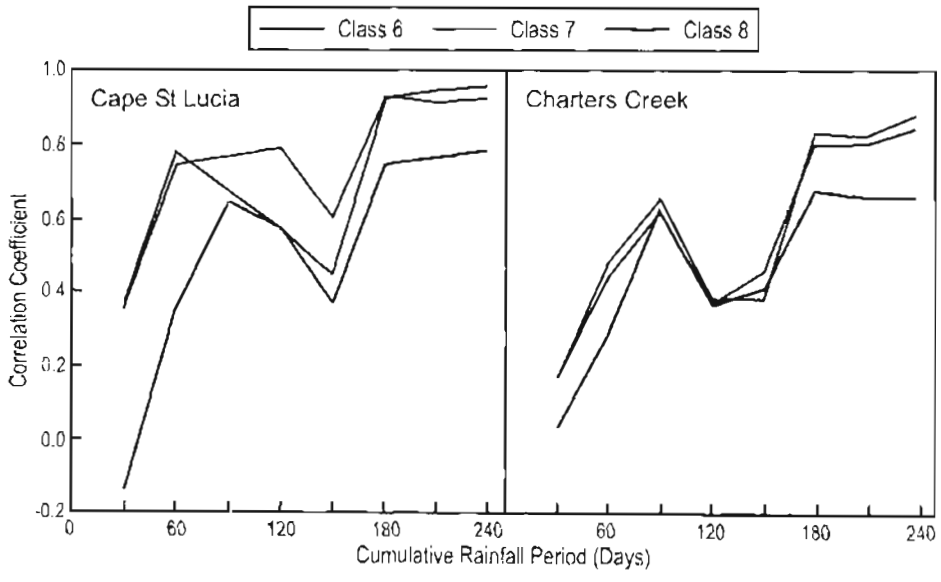

Figure 6.14: Correlation coefficients between cumulative rainfall and water classes 6, 7 and 8.

As with classes 9 and 10, peak correlations occur after six months, reaching 0.95 in some cases. Once again the values for Cape St Lucia are higher although the range of values for this station is much larger than for Charters Creek. The pronounced 90-day peak is again present in the Charters Creek data but shows up as a 60-day peak in the Cape St Lucia data.

Correlations for class 6 are generally lower than classes 7 and 8, an indication, perhaps, of the increasing influence of vegetation in this class.

The high correlation coefficients between the water classes and cumulative rainfall over periods exceeding six months indicate two important things. Firstly, by establishing that mapped water concentrations do indeed fluctuate in tandem with rainfall, they confirm that the application of spectral unmixing to bands 2 to 5 resulted in an accurate mapping of surface water. This is an important result as it allows the results of this mapping technique to be interpreted with confidence. Secondly, it is clear that the extent of surface water on the Eastern Shores has to be interpreted in the context of seasonal rainfall patterns, and not just short-term rainfall events. While short-term rainfall events would undoubtedly cause temporary increases in surface water, it is the cumulative rainfall over periods of six months and longer that are the determining factor in surface water extent.

6.5.2 The effects of fire on classification accuracy

The results of the spectral mixture analysis show the presence of surface water in two fire scars visible in the April and September 2002 images. This apparent increase in water in burnt areas could have been the result of previously hidden water being made visible by the removal of vegetation or else is due to spectral similarities between water and the fire scar. In order to determine whether there really was an increase in water in the fire scars it is quite revealing to examine thermal images of these areas. This is done in Figure 6.15, which shows panchromatic[7] images (ETM+ band 8) on the left, water classes 6 to 10 (all shown in blue) in the middle, and thermal images (ETM+ band 6) on the right. The yellow A symbols mark the positions of the fire scars while the B symbols show the locations of water bodies. In the panchromatic images both the water bodies and fire scars show up clearly as areas that are very dark, almost black. These areas coincide almost exactly with the mapping of water classes 6 to 10, suggesting the presence of surface water in these areas. Examination of the thermal images presents a different picture, however. In these images, which show hotter features in lighter shades and cooler features in darker shades, it can clearly be seen that the fire scars are much warmer than the water bodies, indicating

7. The portion of the electromagnetic spectrum covered by the Landsat ETM+ Panchromatic band (band 8) coincides with that measured by bands 2, 3 and 4. Therefore band 8 covers the same spectral region as three of the four bands used in the mixture analysis of the spectral data.

that these are, in fact, two different feature types. The thermal images show, therefore, that areas which are spectrally similar in the visible and near-infrared (i.e. water and fire scars)

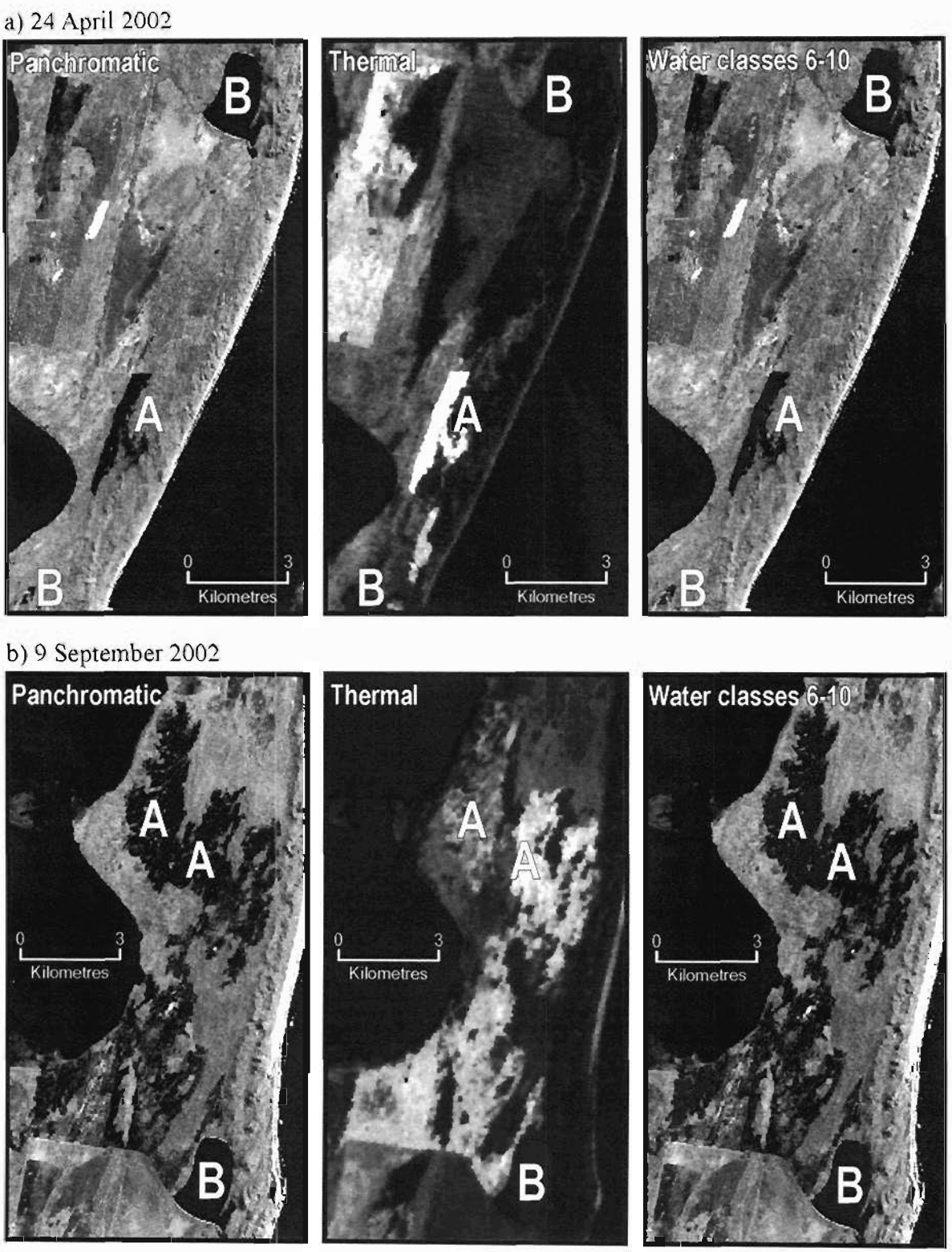

Figure 6.15: The effects of fire scars on the mapping of water for (a) April 2002 and (b) September 2002. The locations of fire scars are indicated by the symbol A while water bodies are shown by the symbol B.

can be separated in the thermal infrared. Based on this evidence it can be concluded that the presence of fire scars has a confounding effect on the accuracy of the spectral mixture analysis and that indications of water within fire scars need to be treated with caution.

Traditional accuracy assessment methods often provide a numerical measure of accuracy, be it producer's accuracy, user's accuracy or even an overall accuracy percentage. In this study, the use of cumulative rainfall as an accuracy test did not lead to such a quantifiable measure but led, instead, to a situation were it could be asserted that the results were 'probably' accurate. This is clearly not an ideal situation, but was the best that could be achieved given the lack of effective methods for assessing the classification accuracy of historical images and/or soft classifications.

6.6 SEASONAL AND SPATIAL DISTRIBUTION OF SURFACE WATER

When interpreting the surface water distribution in the study area it is pertinent to examine the rainfall patterns prior to the study dates. Figure 6.16 presents cumulative rainfall figures for the six months leading up to each of the study dates and clearly shows the presence of a drier period in 2002. This contrasts with the situation in 1991 and 2001 when six-month rainfall was generally much higher.

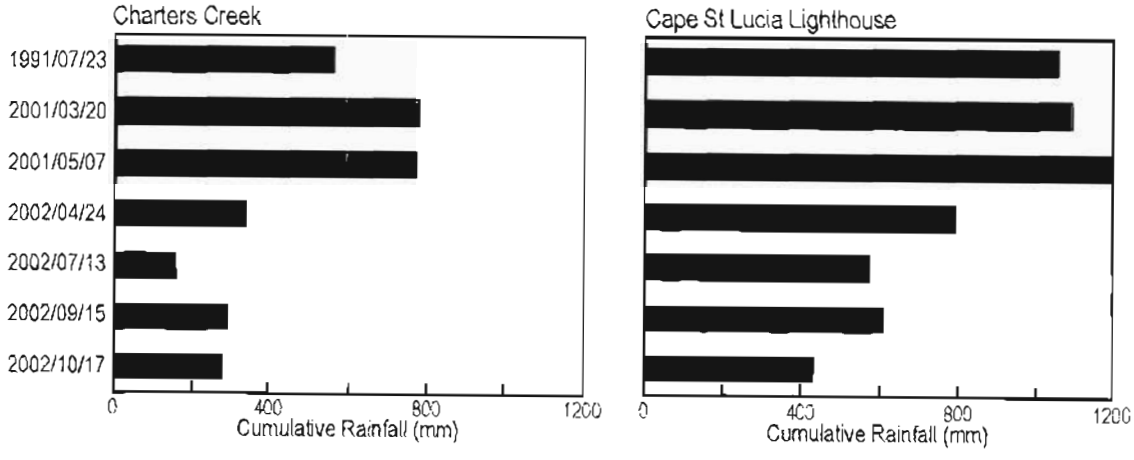

Figure 6.16: Cumulative six-month rainfall measured at Charters Creek (left) and Cape St Lucia Lighthouse (right). Wetter periods are indicated in blue, drier periods in brown (Source: South African Weather Service).

The dry-wet rainfall pattern also manifested itself in the distribution of surface water on the Eastern Shores (see Figure 6.9 on page 107), emphasising the close link that exists between the two. This is most clearly shown in Figure 6.17 which illustrates the similarities in the water distribution from the three study dates in the wet period (shown in blue). The curves for these three dates all show elevated amounts of water in the 11 to 50% range, indicating the presence of extensive, vegetation-dominated areas of water.

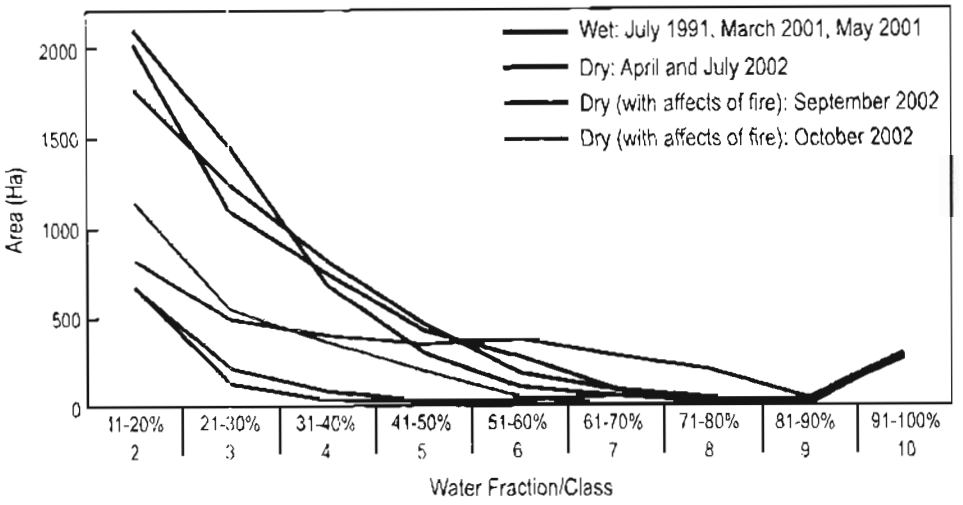

Figure 6.17: Areas, in hectares, covered by the water classes for each study date. Curves are grouped according to rainfall regime. Also shown are the affects of the large fire in September 2002. The 'no water' class is not shown.

The picture presented by the results from the drier period in 2002 is confused by the effects of the fire scars. The curves for April and July (shown in brown) are very similar and indicate the presence of very little water, particularly in the 31 to 80% range. Increases are noted in classes 2 and 3 although these are a lot lower than the values for the wet period. The curves for September (shown in red) and, to a lesser extent, that of October 2002 (green) are unquestionably anomalous and reflect the influence of the large fire scar to the north of Lake Bhangazi. The September curve shows elevated amounts of water in classes 6, 7 and 8 while both the September and October results indicate increases in water in classes 2-5 as compared to April and July 2002. The differences in the September and October curves can be explained by the freshness of the fire scar. In September the fire scar was new and dominated by burnt vegetation. By October the vegetation had started recovering, providing an explanation for why the October curve resembles the September curve for classes 2, 3 and 4 but is more like the dry April and July curves for classes 6 to

10. The April 2002 fire scar (see Figure 6.15a) was very small and did not appear to influence the results shown in Figure 6.17.

A final trend visible in Figure 6.17 is that classes 9 and 10 (81 to 100% water) exhibit similar patterns for all seven study dates. This is not surprising as Lake Bhangazi dominates these two classes, especially class 10 where it makes up over 98% of the area for each of the study dates.

The patterns apparent in Figures 6.16 and 6.17 also manifest themselves in Figure 6.9 on page 107, which illustrates the spatial distribution of water in the study area. The three images in the top row are from the wetter period in 1991 and 2001 and all show similar patterns of water distribution. High concentrations of water are found in the well-defined Mfabeni swamp south of Lake Bhangazi as well as in the wilderness area to the north. The water in the wilderness area is diffuse but widespread during the wetter period, when many regions show concentrations in the 20 to 60% range and some areas reach 90%. Also apparent are regions of water in the Brodies Crossing area, where concentrations of 60% were measured in May 2001. The four images from the drier 2002 all show low concentrations of surface water throughout the study area. Exceptions to this are Lake Bhangazi and the burnt regions discussed in the previous section. Lake Bhangazi, with its fringe of reeds, shows up clearly in all the images.

The distribution of water in the Mfabeni swamp is shown in Figure 6.18. Water concentrations in the core of this swamp reached 80% during the wet period, decreasing

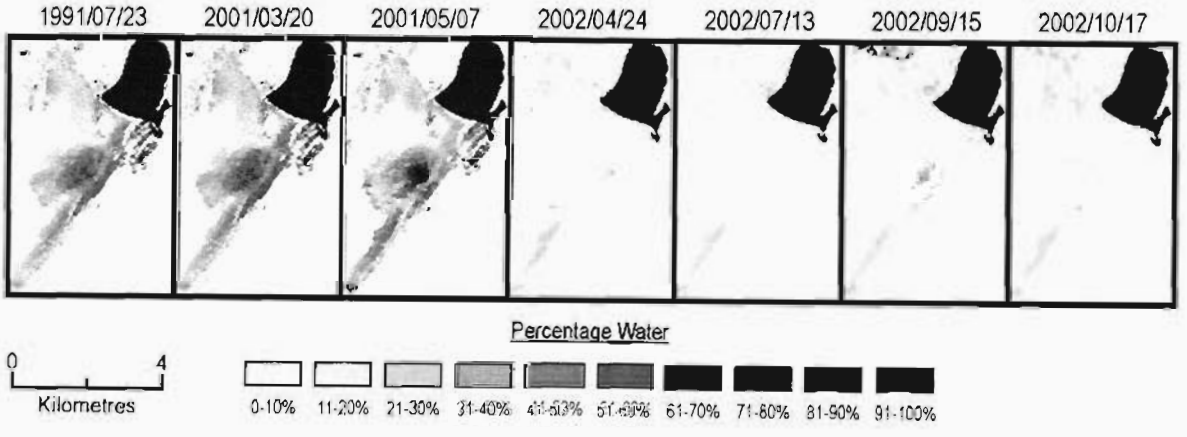

Figure 6.18: Spatial and temporal distribution of water in and around Lake Bhangazi and the Mfabeni swamp.

outwards to the margins of the swamp. During the 2002 drier period the wet core of the Mfabeni was almost absent. However, a secondary linear core at the southern end of the Mfabeni swamp is present throughout, with concentrations in the 21-30% range being recorded even in the dry months. More diffuse patterns of water, discernible to the west of Lake Bhangazi in the wetter periods, were absent or much reduced in 2002.

To conclude this section on the distribution of surface water, it is illuminating to examine those areas that remained the same throughout the study period. Of the 102.8 km^2 that were analysed, 19.6 km^2 were always classed as class 1 while 2.5 km^2 were always mapped as class 10. These areas are shown in Figure 6.19. The pixels in the remaining 80.7 km^2 were assigned a different class classification at least once over the seven study dates. A detailed examination of these pixels that changed class proved difficult given that each pixel could

Figure 6.19: Results of change analysis showing areas of change in pink and areas of no change in blue and green.

have assumed any one of ten class values for each of the seven study dates, resulting in a possible 10 million permutations per pixel.

Areas that remained as class 10 throughout the study (i.e. were always water) are confined to Lake Bhangazi while regions that were always vegetation are found mainly to the west and south-west of the Mfabeni as well as in the southern parts of the study area. The Mfabeni swamp, the wilderness area north of Lake Bhangazi and the area near Brodies Crossing are dominated by change, reflecting areas where fluctuations in surface water occurred. These results, in providing insight into the connectedness and spatial distribution of surface water in the study area, allow the structure of wetlands systems and their relationship with biodiversity to be investigated.

6.7 CONCLUSION

The methodology employed in this study led to a series of results that allowed the temporal and spatial distribution of surface water on the Eastern Shores to be mapped. Each of the steps in this methodology were crucial as the accuracy of their outcomes influenced the success of subsequent stages. The image preparation stage produced a set of geometrically and radiometrically consistent images that facilitated the inter-comparison of these multitemporal datasets. Images could therefore be compared with confidence in the knowledge that differences arising from atmospheric and geometric effects had been largely eliminated.

The application of exclusion masks was an important phase of the study as it reduced the volume of data to be processed in the subsequent image classification stage. This was achieved by eliminating areas where water was not likely to occur, as well as regions where the presence of water was hidden by trees. This process reduced the area to be analysed to just under 103 km^2.

Perhaps the most important part of this study was the interpretation and assessment of the outputs from the different image classification methods. Three different classification methods were applied to both untransformed spectral data and transformed PCA data in order to determine the method best able to map surface water on the Eastern Shores. The

unsupervised cluster analysis and the supervised maximum likelihood classifiers performed rather poorly and were not able to map the complex relationships between water and vegetation in the study area. This was not an unexpected result for these hard classifiers. The results of the spectral mixture analysis were much more encouraging, particularly the unmixing performed on spectral bands 2, 3, 4 and 5 of the spectral data. This output, chosen as the most accurate of the six produced by the image classification, was verified against rainfall measurements. Most of the surface water in the study area was found in Lake Bhangazi, the Mfabeni swamp and the wilderness area in the north. Permanently dry areas were found to the west and south-west of the Mfabeni and also in the south. Possible seasonal variations in water distribution were masked by the dry/wet rainfall regime and, to a lesser extent, by the presence of fire scars.

7. DISCUSSION

7.1 INTRODUCTION

One of the major problems that had to be overcome in this research was that of mapping water in the presence of emergent vegetation. This co-presence of water and vegetation led to unsatisfactory results being obtained from the hard classifiers used in this study. Spectral mixture analysis, on the other hand, produced promising results and this classification method was incorporated into the water mapping protocol described in this chapter.

The chapter commences with a discussion of the geometric and radiometric rectification procedures carried out and compares the results to those described in the literature. The issue of image masking will be dealt with in a similar manner. The outputs of the three different classification methods used in this research will be compared with findings from previous studies, particularly those that attempted to map water and/or wetlands. This is followed by a brief assessment of the accuracy of the results produced by the preferred classification method, spectral mixture analysis. With an understanding of the achieved levels of accuracy in mind, the water concentration maps are analysed and compared to two previous land cover maps of the Eastern Shores. This leads into a description of the water mapping protocol developed in this study, its application, and its constraints.

7.2 IMAGE PREPARATION AND TRANSFORMATION

The image preparation phase commenced with the rectification and georeferencing of the Landsat images for each study date. As recommended by Lunetta (1999) in his discussion on change detection studies, this was a two step process in which a chosen reference image was georegistered to geographic coordinates followed by an image-to-image registration that rectified the remaining images relative to the reference image. The RMS error of 0.80 pixels (24 m) obtained from the rectification of the reference image compared favourably with similar studies. Both Dewidar & Frihy (2003) and Lu *et al.* (2004) reported RMS errors of below 15 m while Frazier *et al.* (2003) obtained values of less than 20 m. Slightly larger RMS errors were obtained by Munyati (2000) (< 28.5 m) and Ringrose *et al.* (2003)

(42 metres). Lunetta (1999) suggested that RMS errors for the relative, or image-to-image, rectifications should not exceed 0.5 pixels. This was achieved in this study where each of the RMS error values from the relative rectification were below 0.5 pixels (see Table 6.2 on page 89). A number of other studies employing relative rectification obtained similar RMS errors, ranging from Frazier *et al.* (2003), who reported values of less than 10 m (0.33 pixels), to the <0.5 pixels of Boresjö Bronge (1999) and the ±0.5 pixels measured by Sader *et al.* (1995). The fact that the accuracies achieved during image rectification were so similar to results presented in the literature suggests that this crucial first stage in the preparation of the satellite images had been performed satisfactorily. This was an important outcome in this study as it allowed multidate images to be compared with confidence.

The preparation of the images continued with the application of radiometric correction procedures. As with the geometric rectification, results obtained were similar to those obtained by other researchers applying relative radiometric normalisation techniques. The types of areas selected as bright and dark targets closely mirrored those selected by Munyati (2000) who used irrigation reservoirs as dark targets and bare, unvegetated soil for the bright targets. As in the current study, the correlations (reported as R^2 values) obtained by Munyati (2000) for the relative normalisation of three Landsat TM images were very high, namely 0.991, 0.998 and 0.999 (Table 7.1). These R^2 values are comparable to those of the current study, which were all above 0.998. Eckhardt *et al.* (1990), in a study of irrigated lands in Nevada, used a deep clear lake as a dark target, and a dry lake bed and a badlands area as the two bright targets. The spectral characteristics of these targets were very similar to the water and beach targets used in the current study. R^2 values reported by Eckhardt *et al.* (1990) for the normalisation of three SPOT HRV images were all above 0.998. Jensen *et al.* (1995) used water and unvegetated, bare soil as pseudoinvariant targets in their research into vegetation in the Florida Everglades. Their resulting correlation coefficients were all in the range 0.95 to 0.99.

Both the image rectification and radiometric normalisation produced results similar to those obtained by other studies. This is not surprising given that the same correction techniques were used. Furthermore, the fact that the results were so similar indicated that the procedures had been correctly applied and that the images had been adequately prepared for the image classification stage of this study.

Table 7.1: Comparison of correlation coefficients obtained by studies employing relative radiometric normalisation techniques.

Study	*Range of R^2 values*	*Sensor*
Current study	**0.998 to 1.000**	**Landsat TM**
Jensen *et al.* (1995)	0.96 to 0.99	Landsat MSS
Jensen *et al.* (1995)	0.95 to 0.99	SPOT XS
Eckhardt *et al.* (1990)	0.998802 to 0.999000	SPOT HRV
Munyati (2000)	0.991 to 0.999	Landsat TM
Munyati (2000)	0.907 to 0.988	Landsat MSS

The final procedure carried out prior to image classification involved the use of ancillary and derived data to mask out areas in which surface water was unlikely to be found. Comparing these results to previous studies is difficult as the specifics of individual studies dictated differences in the types of masking that were used. Although a review of the literature revealed no studies that used masking in exactly the same way it was applied in this study, a few did use digital elevation models (DEMs) in a similar way. Thompson *et al.* (2002) devised a methodology for mapping South African wetlands that used terrain-based modelling to determine areas where water was likely to accumulate. Their terrain model used DEM-derived slope and hydrological variables to exclude non-wetland areas in much the same way that the current study used a slope criterion of 5% to mask out unsuitable zones. Another study using a DEM-derived mask was described by Sader *et al.* (1995), who also used a 5% slope threshold to mask out areas too steep for water to accumulate. This method of Sader *et al.* (1995) was identical to the one employed in the current study. The forest mask used in this study relied on NDVI values to separate forested from non-forested areas. A similar image-based method of forest delineation was used by Sader *et al.* (1995), although in their case they used an unsupervised classification of Landsat TM bands 3, 4 and 5, and not NDVI values, to extract forests. In contrast, Boresjö Bronge (1999) employed a completely different approach to producing a forest mask. In this case, forest data extracted from scanned 1:50000 topographical maps was used to produce a forest mask that aided the classification of boreal vegetation in Sweden. A disadvantage of this method was that it was not image-based but was dependant on the accuracy of the topographical maps.

The value of masking was emphasised by Lunetta (1999) who noted that the reduction of data dimensionality associated with masking enhanced the accuracy of image classification. In this study, the application of slope, sand and forest masks reduced the dimensionality of the remaining spectral data to three main components, namely water, forests and grasslands. This can be seen in scattergrams of the PCA data (see Figure 5.6 on page 80), where the reduction of data to these three components is evident from the triangular pattern exhibited by the plotted pixels. While the use of PCA component data in this study was ultimately not successful, the results from the PCA analysis were important in that they verified the presence of three major components in the spectral data. This finding had important implications for the selection of endmembers in the spectral mixture analysis.

7.3 CLASSIFICATION METHODS

A main aim of this study was to develop a protocol for mapping surface water in the study area. To this end, three different classification methods were applied to both the spectral and principal components datasets, and the different outputs were assessed for accuracy. Selecting which bands to analyse was quite straightforward for the component data as the first three components contained virtually all the information present in the dataset. This characteristic of Landsat TM data has been well documented (e.g. Lillesand & Kiefer, 2000). The selection of bands from the spectral dataset (see Table 7.2) was guided by studies in the literature, particularly those that mapped water and wetlands. TM bands 4 and 5 were widely acknowledged to be the most suitable for detecting water (e.g. De Haan *et al.*, 1991; Wickware *et al.*, 1991; Eastman, 2001; Braga *et al.*, 2003; Frazier *et al.*, 2003) so there was little difficulty in choosing these bands for classification. For wetland classification, all the studies reviewed used TM bands 3 and 4, mainly because of their ability to map the complex water and vegetation patterns present in most wetlands (Wang *et al.*, 1998). The addition of TM band 2 was also found to be useful, especially in combination with band 3 as it allowed saturated surfaces to be distinguished from dark organic soil (Lunetta & Balogh, 1999). Apart from Thompson *et al.* (2002), none of the studies under review used bands 1 or 7 to map wetlands. For the current study it was nevertheless decided to include bands 1 and 7 in the cluster analysis to allow the detection of spectral clusters from the full range of available data. These two bands were not used in the initial cluster seeding process, however.

Table 7.2: Landsat TM bands used for the three different classification methods applied in this study.

Classification Method	*Bands Used*
Unsupervised cluster analysis	3, 4, 5 for seeding; 1, 2, 3, 4, 5, 7 for analysis
Supervised maximum likelihood	2, 3, 4, 5
Spectral mixture analysis	2, 3, 4, 5

With the selection of spectral bands having been guided by previous studies, it is illuminating to assess the performance of the classification techniques themselves.

7.3.1 Hard classifiers

Two previous attempts at mapping land cover using hard classifications of Landsat data produced comparable results for the Eastern Shores (Figure 7.1). A national land cover classification for South Africa (CSIR/ARC, 1998) mapped unimproved grassland, wetlands, and thicket & bushland as the main cover types in the unmasked area of the Eastern Shores. Also mapped were smaller areas of forest and water. Smith (2001) used a more detailed land cover classification in mapping Maputaland, finding the unmasked part of the Eastern Shores to be dominated by hygrophilous grasslands[8], woody grasslands[9], and sedge & grass swamp. Also present were smaller amounts of open water, plantations and mud flats. Both these classifications produced maps of all land cover types, not just water, and neither attempted to map the temporal fluctuations in surface water. In a third mapping exercise, Walsh (2004) mapped swamp forest in Maputaland but found it very difficult to differentiate swamp forest from other forest types based on spectral information alone. In this case, mapping accuracy was improved by incorporating DEM data.

Both CSIR/ARC (1998) and Smith (2001) found the main Eastern Shores land cover types to be grasslands and wetlands/hygrophilous grasslands. In testing the applicability of hard classifiers to the mapping of surface water, the current study used similar land cover categories, namely wetland and grassland, as well as a water class. Classification of the clusters from the unsupervised cluster analysis was done by referral to field data, aerial

8. Hygrophilous grasslands are waterlogged for most of the year and are found on flat ground and in depressions between dunes.

9. Woody grasslands occur mainly on dune crests, slopes and relatively high lying level plains.

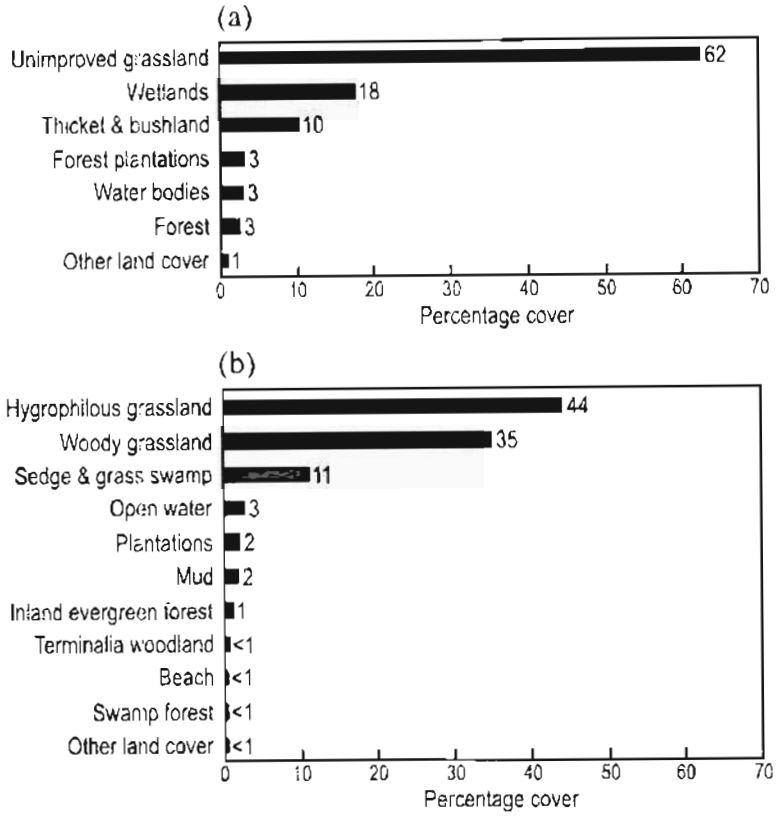

Figure 7.1: Percentage of the study area covered by the land cover classes of (a) the CSIR/ARC (1998) classification, and (b) the Smith (2001) classification. Figures are for the unmasked portion of the Eastern Shores study area only.

photographs and colour composite images. In performing this classification it was apparent that many clusters could not be assigned to any of the three classes but appeared to be mixed classes, containing elements that were partly grass and partly wetland. These mixed classes were assigned to a new class called grassland/wetland. The numbers of clusters allocated to the wetland class seemed to indicate that these environments were a lot more complex than grasslands, which generally tended to contain fewer clusters. It was also noted that there was less confusion between grasslands and wetlands in wetter years. This ties in with the findings of Pillay (2001) who achieved greater accuracies when mapping wetlands of the Midmar sub-catchment using images from the wet season.

The maximum likelihood classification also mapped pixels into classes of water, grassland and wetland. The major problem with this classification lay in the large number of pixels left unclassified. As discussed in the previous chapter, this could have been due to poorly chosen training sites, but it is much more likely that the landscape was too complex to be

mapped into just three classes. This is similar to the problem experienced with the cluster analysis where considerable confusion existed between grassland and wetland clusters.

The problem with the spectral separation of different land cover types has been commented on by a number of researchers. Smith (2001) found that the maximum likelihood classifier struggled to distinguish hygrophilous grasslands from woody grasslands, but that mapping accuracy could be improved through the incorporation of ancillary DEM and vegetation data. Similarly, Boresjö Bronge & Näslund-Landenmark (2002) discovered that Scandinavian marshes were difficult to map using spectral data alone, and so used ancillary data derived from topographical maps to enhance classification accuracy. The presence of mixed classes was commented on by Jensen *et al.* (1995), who noted the presence of 'intermediate' clusters in their mapping of aquatic vegetation of the Florida Everglades. These, they surmised, contained different mixtures of the land cover types they were attempting to map.

Both hard classifiers produced good estimates of the amount of open water in the study area. This was in line with findings by Smith (2001) who reported a water mapping accuracy of 100% for Maputaland using Landsat imagery. Open water proved easy to map because of the uniqueness of its reflectance signal, a fact noted in numerous studies. Wickware *et al.* (1991), Lunetta & Balogh (1999) and Frazier *et al.* (2003) among others, were all able to map water fairly easily using data from near- or mid-infrared bands.

In terms of a hard classification approach, very few of the reviewed studies relied solely on an unsupervised approach to map water and/or wetlands. The preference was to use either a supervised maximum likelihood classification or else to employ a hybrid classification technique. Even so, some studies found even the maximum likelihood classification unsatisfactory for mapping wetland-type environments (e.g. Wickware *et al.*, 1991). Smith (2001) surmised that the accuracy of the maximum likelihood classifier could be improved by incorporating ancillary data like elevation and water table heights. Those studies that used hybrid classifications (e.g. Jensen *et al.* 1995; Lunetta & Balogh, 1999; Munyati 2000) all used clusters from an unsupervised cluster analysis as input into a supervised maximum likelihood classification. This was done in an attempt to overcome the limitations of hard classifiers.

The limitations of hard classifiers found in this study mirror those reported by other researchers. The main reason for the difficulty in applying hard classification techniques to wetland mapping is that the spectral characteristics of these environments represent a continuum from open water with no emergent vegetation through to complete vegetation cover where no water is visible. These complex landscapes do not lend themselves to hard classification and are much better served by sub-pixel classification methods.

7.3.2 Spectral mixture analysis

The particular application of spectral mixture analysis in this study was quite different from other research projects, with most of the reviewed studies interpreting the fraction images in terms of specific land cover types. This was achieved by 'hardening' the fraction images to produce land cover distribution maps. Those few studies that interpreted the fraction images as varying amounts of a particular feature (as was done in this study) invariably did so for vegetation and not for water. Nevertheless, similarities between the reviewed studies and the current project do exist, particularly in the selection of endmembers.

Ideally, endmembers should represent pure examples of each land cover class present in the study area and can be either image- or laboratory-derived. A good indication of the number of endmembers to use can be gained by examining the results of a principal components analysis of the spectral data. In this study, a PCA indicated that three endmembers were required to model land cover in the study area. This was evident from the fact that the first three components of the PCA for each of the image dates contained over 99% of all the information in the image bands (see Table 5.3 on page 74). This method of determining the optimum number of endmembers was discussed by Bateson & Curtiss (1996) who suggested that a PCA provided a useful guide for endmember determination. Of course, the number of available spectral bands provides an upper limit to how many endmembers can be used, meaning that the actual number of endmembers selected is often a trade-off between the number of major land cover types and the available spectral bands. In this study, the availability of six Landsat TM bands was not a serious constraint as three endmembers adequately described the land cover in the unmasked study area.

Table 7.3 compares the endmembers used by a number of other studies with those applied in this study. Each of the studies included a 'dark' endmember, often called shade but sometimes referred to as clear water, or just water. Some authors commented on the spectral similarities of shade and clear water and indicated that these endmembers were usually interchangeable (e.g. Mertes *et al.*, 1995). Shade was increased by the presence of trees (Adams *et al.*, 1995) but was considered less of an issue in the grassland and wetland environments of the Eastern Shores. Each of the reviewed studies also included at least one vegetation endmember, mostly representing dark green, leafy vegetation. In the current study, two vegetation endmembers were used, one called woody, the other non-woody. The inclusion of these vegetation endmembers was crucial for the success of this study as it allowed the complex mixing of water and vegetation to be described. These two endmembers did not represent specific vegetation species, but grouped together classes of vegetation types with similar spectral characteristics. Indeed, Adams *et al.* (1995) noted that it was not appropriate to interpret vegetation endmembers as actual vegetation species but rather as a grouping of vegetation types. The woody vegetation endmember represented all green, leafy vegetation that had not been excluded by the masking process, while the non-woody endmember was chosen to represent all grassland and wetland vegetation.

Table 7.3: Comparison of endmembers used in the current study and those used in studies reported in the literature.

Study	*Endmembers selected*
Current study	**Water, woody, non-woody**
Mertes *et al.* (1993)	Shade, soil, vegetation, various water/sediment mixtures
Adams *et al.* (1995)	Shade, green vegetation, non-photosynthetic vegetation, soil
Mertes *et al.* (1995)	Shade/clear water, vegetation, sediment-laden water
Mertes (1997)	Clear water, muddy water, vegetation
Binaghi *et al.* (1999)	Water, wetland
Elmore et al. (1999)	Shade, vegetation, light soil, dark soil
Roberts *et al.* (1999)	Shade, green vegetation, non-photosynthetic vegetation, soil
Small (2001)	High albedo, low albedo, vegetation
Lu *et al.* (2004)	Shade, soil, green vegetation
Théau & Duguay (2004)	Shade, canopy, lichen

In keeping with the largely image-based techniques utilised in this study, endmembers were selected from the images themselves and no reliance was placed on laboratory

measurements. This was similar to the techniques described by Mertes *et al.* (1995). Binaghi *et al.* (1999), Elmore *et al.* (1999), Small (2001) and Lu *et al.* (2004), among others, who all used image-derived endmembers in their research. The actual method of image endmember selection varied from study to study, with some identifying endmembers from scattergrams and others using ground truth data. Bateson & Curtiss (1996) described a method for selecting endmembers from scattergram displays of spectral data in multidimensional space but conceded that the method suffered from user subjectivity. This problem was apparent in the current project where the selection of endmembers from component data scattergrams produced unsatisfactory results. It is quite likely that another user would select a different set of endmembers from the same scattergrams, and in so doing obtain different (and perhaps more accurate) results from the mixture analysis. This was demonstrated by Théau & Duguay (2004) who, in using spectral mixture analysis to map lichen in northern Canada, tested different sets of scattergram-selected endmembers and obtained slightly different results each time. The scattergram approach to selecting endmembers obviously needs to be performed with care and requires numerous iterations before producing accurate endmembers. Nevertheless, a number of studies have reported success with this method. Small (2001) found that two different sets of endmembers selected from scattergrams both provided reasonable estimates of vegetation cover fractions. Similarly, Théau & Duguay (2004) selected shade, lichen and canopy endmembers from the vertices of a TM 3 and 4 scattergram and reported high accuracies in mapping lichen cover.

The other method of selecting image endmembers involves locating endmembers on the images themselves. This is similar to the training site technique used in supervised classification but differs in that endmember sites represent purest examples of endmembers and do not contain mixtures of other elements (as can happen with traditional training sites). Locating water or shade endmembers is easy, with most studies using water bodies for this purpose (e.g. Elmore *et al.*, 1999; Lu *et al.*, 2004). Finding vegetation endmembers is rather more difficult as pure examples rarely exist in nature. For instance, trees are invariably accompanied by shade while the 30 m pixel size of Landsat TM images makes it almost inevitable that some degree of mixing occurs within pixels. In this study, maximum NDVI values were used to define the woody vegetation endmembers. In doing this it was assumed that the presence of shade would lower NDVI values and that those pixels with the highest NDVI values represented forest with the least amount of shade. The non-woody

vegetation endmembers were selected from the modal pixel values of the training sites on the assumption that these were the most representative pixels. These non-woody vegetation endmembers where also assumed to be representative of all the vegetation species found in the grassland and wetland environments in the study area. In a similar manner, Elmore *et al.* (1999) used riparian vegetation along a river to define an endmember representing all vegetation in their study area while Lu *et al.* (2004) used areas of dense pasture to define an endmember for all green vegetation.

Both Adams *at al.* (1995) and Small (2001) noted the ease with which fraction images could be interpreted, being more intuitive than digital numbers (DN) and also facilitating the comparison of multitemporal images. Interpretation of fraction images is further aided by classifying the fractions into different classes. This generally involves applying user-defined land cover thresholds to the endmember fraction images to produce a land cover map. In this study, where water was the land cover of interest, the water fraction images were classified into ten classes representing water concentrations at 10% intervals. This greatly reduced the volume of information to be processed and facilitated the interpretation of results. Compare this to Lu *et al.* (2004) who used fraction images to produce maps of mature forest, advanced secondary succession, initial secondary succession, pasture, agricultural lands, bare lands and water. No attempt was made to map varying concentrations of vegetation within pixels, the fractions being used instead to define boundaries for the different land cover classes. Similar methods were also employed by Adams *et al.* (1995), Mertes *et al.* (1995) and Roberts *et al.* (1999). In all these studies, spectral mixture analysis was used to determine sub-pixel mixing, which in turn was used to define class boundaries in a manner not possible with hard classifiers. The results were land cover maps, not maps showing concentrations of a particular feature. This, then, is the crucial difference between the current study and other studies reviewed in the literature: this study used mixture analysis to produce maps of water concentration whereas most other studies produced maps depicting the distribution of different feature types.

7.4 ASSESSING THE ACCURACY OF RESULTS

As noted in the previous section, the use of spectral mixture analysis to map water concentration is unique when compared to other studies reviewed from the literature. So

too is the use of cumulative rainfall for verification, with a review of current literature not revealing any other studies using this technique. While the need for accuracy assessment is universally accepted, how best to achieve this for soft classification is still under debate. Binaghi *et al.* (1999) proposed using a 'standard error of estimate' between reference data and classified data while other studies calculated correlation coefficients between classified and ground truth data (e.g. Théau & Duguay, 2004). Both Binaghi *et al.* (1999) and Lu *et al.* (2004) applied an error matrix approach but did so on hardened classifications of the fraction images. All these methods relied on the presence of ground truth data, something not always available in historical and/or multitemporal studies. In the absence of ground truth data, ancillary or derived datasets may be used to assess classification accuracy. Small (2001) used aerial photos for classification verification while Mertes *et al.* (1995) compared their classification results to radar data. In an earlier study, Mertes *et al.* (1993) used residual images to explore accuracy while at the same time noting that contemporary field measurements provided the best means of checking for errors.

For the current study, both ancillary (cumulative rainfall) and derived (residual images) datasets were used to assess accuracy. The residual images provided a useful guide of how well the fraction images modelled reality, with high residuals indicating a poor match. The 5% of pixels that were most poorly modelled by the mixture analysis were excluded. Using rainfall to gauge the accuracy of water mapping was perhaps an obvious choice, particularly as the limited hydrological inputs and outputs on the Eastern Shores result in the area having a rainfall-dominated hydrology. The high correlations between cumulative rainfall and the water classes verified the accuracy of spectral mixture analysis as a technique for mapping surface water (see Figures 6.13 on page 112 and 6.14 on page 113). The use of meteorological data to verify classification is not common, with only one of the reviewed studies doing so. Although not an application of spectral mixture analysis, Vicente-Serrano *et al.* (2004) used rainfall to verify a map of soil moisture that had been produced from Landsat ETM+ and NOAA AVHRR data. The two datasets were found to be highly correlated leading to the conclusion that estimates of soil moisture from satellite data were accurate. The main advantage of using ancillary data for assessment is that these datasets obviate the need for contemporary ground truthing data. This was crucial for a study such as this one, where the ephemeral nature of the water being mapped, as well as the historical nature of the satellite images, precluded the use of ground truthing.

A final point on the accuracy of the water mapping relates to the effect of fire scars on classification. This is something that had been noted by Munyati (2000) who found that freshly burnt grassland was spectrally similar to deep, tranquil open water, with the same being true for old burnt areas with fresh grass shoots and water with emergent vegetation. This similarity was noted in the results of this study, where large fire scars in April and September 2002 skewed the results of the water mapping. An examination of thermal images from these dates revealed that the apparent presence of water in these burnt areas was not correct, and that the mapping of these areas as water was due to the spectral similarity between water and burnt vegetation. Interpretation of image classifications in the presence of fire scars needs to be done with care.

7.5 SURFACE WATER ON THE EASTERN SHORES

Inundation by water can occur in a number of ways: through direct precipitation, from groundwater exchange, or via overland flow from surrounding slopes or streams. For the Eastern Shores study area, where no large streams are found, rainfall and groundwater are the main determinants of surface water inundation. While short-term rainfall events undoubtedly increase surface inundation, it is clear that these increases are temporary and that seasonal rainfall patterns, expressed through groundwater levels, are the main controlling factors of inundation on the Eastern Shores. That this is true is shown by the high correlation between surface water extent and cumulative rainfall over periods of six months and more. Seasonal rainfall patterns appear to have long-term effects on groundwater levels, leading to patterns of inundation that reflect rainfall events that might have occurred many months previously.

Also of importance in this study is the possible presence of water in areas excluded by the forest mask. In defining the forest mask, the maximum extent of forest during the period covered by the satellite images was used, leading to a possible underestimation of the water resource on the Eastern Shores. While many hectares of plantation forest were felled during the period between July 1991 and October 2002, none of these areas were analysed in the study. With the removal of trees from these areas, it is very likely that surface water would reappear. The forest mask also excluded large patches of swamp forest from the analysis[10].

10. Smith (2001) found that swamp forests on the Eastern Shores covered an area of just over 6 km^2.

Swamp forests are characterised by the presence of waterlogged ground, and surface water would certainly occur in these areas. Excluding these forests from analysis would therefore result in an underestimation of surface water on the Eastern Shores. The amount of surface water thus excluded could also be estimated using methods developed by Walsh (2004) who used a hybrid classification system supported by ancillary DEM data to map swamp forests in Maputaland.

Apart from Lake Bhangazi, virtually all the surface water on the Eastern Shores occurs in conjunction with emergent vegetation. These areas, which are either permanently saturated or else undergo regular or occasional inundation, are likely to be characterised by distinctive vegetation communities. It is therefore illuminating to compare the areas of inundation obtained in this study with the land cover mappings obtained by CSIR/ARC (1998) and Smith (2001). As mentioned previously, the CSIR/ARC (1998) study mapped unimproved grassland, wetlands, and thicket & bushland as the main cover types on the Eastern Shores, while Smith (2001) found the area to be dominated by hygrophilous grasslands, woody grasslands, and sedge & grass swamp. Care should be taken when comparing these results with the current study as the classifications were produced using different methods and with satellite imagery from different dates. This fact, along with possible misregistration between the datasets, can lead to differences in the outputs from the different classifications.

A cross-tabulation of the pixels from water class 10 (i.e. 91 to 100% water concentration) against the equivalent classes in the CSIR/ARC (1998) and Smith (2001) classifications reveals high agreement between the three different classifications (Table 7.4). When compared to the Smith (2001) water body class there was a 90.1% agreement while a slightly lower value of 88.4% was obtained against the CSIR/ARC (1998) open water class. That there is such good agreement between the three methods is not surprising given the unique spectral characteristics of open water and the relative ease with which it can be mapped. All three classifications were based on Landsat TM images and, hence, used data with the same spectral characteristics.

Table 7.4: Percentage of pixels from water class 10 (91 to 100%) that occurred in the water land cover classes of the CSIR/ARC (1998) and Smith (2001) classifications.

Date	*CSIR/ARC (1998) Class: Water bodies*	*Smith (2001) Class: Open water*
1991/07/23	87	90
2001/03/20	88	89
2001/05/07	87	88
2002/04/24	89	91
2002/07/13	92	94
2002/09/15	87	89
2002/10/17	89	90
Average	88.4	90.1

Moving on to water classes 1 to 9, it is enlightening to examine the peak distribution of each class within the Smith (2001) and CSIR/ARC (1998) classifications. To this end, an analysis of the land cover class in which each water class occurred most often is presented in Table 7.5. From this table it can be seen that pixels in the different water classes occurred most often in the hygrophilous grassland class of the Smith (2001) dataset and in the unimproved grassland class of the CSIR/ARC (1998) classification. Smith (2001) defined hygrophilous grasslands as being waterlogged for most of the year, a fact confirmed by the results from this study where on 44 occasions out of 63 (9 classes, 7 study dates) the majority of pixels in a water concentration class were located in hygrophilous grasslands. According to the Smith (2001) classification, 44% of the (unmasked) study area comprised hygrophilous grasslands with woody grasslands making up 35% and sedge & grass swamp another 11%. The high concordance between the hygrophilous grassland mapping from Smith (2001) and the water classes from the current study indicates that the different classification methods[11] have produced complimentary results: the spectral mixture analysis has mapped water where Smith (2001) found hygrophilous grasslands, and *vice versa*.

11. Smith (2001) used a maximum likelihood classifier, supplemented with ancillary datasets, to produce the land cover map of Maputaland. Mapping accuracy of hygrophilous grasslands was improved through the incorporation of a DEM and various aquatic vegetation datasets that provided indicators of the likelihood of occurrence of this land cover type.

Table 7.5: Land cover class in which each water concentration class occurred most often across the seven study dates for (a) the Smith (2001) dataset and (b) the CSIR/ARC (1998) dataset. The figures show how often the maximum number of water class pixels occurred in a particular land cover class. Percentages in brackets refer to the size of each land cover class as shown in Figure 7.1. Water class 10 is not shown since it was shown in Table 7.4.

(a) Smith (2001)

	Water Class									
	1	*2*	*3*	*4*	*5*	*6*	*7*	*8*	*9*	*Total*
Hygrophilous grasslands (44%)	4	7	6	7	5	5	6	3	1	44
Woody grassland (35%)	3				1			2	1	7
Open water (3%)								1	4	5
Sedge & grass swamp (11%)			1		1	1				3
Beach (<1%)								1	1	2
Mud (2%)						1	1			2

(b) CSIR/ARC (1998)

	Water Class									
	1	*2*	*3*	*4*	*5*	*6*	*7*	*8*	*9*	*Total*
Unimproved grassland (62%)	7	6	5	4	3	5	6	6	6	48
Wetlands (18%)		1	2	3	3	1	1	1		12
Thicket & bushland (10%)					1	1				2
Water bodies (3%)									1	1

In analysing the comparison with the CSIR/ARC (1998) classification it should be remembered that this land cover map was produced for the whole of South Africa and land cover classes had, of necessity, to be broad enough to capture the main land cover types in the country. The unimproved grassland class, for instance, represented a generic grassland land cover and no attempt was made to capture the subtle variations in grassland found throughout the country. It is not surprising, therefore, that most of the water classes from this study coincided with the unimproved grassland class, with a smaller peak being located in the wetland class. Nevertheless, based on this comparison it is clear that the CSIR/ARC (1998) mapping of wetlands is poor.

Comparing the results from this study against both cumulative rainfall and the land cover maps of CSIR/ARC (1998) and Smith (2001) allowed the accuracy of the spectral mixture analysis technique to be appraised. All indications are that this technique is able to unravel

the complex water/vegetation mixtures on the Eastern Shores and, in so doing, allow accurate maps of water inundation to be produced. The protocol for performing this mapping is presented in the next section.

7.6 A PROTOCOL FOR MAPPING SURFACE WATER

One of the major aims of this study was to develop a protocol for mapping the distribution of surface water in the study area by using remotely sensed data. It is clear from the literature that mapping of open water is fairly easy but that problems arise when water occurs in conjunction with emergent vegetation. The spectral complexities introduced by the mixing of water and vegetation are such that standard hard classification methods struggle to produce accurate classifications of these landscapes. In order to overcome this problem, a soft classifier based on spectral mixture analysis was incorporated into the protocol so that the sub-pixel mixing of water and vegetation could be measured. The protocol has the further advantage of being almost completely image-based. Unlike traditional methods, which rely on ground truthing for accuracy assessment, the protocol uses cumulative rainfall as a verification tool. This frees the user from having to collect field data to verify the results, thereby allowing the protocol to be applied to both historical studies and scenario modelling.

7.6.1 Description

The protocol is presented as a series of steps describing the complete processing of images, from their initial acquisition through to the interpretation of the classified results (Table 7.6). The first step covers the acquisition of suitable images, while the next three steps outline the process of rectification, radiometric correction and masking. By the end of step four, preparation of the images is complete and the classification process can begin. This takes the form of endmember selection in step five and spectral mixture analysis in step six. The protocol ends with the important steps of accuracy assessment and interpretation of results. Although the protocol is presented as a series of sequential steps, it is envisaged that certain portions of the protocol will be performed iteratively. This is particularly so for steps five, six and seven, which might need several iterations before endmembers are correctly chosen and an accurate classification obtained. Furthermore, the

fact that only two ancillary datasets are specified by the protocol (digital elevation data for the slope mask and rainfall for accuracy assessment) does not preclude the use of other ancillary data in the production of image masks. While the protocol has only been tested on Landsat TM data, the methodology should be applicable to any sensors operating in the visible, near- and mid-infrared parts of the electromagnetic spectrum.

Table 7.6: A protocol for mapping the distribution of surface water.

Step	*Description*
Step 1 - Image acquisition	Acquire cloud-free imagery of a suitable spatial and spectral resolution.
Step 2 - Image rectification	Perform a geometric rectification of the image bands. If multidate images are being used, choose a reference image and rectify the remaining images relative to the reference image.
Step 3 - Radiometric correction	Select a suitable correction method and radiometrically correct the image bands. If multidate images are being used, choose a reference image and use pseudoinvariant dark and light targets to normalise the remaining images relative to the reference image.
Step 4 - Masking	Exclude all areas which fall outside the study area. Also mask out areas in which surface water is unlikely to occur. For steep slopes use a 5% threshold. For forests use NDVI threshold values. Other areas to mask out could include urban areas, beaches and fire scars. Use ancillary data where necessary.
Step 5 - Endmember selection	Select two or more endmembers that represent pure examples of surface features in the study area. At least one of the endmembers must be a water endmember, while endmembers representing emergent vegetation must also be chosen.
Step 6 - Spectral mixture analysis	Using the endmembers selected in step 5, perform spectral mixture analysis on selected visible, near- and mid-infrared bands of the image data. Use the resulting residual images to exclude poorly modelled areas from the water fraction images produced by the mixture analysis.
Step 7 - Accuracy assessment	Use six month cumulative rainfall to verify the accuracy of the water fraction images.
Step 8 - Interpretation of results	Describe the spatial and temporal distribution of surface water by examining the water fraction images generated in step 6.

7.6.2 Constraints and limitations

There are a number of constraints and limitations that should be borne in mind when applying the protocol. The first of these is that the protocol specifically excludes forests from classification. In the context of the Eastern Shores this also leads to the exclusion of

all swamp forests; areas where permanent surface water is known to occur. The protocol excludes forests as the closed nature of their canopies prevents surface water from being visible to the satellite. This is particularly true for swamp forests. While success at measuring water through canopies has been obtained by means of radar (e.g. Wang *et al.*, 1998; Bourgeau-Chavez *et al.*, 2005), much of this has been in mangroves or in northern hemisphere forested wetlands. These techniques need to be tested on swamp forests and, if successful, would be a valuable addition to the protocol.

The problem relating to closed forest canopies highlights one of the main drawbacks of the protocol: water can only be detected if it is visible to the satellite. If the presence of water is hidden by dense wetland vegetation then application of the protocol will lead to an underestimation of the extent of surface water. This is a problem experienced by all passive sensors operating at visible and near-infrared wavelengths and needs to be borne in mind when applying this protocol.

A further constraint that needs to be considered is the availability of reliable rainfall data. Although the lack of rainfall records does not prevent the protocol from being applied, it does remove the main verification method used by the protocol. Failure to verify the accuracy of the protocol results leads to uncertainty in their interpretation and also raises a question mark over their validity. Water table heights, if available, could be used for verification in the absence of rainfall data.

7.7 PROTOCOL APPLICATION: MAPPING WATER IN MAPUTALAND

In order to test its applicability, the water mapping protocol was applied to an area encompassing southern Maputaland, from St Lucia in the south to Lake Sibaya in the north and inland to the Lebombo Mountains. The protocol was applied to bands 2, 3, 4 and 5 of the 7 May 2001 image and unmixing was performed using the same three endmembers used to process the Eastern Shores data. Forests and slopes steeper than 5% were excluded.

An analysis of the protocol output shows that the three main bodies of water in the area - the Indian Ocean, Lake St Lucia and Lake Sibaya - have been successfully mapped (Figure 7.2a). Also present on the Eastern Shores and on the coastal strip north of Lake St

Lucia are areas of water with concentrations of 30% and upwards. These map out the coastal wetlands that are so characteristic of the region. The pans associated with the Mkuze wetlands are also mapped but the large diffuse areas of water around the Lebombo Mountains in the west are probably inaccurate. These zones, with water concentrations of 10 to 30%, are probably due to the fact that the vegetation endmembers used in the unmixing were derived from coastal vegetation sites on the Eastern Shores. The vegetation found along the Lebombo Mountains, particularly the woody vegetation, is quite different

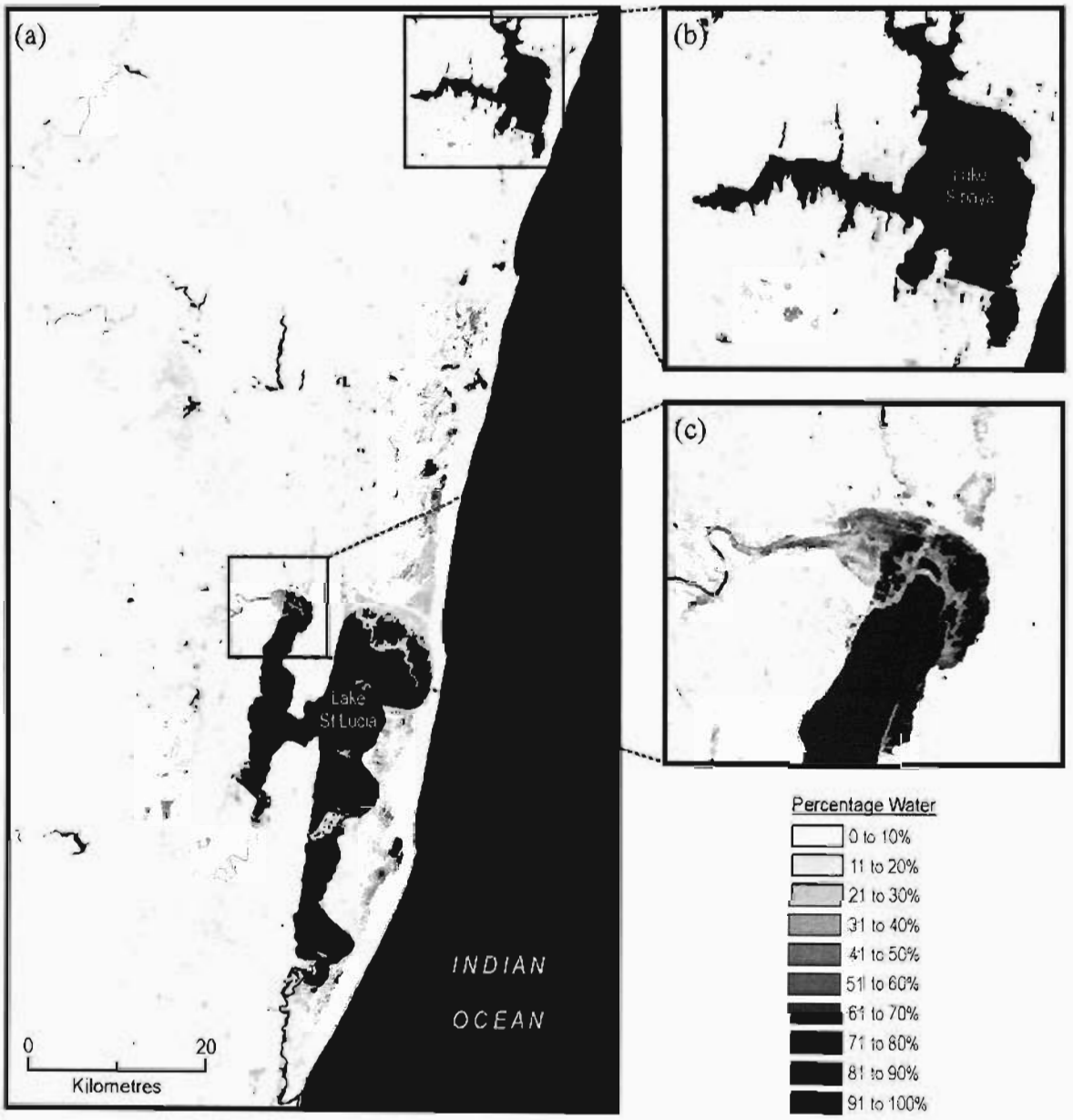

Figure 7.2: Application of the water mapping protocol to Maputaland showing the water concentrations for (a) the whole region, (b) Lake Sibaya, and (c) the mouth of the Mzinene River. Masked areas are shown in white.

from that found on the Eastern Shores, and would most likely require different endmembers.

From Figure 7.2b, which shows the mapping of Lake Sibaya, it can be seen that the outline of the lake is accurately captured by water class 10 (i.e. 91 to 100% concentration). Furthermore, the fringe of water and reeds surrounding the lake has also been mapped, particularly on the southern and northern shores. Further evidence of the effectiveness of the water mapping protocol is presented in Figure 7.2c, which shows the Mzinene River as it enters Lake St Lucia from the west. The river is initially confined to a fairly narrow channel but spreads out into a delta as it enters the lake. This delta is clearly visible as a region of mixed water and vegetation, with water concentrations ranging from 20% up to 100%.

The water mapping protocol, developed using conditions on the Eastern Shores of Lake St Lucia, has successfully mapped the water/vegetation mix occurring in other parts of Maputaland. This has demonstrated the robustness, applicability and transferability of the techniques incorporated in the protocol. However, this application of the protocol has also shown that endmembers need to match the actual conditions in a region. The implication of this is twofold. Firstly, some regions might need more endmembers than the three used in this study. A possible scenario could be where water occurs in silt-laden rivers as well as in clear lakes, requiring the use of two different water endmembers. The second implication is that different regions within a study area might require different sets of endmembers and, hence, need to be processed separately. For Maputaland this would mean deriving different vegetation endmembers for the coastal and inland regions and processing each region separately.

7.8 CONCLUSION

To conclude this chapter, it is worth remembering that the environment this study attempted to map is a complex one, being characterised by gradual transitions from vegetation to water. This co-presence of water and vegetation results in heterogeneity that is difficult, if not impossible, to map using traditional hard classifiers. This was confirmed

by the results of other studies that attempted to map wetlands, with many of them resorting to hybrid classification techniques in an attempt to increase mapping accuracy.

The water mapping protocol presented in this chapter uses spectral mixture analysis to tease out the complexities of sub-pixel water/vegetation mixing occurring on the Eastern Shores. Results from this technique compared favourably with cumulative rainfall and also showed close concordance with hygrophilous grasslands mapped by Smith (2001). It is also clear from these results that seasonal rainfall patterns play a crucial role in the amount of surface water in the study area. This is shown by the high correlations between cumulative rainfall over periods of six months and longer and the amounts of water mapped by the protocol.

Although the protocol has shown that surface water can be mapped successfully in the presence of vegetation, this can only be done if the water is actually visible from above. Water hidden by dense vegetation will not be mapped. Nevertheless, the water mapping protocol is a powerful tool, particularly as it applies image-based techniques that do not rely on ground truthing. This opens the way for studies of important historical events like the Demoina floods while at the same time providing a valuable tool for modelling the effects of changing rainfall patterns produced by global warming.

8. CONCLUSION AND RECOMMENDATIONS

8.1 ACHIEVEMENT OF THE PROJECT AIM AND OBJECTIVES

The aim of this research project, which was to 'use satellite remote sensing to ascertain the spatial and temporal distribution of surface water on the Eastern Shores of Lake St Lucia', was achieved by working towards the project objectives outlined in Chapter One. These objectives were attained as follows :

Objective 1: Assess the suitability of available remotely sensed products.

A review of currently operating earth observation satellites showed that Landsat and SPOT were the only two suitable candidates. Data from the Landsat Thematic Mapper sensor were preferred over SPOT data because of the better spectral resolution, larger footprint, lower cost, and the presence of continuous measurements back to 1982.

Objective 2: Acquire satellite images suitable for mapping surface water.

This objective was achieved by reviewing archived Landsat images and selecting a series of six cloud-free images covering a complete seasonal cycle during 2001 and 2002. The dates of these images are listed in Table 5.1 on page 68. A single Landsat-5 image from 1991 was also obtained.

Objective 3: Geometrically and radiometrically correct the chosen satellite images.

The geometric and radiometric correction steps both involved a two stage process. For the geometric correction, a reference image was chosen and georeferenced to the South African LO33 coordinate system. The six remaining images were then rectified relative to the reference image using a series of ground control points. The first step in the radiometric correction was to apply an absolute correction to the reference image using Chavez's COST method. The remaining six images were radiometrically normalised to the target image using a series of invariant dark and bright targets.

Objective 4: Develop a set of spectral signatures to detect the presence of surface water on the Eastern Shores.

Three different image classification methods were applied to two different datasets (i.e. spectral and component datasets) resulting in six different characterisations of the Eastern Shores water bodies. However, only the spectral mixture analysis of the spectral dataset produced satisfactory results. This classification produced a set of endmember spectra (see Figure 6.7 on page 103) that were used to map the presence of surface water in the study area as well as the varying concentrations of the water-vegetation mix.

Objective 5: Map the distribution of surface water on the Eastern Shores.

These maps, produced using spectral mixture analysis and depicted in Figure 6.9 on page 107, show how surface water is distributed in the study area.

Objective 6: Develop a protocol for mapping the distribution of surface water.

The techniques applied in this study were used to produce the water mapping protocol shown in Table 7.6 on page 139. Important characteristics of this protocol are the use of image masking, the application of spectral mixture analysis and the assessment of results against cumulative rainfall.

All six of these objectives have been attained in this project, resulting in a greater understanding of surface water distribution on the Eastern Shores. Furthermore, the development of a water mapping protocol, in addition to allowing the effects of changes in past and future rainfall patterns to be examined, enables the water reserve in the greater Maputaland region to be mapped.

8.2 IMPORTANT RESULTS ARISING OUT OF THIS STUDY

In using spectral mixture analysis to map the mixing of water and vegetation at a sub-pixel level, the following trends are visible:

- Inundation on the Eastern shores is best interpreted in the light of seasonal rainfall patterns and not individual rainfall events.

- Surface water is concentrated around Lake Bhangazi, the Mfabeni swamp and in the wilderness area.
- Lake Bhangazi aside, virtually all the surface water on the Eastern Shores occurs in conjunction with emergent vegetation.
- Areas to the west and south-west of the Mfabeni, as well as the southern parts of the study area are rarely flooded.

In designing a water mapping protocol, this study has developed a number of new techniques while at the same time applying existing techniques in new ways. The protocol also provides a powerful tool for researching and modelling the distribution of water and wetlands. In particular, the following points are noteworthy:

- The use of spectral mixture analysis to map water-vegetation concentrations is unique when compared to other studies reviewed in the literature.
- A review of the literature has also not revealed any other remote sensing studies using cumulative rainfall as a verification of water mapping accuracy.
- The protocol has the advantage of being an image-based method and does not rely on ground truthing for verification.
- Determining the presence of water and emergent vegetation allows the presence of wetlands to be inferred. Not only does this allow wetlands to be delineated without using traditional wetland indicators such as soils and vegetation, it also provides a means of estimating the water reserve associated with wetlands.
- By establishing a link between surface water and cumulative rainfall, the protocol will allow the effect of past and future rainfall events on the distribution of surface water on the Eastern Shores to be modelled.

When interpreting the results of the water mapping protocol, a number of caveats should be remembered. Foremost among these are:

- The protocol does not map water that cannot be seen. As the protocol is based on spectral reflectance patterns of surface features, water will not be detected if it is obscured by vegetation or cloud.
- Interpretation of results in the presence of fire scars needs to be done with care. It has been shown that the presence of fresh fire scars leads to inaccurate spectral unmixing, resulting in an overestimation of the amount of surface water.

This section has summarised a number of important findings and issues raised by this research. Many of these findings will provide information valuable for the management of the Eastern Shores, particularly in light of it being part of a World Heritage Site. These findings will hopefully provide a stimulus for further research in the region.

8.3 RECOMMENDATIONS FOR FUTURE STUDIES

The research presented in this thesis, informed and influenced as it was by previous research described in the literature, has helped to provide a greater understanding of the surface waters and, by association, the wetlands of the Eastern Shores. At the same time, this research has raised new questions and presented new opportunities for further investigation.

8.3.1 Protocol validation

A number of assumptions were made during the development of the water mapping protocol. Some of these concerned the development of endmembers used to determine the mixing of water and vegetation, while others concerned the use of the Landsat Thematic Mapper. These assumptions suggest that a number of follow-up studies may be useful:

- **Verify the vegetation endmembers used in the protocol.** The principal components analysis revealed that three endmembers would be sufficient to unmix the spectral data in the study area. These endmembers were shown to be water, woody and non-woody vegetation. In defining the non-woody vegetation endmember, it was assumed that the spectral reflectance characteristics of wetland and grassland vegetation are similar, and that a grassland endmember would adequately represent all non-woody vegetation. Measuring the actual reflectance characteristics of both grassland and wetland vegetation would verify whether this assumption was valid.
- **Test whether the protocol works on other satellites.** The water mapping protocol was developed using the spectral and spatial resolution of the Landsat Thematic Mapper. The protocol needs to be tested on data measured by satellites that have different spatial and spectral characteristics. This will provide an indication of the transferability of the protocol.

In addition to testing the influence of the satellite platform and endmember selection on the water mapping protocol, the inputs and outputs of the protocol can also be tested. In particular, it would be useful to examine the following:

- **Use groundwater data to test the validity of the protocol.** A link has already been established between cumulative rainfall and surface water extent. There is a need to extend this link to groundwater levels. The establishment of such a link would allow groundwater levels to be used in place of rainfall for verifying the protocol outputs.
- **Examine the effects of fire scars on the protocol.** Analysis of fire scars in the study area revealed that these scars have spectral similarities to water. The effect of fire scars on mapping accuracy needs to be determined and ways of overcoming these effects need to be incorporated into the protocol.
- **Determine the applicability of the protocol to other areas of Maputaland and South Africa.** The water mapping protocol was developed using the environmental conditions present on the Eastern Shores of Lake St Lucia. The accuracy of the water mapping capability of the protocol still needs to be tested for other areas of South Africa.

8.3.2 Relating water distribution and concentration to wetlands

The aim of this research was to map the surface water of the Eastern Shores. This has resulted in a series of water concentration maps depicting the spatial and temporal distribution of surface water in the study area. The availability of these maps allows a number of follow-up studies to be conducted:

- **Comparison between water concentration and vegetation.** The water concentration maps indicate the distribution of water, usually in the presence of vegetation. A useful study would be to relate the different water concentration levels to wetland vegetation type, thereby allowing vegetation and wetland distribution maps for other regions to be produced based on the relationships established between water concentration and vegetation.
- **Relate water concentration to wetland hydroperiod.** Wetlands can be defined in terms of the hydroperiod, which describes the pattern of flooding in the wetland. The series of maps depicting water distribution and concentration that were

produced in this study provide an indication of the hydroperiod for the whole of the study area. Linking these patterns of inundation to actual hydroperiod definitions will allow the different types of wetlands on the Eastern Shores to be classified on the basis of both physical and biological characteristics.

8.3.3 Modelling

The development of a water mapping protocol, which uses an established link between surface water and cumulative rainfall, allows the modelling of different scenarios to be undertaken. These include:

- **Investigate the effects of global warming-induced changes in rainfall patterns on the distribution of surface water.** Most studies indicate that global warming will lead to changes in the world's rainfall. The effects of changing rainfall on the Eastern Shores, whether increasing or decreasing, can be examined by utilising the relationship that has been established between cumulative rainfall and surface water distribution.
- **Examine past patterns of surface water distribution based on historical rainfall patterns.** By knowing the current relationship between rainfall and surface water distribution, past patterns of water distribution can be deduced from historical rainfall patterns. These rainfall patterns can either be obtained directly (i.e. from rain gauge records) or be inferred from proxy indicators like tree rings or sediments.
- **Examine the effects of removing the Eastern Shores plantations.** The removal of the 5600 ha of commercial pine plantations, and the consequent reduction in evapotranspiration, is likely to have a measurable impact on the hydrology of the region. These impacts can be investigated by running the protocol without a forest mask, and then using topography and existing water distribution patterns to predict where surface water will reappear following the removal of plantations.
- **Examine the effects of sea level rise on surface water.** Rising sea levels, induced by global warming, are likely to cause higher groundwater levels on the Eastern Shores. If it were possible to establish a link between groundwater levels and surface water distribution (as was done between rainfall and surface water in this study), then the protocol could be used to examine the effects of sea level rise on the surface water of the Eastern Shores.

8.4 CONCLUDING REMARKS

This study, through the development and application of an image-based water mapping protocol, has shown that fluctuations in surface water on the Eastern Shores are driven mainly by cumulative rainfall. Almost all this water occurs in conjunction with emergent vegetation and is concentrated in Lake Bhangazi, the Mfabeni Swamp and the wilderness area. The protocol developed to map this surface water uses image-based methods and rainfall validation and will hopefully prove a valuable tool for delineating wetlands and for helping to determine their water reserve. This in turn will shed light on the structure of wetlands and the relationship between wetland structure and biodiversity. It is also hoped that the water distribution maps produced by this study will go a long way towards providing an understanding of the complex environmental interactions occurring on the Eastern Shores, thereby contributing to the effective management of this unique environment.

REFERENCES

Adams, J.B., Sabol, D.E., Kapos, V., Almeida Filho, R., Roberts, D.A., Smith, M.O. and Gillespie, A.R., 1995. Classification of Multispectral Images Based on Fractions of Endmembers: Application to Land-Cover Change in the Brazilian Amazon, *Remote Sensing of the Environment*, 52, 137-154.

Aldrich, S.A., Aldrich, F.T. and Rudd, R.D., 1971. An Effort to Identify the Canadian Forest-Tundra Ecotone Signature on Weather Satellite Imagery, *Remote Sensing of the Environment*, 2(1), 9-20.

Anuta, P.E. and MacDonald, R.B., 1971. Crop Surveys from Multiband Satellite Photography Using Digital Techniques, *Remote Sensing of the Environment*, 2(1), 53-67.

Ardö, J., Pilesjö, P. and Skidmore, A., 1997. Neural Networks, Multitemporal Landsat Thematic Mapper Data and Topographic Data to Classify Forest Damages in the Czech Republic, *Canadian Journal of Remote Sensing*, 23(3), 217-229.

Ashley, M.D. and Rea, J., 1975. Seasonal Vegetation Differences from ERTS Imagery, *Photogrammetric Engineering and Remote Sensing*, 41(6), 713-719.

Bateson, A. and Curtiss, B., 1996. A Method for Manual Endmember Selection and Spectral Unmixing, *Remote Sensing of the Environment*, 55, 229-243.

Binaghi, E., Brivio, P.A., Ghezzi, P., Rampini, A. and Zilioli, E., 1999. Investigating the Behaviour of Neural and Fuzzy-Statistical Classifiers in Sub-Pixel Land Cover Estimations, *Canadian Journal of Remote Sensing*, 25(2), 171-188.

Boresjö Bronge, L., 1999. Mapping Boreal Vegetation Using Landsat-TM and Topographic Map Data in a Stratified Approach, *Canadian Journal of Remote Sensing*, 25(5), 460-474.

Boresjö Bronge, L. and Näslund-Landenmark, B., 2002. Wetland classification for Swedish CORINE Land Cover adopting a semi-automatic interactive approach, *Canadian Journal of Remote Sensing*, 28(2), 139-155.

Bourgeau-Chavez, L.L., Smith, K.B., Brunzell, S.M., Kasischke, E.S., Romanowicz, E.A. and Richardson, C.J., 2005. Remote Monitoring of Regional Inundation Patterns and Hydroperiod in the Greater Everglades using Synthetic Aperture Radar, *Wetlands*, 25(1), 176-191.

Boyes, S., Brett, M.R., Combrink, A., Long, B., Nkhoma, R., Shepherd, A. and Steytler, B., 2002. *The Greater St Lucia Wetland Park - Critical Issues, Analysis and Management Recommendations*, Joint report prepared for Protected Area Management Course of the Masters in Environment and Development, Centre for Environment and Development, University of Natal, Pietermaritzburg.

Braga, C.Z.F., Vianna, M.L. and Kjerfve, B., 2003. Environmental characterization of a hypersaline coastal lagoon from Landsat-5 Thematic Mapper data. *International Journal of Remote Sensing*, 24(16), 3219-3234.

Brooks, D.J., 1975. LANDSAT Measures of Water Clarity. *Photogrammetric Engineering and Remote Sensing*, 41(10), 1269-1272.

Chavez, P.S., 1996. Image-Based Atmospheric Corrections - Revisited and Improved. *Photogrammetric Engineering and Remote Sensing*, 62(9), 1025-1036.

Chavez, P.S., 1988. An Improved Dark-Object Subtraction Technique for Atmospheric Scattering Correction of Multispectral Data. *Remote Sensing of the Environment*, 24, 459-479.

Chen, Z., Elvidge, C.D. and Groeneveld, D.P., 1999. Vegetation Change Detection Using High Spectral Resolution Vegetation Indices. In: *Remote Sensing Change Detection: Environmental Monitoring Methods and Applications*, Lunetta, R.S. and Elvidge, C.D. (Eds.), 1st Edition, 181-190, Taylor and Frances, London.

Cihlar, J., Latifovic, R. and Beaubien, J., 2000. A Comparison of Clustering Strategies for Unsupervised Classification. *Canadian Journal of Remote Sensing*, 26(5), 446-454.

Congalton, R.G., 1991. A Review of Assessing the Accuracy of Classifications of Remotely Sensed Data. *Remote Sensing of the Environment*, 37, 35-46.

Congalton, R.G. and Green, K., 1999. *Assessing the Accuracy of Remotely Sensed Data: Principles and Practices*, 1st Edition, Lewis Publishers, Boca Raton.

CSIR/ARC. Thompson, M.W., 1998. CSIR/ARC National Land-Cover Database Project, *Data Users Manual: final report reference*, CSIR contract report ENV/P/C 98122.

De Haan, J.F., Hovenier, J.W., Kokke, J.M.M. and Van Stokkom, H.T.C., 1991. Removal of Atmospheric Influences on Satellite-Borne Imagery: A Radiative Transfer Approach. *Remote Sensing of the Environment*, 37, 1-21.

Dewidar, K.H.M. and Frihy, O.E., 2003. Thematic Mapper analysis to identify geomorphologic and sediment texture of El Tineh plain, north-western coast of Sinai, Egypt. *International Journal of Remote Sensing*, 24(11), 2377-2385.

Diab, R.D., 1995. *Wind Atlas of South Africa*. Report prepared for the Department of Mineral and Energy Affairs, Pretoria.

Donoghue, D.N.M., 2000. Remote sensing: sensors and applications. *Physical Geography*, 24(3), 407-414.

DWAF, 2003. *A practical field procedure for identification and delineation of wetlands and riparian areas*. Department of Water Affairs and Forestry, South Africa. February 2003.

Eastman, R.J., 2001. *Guide to GIS and Image Processing*. Clark Labs, Worcester, MA.

Eckhardt, D.W., Verdin, J.P. and Lyford, G.R., 1990. Automated Update of an Irrigated Lands GIS Using SPOT HRV Imagery, *Photogrammetric Engineering and Remote Sensing*, 56(11), 1515-1522.

Edgley, E. and Werstak, C.E., 1998. Use of Landsat Thematic Data for Waterfowl Habitat Inventory in Idaho and Western Wyoming, Online, <http://www.nr.usu.edu/~lcma/duckhab/duckfinrpt.htm> (accessed 15 December 2004).

Ellery, W.N., 2006a, pers. comm. Private correspondence with Professor Ellery, School of Environmental Sciences, University of KwaZulu-Natal, January 2006.

Ellery, W.N., 2006b, pers. comm. Private correspondence with Professor Ellery, School of Environmental Sciences, University of KwaZulu-Natal, June 2006.

Ellery, W.N. and Mentis, M.T., 1992. How old are South Africa's grasslands?, In: *Forest - Savanna Boundaries*, Furley, P., Proctor, J. and Ratter, J.A. (Eds.), 283-292, Chapman and Hall, London.

Elmore, A.J., Mustard, J.F., Manning, S.J. and Lobell, D.B., 1999. Precision and Accuracy of Remotely Sensed Data for Quantitative Analysis of Vegetation Change in a Semi-arid Region, *Proceedings of the International Symposium on Digital Earth*, 1-8. Science Press.

Emrahoğlu, N., Yeğinlil, I., Peştemalci, V., Şenkal, O. and Kandirmaz, H.M., 2003. Comparison of a new algorithm with the supervised classifications, *International Journal of Remote Sensing*, 24(4), 649-655.

Foody, G.M., Lucas, R.M., Curran, P.J. and Honzak, M., 1996. Estimation of the areal extent of land cover classes that only occur at a sub-pixel level, *Canadian Journal of Remote Sensing*, 22(4), 428-432.

Frazier, P.S. and Page, K.J., 2000. Water Body Detection and Delineation with Landsat TM Data. *Photogrammetric Engineering and Remote Sensing*, 66(12), 1461-1467.

Frazier, P., Page, K., Louis, J., Briggs, S. and Robertson, A.I., 2003. Relating wetland inundation to river flow using Landsat TM data, *International Journal of Remote Sensing*, 24(19), 3755-3770.

Gao, B.-C., 1996. NDWI - A Normalized Difference Water Index for Remote Sensing of Vegetation Liquid Water From Space, *Remote Sensing of the Environment*, 58, 257-266.

Gausman, H.W., Gerbermann, A.H. and Wiegland, C.L., 1975. Use of ERTS-1 Data to Detect Chlorotic Grain Sorghum, *Photogrammetric Engineering and Remote Sensing*, 41(2), 177-179.

Glackin, D.L., 1998. International Space-Based Remote Sensing Overview: 1980-2007. *Canadian Journal of Remote Sensing*, 24(3), 307-314.

Greenwood, J.A., Nathan, A., Neumann, G., Pierson, W.J., Jackson, F.C. and Pease, T.E., 1969a. Radar Altimetry from a Spacecraft and Its Potential Applications to Geodesy, *Remote Sensing of the Environment*, 1(1), 59-70.

Greenwood, J.A., Nathan, A., Neumann, G., Pierson, W.J., Jackson, F.C. and Pease, T.E., 1969b. Oceanographic Applications of Radar Altimetry from a Spacecraft, *Remote Sensing of the Environment*, 1(1), 71-80.

Hadjimitsis, D.G., Clayton, C.R.I. and Hope, V.S., 2004. An assessment of the effectiveness of atmospheric correction algorithms through the remote sensing of some reservoirs, *International Journal of Remote Sensing*, 25(18), 3651-3674.

Hall, F.G., Strebel, D.E., Nickeson, J.E. and Goetz, S.J., 1991. Radiometric Rectification: Toward a Common Radiometric Response Among Multidate, Multisensor Images, *Remote Sensing of the Environment*, 35, 11-27.

Harris, R., 2003. Remote sensing of agriculture change in Oman, *International Journal of Remote Sensing*, 24(23), 4835-4852.

Hutchison, I.P.G. and Pitman, W.V., 1973. *Hydrology and Climatology of the St. Lucia Lake system*, Report No. 1/73, Joint CSIR - University Council Hydrological Research Unit report.

Jensen, J.R., Christensen, E.J. and Sharitz, R., 1984. Nontidal Wetland Mapping in South Carolina Using Airborne Multispectral Scanner Data, *Remote Sensing of the Environment*, 16, 1-12.

Jensen, J.R., Rutchey, K., Koch, M.S. and Narumalani, S., 1995. Inland Wetland Change Detection in the Everglades Water Conservation Area 2A Using a Time Series of Normalised Remotely Sensed Data, *Photogrammetric Engineering and Remote Sensing*, 61(2), 199-209.

Justice, C. and Townshend, J., 1982. A Comparison of Unsupervised Classification Procedures on Landsat MSS Data for an Area of Complex Surface Conditions in Basilicata, Southern Italy, *Remote Sensing of the Environment*, 12, 407-420.

Kauth, R.J. and Thomas, G.S., 1976. The Tasseled Cap - a graphic description of the spectral-temporal development of agricultural crops as seen by Landsat, *Proceedings of the Symposium on Machine Processing of Remotely Sensed Data*, 4b41-4b51, Purdue University, West Lafayette.

Keddy, P.A., 2000. *Wetland Ecology: Principles and Conservation*, Cambridge University Press.

Kelbe, B., 2005, pers. comm. Private e-mail correspondence with Professor Bruce Kelbe, Department of Hydrology, University of Zululand, 2 December 2005.

Klemas, V., Borchardt, J.F. and Treasure, W.M., 1973. Suspended Sediment Observations from ERTS-1, *Remote Sensing of the Environment*, 2(4), 205-221.

Kondratyev, K.Y., Vassilyev, O.B., Grigoryev, A.A. and Ivanian, G.A., 1973. An Analysis of the Earth's Resources Satellite (ERTS-1) Data, *Remote Sensing of the Environment*, 2(4), 273-283.

Lawrence, R.D. and Herzog, J.H., 1975. Geology and Forestry Classification from ERTS-1 Digital Data, *Photogrammetric Engineering and Remote Sensing*, 41(10), 1241-1251.

Lillesand, T.M. and Kiefer, R.W., 2000. *Remote Sensing and Image Interpretation*, 4th Edition, John Wiley & Sons, Inc., New York.

Lu, D., Mausel, P., Batistella, M. and Moran, E., 2004. Comparison of Land-Cover Classification Methods in the Brazilian Amazon Basin, *Photogrammetric Engineering and Remote Sensing*, 70(6), 723-731.

Lunetta, R.S., 1999. Applications, Project Formulations, and Analytical Approach, In: *Remote Sensing Change Detection: Environmental Monitoring Methods and Applications*, Lunetta, R.S. and Elvidge, C.D. (Eds.), 1st Edition, 1-19, Taylor and Frances, London.

Lunetta, R.S. and Balogh, M.E., 1999. Application of Multi-Temporal Landsat 5 TM Imagery for Wetland Identification, *Photogrammetric Engineering and Remote Sensing*, 65(11), 1303-1310.

Malthus, T.J. and Mumby, P.J., 2003. Remote sensing of the coastal zone: an overview and priorities for future research, *International Journal of Remote Sensing*, 24(13), 2805-2815.

Markham, B.L., Boncyk, W.C., Helder, D.L. and Barker, J.L., 1997. Landsat-7 Enhanced Thematic Mapper Plus Radiometric Calibration, *Canadian Journal of Remote Sensing*, 23(4), 318-332.

Masry, S.E., Crawley, B.G. and Hilborn, W.H., 1975. Difference Detection, *Photogrammetric Engineering and Remote Sensing*, 41(9), 1145-1148.

McCauley, S. and Goetz, S.J., 2004. Mapping residential patterns using multitemporal Landsat data and a decision-tree classifier, *International Journal of Remote Sensing*, 25(6), 1077-1094.

Mertes, L.A.K., 1997. Documentation and significance of the perirheic zone on inundated floodplains, *Water Resources Research*, 33(7), 1749-1762.

Mertes, L.A.K., Daniel, D.L., Melack, J.M., Nelson, B., Martinelli, L.A. and Forsberg, B.R., 1995. Spatial patterns of hydrology, geomorphology, and vegetation on the floodplain of the Amazon River in Brazil from a remote sensing perspective, *Geomorphology*, 13, 215-232.

Mertes, L.A.K., Smith, M.O. and Adams, J.B., 1993. Estimating Suspended Sediment Concentrations in Surface Waters of the Amazon River Wetlands from Landsat Images, *Remote Sensing of the Environment*, 43, 281-301.

Mispan, M.R. and Mather, P.M., 1997. Multi-Sensor Radiometric Correction: A Case Study from Malaysia. Online, <http://www.gisdevelopment.net/aars/acrs/1997/ps2/ps4022pf.htm> (accessed 23 August 2004).

Munyati, C., 2000. Wetland change detection on the Kafue Flats, Zambia, by classification of a multitemporal remote sensing image dataset. *International Journal of Remote Sensing*, 21(9), 1787-1806.

Myneni, R.B. and Asrar, G., 1994. Atmospheric Effects and Spectral Vegetation Indices, *Remote Sensing of the Environment*, 47, 390-402.

National Water Act, 1998. Act No 36 of 1998. *Government Gazette: Republic of South Africa*, Vol. 398, No 19182, 26 August 1998.

Pedroni, L., 2003. Improved classification of Landsat Thematic Mapper data using modified prior probabilities in large and complex landscapes. *International Journal of Remote Sensing*, 24(1), 91-113.

Pillay, D.L., 2001. An Investigation into Mapping Wetlands Using Satellite Imagery: The Case of Midmar Sub-Catchment. Unpublished M.Sc. thesis, University of Natal, Pietermaritzburg.

Ricotta, C., 2004. Evaluating the classification accuracy of fuzzy thematic maps with a simple parametric measure. *International Journal of Remote Sensing*, 25(11), 2169-2176.

Ringrose, S., Vanderpost, C. and Matheson, W., 2003. Mapping ecological conditions in the Okavango delta, Botswana using fine and coarse resolution systems including simulated SPOT vegetation imagery. *International Journal of Remote Sensing*, 24(5), 1029-1052.

Roberts, D.A., Batista, G.T., Pereira, J.L.G, Waller, E.K. and Nelson, B.W., 1999. Change Identification Using Multitemporal Spectral Mixture Analysis: Applications in Eastern Amazonia, In: *Remote Sensing Change Detection: Environmental Monitoring Methods and Applications*, Lunetta, R.S. and Elvidge, C.D. (Eds.), 1st Edition, 137-161, Taylor and Frances, London.

Sader, S.A., Ahl, D. and Liou, W.-S., 1995. Accuracy of Landsat-TM and GIS Rule-Based Methods for Forest Wetland Classification in Maine. *Remote Sensing of the Environment*, 53, 133-144.

Salvador, R. and San-Miguel-Ayanz, J., 2003. The effect of histogram discontinuities on spectral information and non-supervised classifiers. *International Journal of Remote Sensing*, 24(1), 115-131.

San Miguel-Ayanz, J. and Biging, G.S., 1997. Comparison of Single-Stage and Multi-Stage Classification Approaches for Cover Type Mapping with TM and SPOT Data. *Remote Sensing of the Environment*, 59, 92-104.

Schott, J.R., Salvaggio, C. and Volchok, W.J., 1988. Radiometric Scene Normalization Using Pseudoinvariant Features. *Remote Sensing of the Environment*, 26, 1-16.

Schowengerdt, R.A., 1997. *Remote Sensing, Models and Methods for Image Processing*, 2nd Edition, Academic Press, San Diego.

Settle, J.J. and Drake, N.A., 1993. Linear mixing and the estimation of ground cover proportions, *International Journal of Remote Sensing*, 14(6), 1159-1177.

Shaghude, Y.W., Wannäs, K.O. and Lundén, B., 2003. Assessment of shoreline changes in the western side of Zanzibar channel using satellite remote sensing, *International Journal of Remote Sensing*, 24(23), 4953-4967.

Shao, G., Liu, D. and Zhao, G., 2001. Relationships of Image Classification Accuracy and Variation of Landscape Statistics. *Canadian Journal of Remote Sensing*, 27(1), 33-43.

Shoshany, M., 2000. Satellite remote sensing of natural Mediterranean vegetation: a review within an ecological context, *Progress in Physical Geography*, 24(2), 153-178.

Small, C., 2001. Estimation of urban vegetation abundance by spectral mixture analysis, *International Journal of Remote Sensing*, 22(7), 1305-1334.

Smith, R.J., 2001. Designing an integrated protected area network for Maputaland, South Africa, Unpublished Ph.D. thesis, Durrell Institute of Conservation & Ecology, University of Kent at Canterbury.

Strahler, A.H., 1980. The Use of Prior Probabilities in Maximum Likelihood Classification of Remotely Sensed Data, *Remote Sensing of the Environment*, 10, 135-163.

Tanre, D., Deroo, C., Dahaut, P., Herman, M. and Morcrette, J.J., 1990. Description of a computer code to simulate the satellite signal in the solar spectrum: the 5S code, *International Journal of Remote Sensing*, 11, 659-688.

Tassan, S. and Ribera d'Alcalá, M., 1993. Water Quality Monitoring by Thematic Mapper in Coastal Environments. A Performance Analysis of Local Biooptical Algorithms and Atmospheric Correction Procedures. *Remote Sensing of the Environment*, 45, 177-191.

Teillet, P.M., 1997. A Status Overview of Earth Observation Calibration/Validation for Terrestrial Applications, *Canadian Journal of Remote Sensing*, 23(4), 291-298.

Teillet, P.M. and Fedosejevs, G., 1995. On the Dark Target Approach to Atmospheric Correction of Remotely Sensed Data, *Canadian Journal of Remote Sensing*, 21(4), 374-387.

Théau, J. and Duguay, C.R., 2004. Lichen mapping in the summer range of the George River caribou herd using Landsat TM imagery, *Canadian Journal of Remote Sensing*, 30(6), 867-881.

Thompson, M., Marnewick, G., Bell, S., Kotze, D., Muller, J., Cox, D. and Clark, R., 2002. Satellite Image Mapping. In: *A Methodology Proposed for a South African National Wetland Inventory*. Report prepared for the Wetlands Conservation Programme, Department of Environmental Affairs and Tourism.

Thompson, G., 2002. The dynamics of ecological change in an era of political transformations: An environmental history of the Eastern Shores of Lake St Lucia. In: *South Africa's Environmental History: Cases & Comparisons*, Dovers, S., Edgecombe, R. and Guest, B. (Eds.), 191-212. Ohio University Press, Athens.

Ustin, S.L., Roberts, D.A. and Hart, Q.J., 1999. Seasonal Vegetation Patterns in a California Coastal Savanna Derived from Advanced Visible/Infrared Imaging Spectrometer (AVIRIS) Data. In: *Remote Sensing Change Detection: Environmental Monitoring Methods and Applications*, Lunetta, R.S. and Elvidge, C.D. (Eds.), 1st Edition, 163-180, Taylor and Frances, London.

Van der Meer, F. and De Jong, S. M., 2000. Improving the results of spectral unmixing of Landsat Thematic Mapper imagery by enhancing the orthogonality of end-members, *International Journal of Remote Sensing*, 21(15), 2781-2797.

Vermote E., Tanré D., Deuzé J. L., Herman M. and Morcrette J. J., 1997. *Second Simulation of the Satellite Signal in the Solar Spectrum (6S): User Guide Version 2.*

Vicente-Serrano, S.M., Pons-Fernández, X. and Cuadrat-Prats, J.M., 2004. Mapping soil moisture in the central Ebro river valley (northeast Spain) with Landsat and NOAA satellite imagery: a comparison with meteorological data, *International Journal of Remote Sensing*, 25(20), 4325-4350.

Vrdoljak, S.M., 2004. Spatial and temporal dynamics of freshwater wetlands on the Eastern Shores of St Lucia, as reflected by their macrofaunal composition and distribution, Unpublished M.Sc. thesis, University of KwaZulu-Natal, Pietermaritzburg.

Walsh, B.J., 2004. The Use of Remote Sensing to Map Swamp Forest of the Greater St Lucia Wetland Park. Unpublished B.Sc.(Hons) thesis, University of KwaZulu-Natal, Durban.

Wang, F., 1990. Improving Remote Sensing Image Analysis through Fuzzy Information Representation, *Photogrammetric Engineering and Remote Sensing*, 56(8), 1163-1169.

Wang, J., Shang, J., Brisco, B. and Brown, R.J., 1998. Evaluation of Multidate ERS-1 and Multispectral Landsat Imagery for Wetland Detection in Southern Ontario, *Canadian Journal of Remote Sensing*, 24(1), 60-68.

Wannenburgh, A. and Mabena, S., 2002. National Indigenous Forest Inventory. In: *Multiple Use Management of Natural Forests and Savanna Woodlands: Policy Refinements and Scientific Progress*, Seydack, A.H.W., Vorster, T., Vermuelen, W.S. and Van der Merwe, I.J. (Eds.), 79-90, Proceedings of Natural Forests and Savanna Woodlands Symposium III, Kruger National Park, 6-9 May 2002.

Watkeys, M.K., Mason, T.R. and Goodman, P.S., 1993. The rôle of geology in the development of Maputaland, South Africa, *Journal of African Earth Sciences*, 16(1), 1-16.

Wickware, G.M., Hélie, R.G. and Strome, W.M., 1991. Quantitative assessment of surface water resources in Quebec and the Kejimkujik calibrated watershed in Nova Scotia: A remote sensing approach, *Canadian Journal of Remote Sensing*, 17(1), 56-62.

Wong, K.W., 1975. Geometric and Cartographic Accuracy of ERTS-1 Imagery, *Photogrammetric Engineering and Remote Sensing*, 41(5), 621-635.

Appendix 1: Normalisation equations

Regression equations used to perform relative radiometric normalisation of the bands from the six target images:

23 July 1991

```
band1_normalised = 0.529 * [band1] - 18.872
band2_normalised = 1.177 * [band2] - 13.524
band3_normalised = 1.021 * [band3] -  8.358
band4_normalised = 1.191 * [band4] -  5.588
band5_normalised = 0.771 * [band5] -  2.240
band7_normalised = 1.159 * [band7] -  2.657
```

20 March 2001

```
band1_normalised = 0.328 * [band1] - 17.559
band2_normalised = 0.428 * [band2] - 14.512
band3_normalised = 0.392 * [band3] -  8.548
band4_normalised = 0.866 * [band4] -  7.817
band5_normalised = 0.522 * [band5] -  4.528
band7_normalised = 0.550 * [band7] -  4.506
```

24 April 2002

```
band1_normalised = 0.356 * [band1] - 16.056
band2_normalised = 0.432 * [band2] - 10.534
band3_normalised = 0.407 * [band3] -  6.283
band4_normalised = 0.625 * [band4] -  6.626
band5_normalised = 0.577 * [band5] -  4.738
band7_normalised = 0.604 * [band7] -  4.878
```

13 July 2002

```
band1_normalised = 0.543 * [band1] - 26.346
band2_normalised = 0.648 * [band2] - 20.023
band3_normalised = 0.557 * [band3] - 12.084
band4_normalised = 0.781 * [band4] - 10.062
band5_normalised = 0.674 * [band5] -  5.390
band7_normalised = 0.694 * [band7] -  5.434
```

15 September 2002

```
band1_normalised = 0.310 * [band1] - 15.814
band2_normalised = 0.392 * [band2] - 12.673
band3_normalised = 0.355 * [band3] -  7.435
band4_normalised = 0.796 * [band4] -  7.036
band5_normalised = 0.476 * [band5] -  4.268
band7_normalised = 0.478 * [band7] -  4.133
```

17 October 2002

```
band1_normalised = 0.410 * [band1] - 33.629
band2_normalised = 0.449 * [band2] - 23.909
band3_normalised = 0.389 * [band3] - 16.320
band4_normalised = 0.834 * [band4] - 14.041
band5_normalised = 0.456 * [band5] -  6.002
band7_normalised = 0.425 * [band7] -  5.650
```

Appendix 2: Transformation Data for the Reference Image

Resample : Summary of Transformation of reference image

Computed polynomial surface : Quadratic (based on 12 control points)

Coefficient	X	Y
b0	-10304.764422133564950	104145.766893818974500
b1	0.032434177135986	0.007857693095627
b2	-0.004612558040406	0.031816618904869
b3	-0.000000001460287	-0.000000000123722
b4	-0.000000000091519	0.000000000849009
b5	0.000000000105791	-0.000000000184827

Note : Formula shown is the back transformation (new to old).

Control points used in the transformation :

Old X	Old Y	New X	New Y	Residual
2526.827370	1676.848590	-83531.720000	-3149383.800000	1.290376
1558.266650	4745.134440	-97679.060000	-3053799.000000	0.033188
3808.409860	5317.795930	-34226.370000	-3046585.660000	0.162809
2864.211090	3901.853150	-63004.350000	-3084965.180000	1.249575
2848.692060	4670.034570	-59839.550000	-3062179.060000	0.668011
2767.595760	4553.158020	-62806.320000	-3065224.750000	0.503075
2586.676470	346.911560	-88066.470000	-3189034.760000	0.242723
2559.191980	1834.309820	-81879.300000	-3144832.080000	1.003087
2191.700410	2245.807790	-90764.600000	-3130885.630000	1.050124
2427.446520	2913.710920	-80643.220000	-3112261.900000	1.259004
3323.852170	2133.525360	-67778.370000	-3139586.670000	0.092345
3028.953110	2038.984940	-66972.150000	-3140966.170000	0.230289

Overall RMS = 0.804569

Note : RMS Error is expressed in input image units.

Appendix 3: Correlation Matrices for the Spectral and Component Datasets

23 July 1991

	Band 1	*Band 2*	*Band 3*	*Band 4*	*Band 5*	*Band 7*
Band 1	**1.000**					
Band 2	0.871	**1.000**				
Band 3	0.845	0.962	**1.000**			
Band 4	0.012	0.277	0.263	**1.000**		
Band 5	0.140	0.393	0.428	0.799	**1.000**	
Band 7	0.269	0.490	0.540	0.655	0.931	**1.000**

	Comp 1	*Comp 2*	*Comp 3*	*Comp 4*	*Comp 5*	*Comp 6*
Comp 1	**1.000**					
Comp 2	0.000	**1.000**				
Comp 3	0.001	0.000	**1.000**			
Comp 4	0.003	-0.001	-0.012	**1.000**		
Comp 5	-0.005	0.005	-0.005	-0.072	**1.000**	
Comp 6	0.001	-0.006	-0.028	0.058	-0.002	**1.000**

20 March 2001

	Band 1	*Band 2*	*Band 3*	*Band 4*	*Band 5*	*Band 7*
Band 1	**1.000**					
Band 2	0.888	**1.000**				
Band 3	0.828	0.963	**1.000**			
Band 4	-0.138	0.172	0.153	**1.000**		
Band 5	-0.080	0.220	0.270	0.835	**1.000**	
Band 7	0.034	0.293	0.381	0.658	0.939	**1.000**

	Comp 1	*Comp 2*	*Comp 3*	*Comp 4*	*Comp 5*	*Comp 6*
Comp 1	**1.000**					
Comp 2	0.000	**1.000**				
Comp 3	0.000	-0.004	**1.000**			
Comp 4	-0.006	-0.003	0.004	**1.000**		
Comp 5	0.014	0.010	-0.005	0.128	**1.000**	
Comp 6	-0.008	-0.070	0.047	-0.091	0.168	**1.000**

7 May 2001

	Band 1	*Band 2*	*Band 3*	*Band 4*	*Band 5*	*Band 7*
Band 1	**1.000**					
Band 2	0.900	**1.000**				
Band 3	0.829	0.948	**1.000**			
Band 4	-0.120	0.131	0.165	**1.000**		
Band 5	-0.055	0.198	0.296	0.829	**1.000**	
Band 7	0.059	0.283	0.406	0.647	0.932	**1.000**

	Comp 1	*Comp 2*	*Comp 3*	*Comp 4*	*Comp 5*	*Comp 6*
Comp 1	**1.000**					
Comp 2	0.001	**1.000**				
Comp 3	0.001	-0.005	**1.000**			
Comp 4	0.009	0.019	-0.016	**1.000**		
Comp 5	-0.018	-0.006	0.011	0.117	**1.000**	
Comp 6	-0.011	-0.046	0.059	0.047	-0.041	**1.000**

24 April 2002

	Band 1	*Band 2*	*Band 3*	*Band 4*	*Band 5*	*Band 7*
Band 1	**1.000**					
Band 2	0.842	**1.000**				
Band 3	0.768	0.961	**1.000**			
Band 4	-0.030	0.273	0.268	**1.000**		
Band 5	0.097	0.379	0.441	0.837	**1.000**	
Band 7	0.260	0.497	0.577	0.694	0.951	**1.000**

	Comp 1	*Comp 2*	*Comp 3*	*Comp 4*	*Comp 5*	*Comp 6*
Comp 1	**1.000**					
Comp 2	0.000	**1.000**				
Comp 3	0.000	0.000	**1.000**			
Comp 4	0.006	-0.016	-0.006	**1.000**		
Comp 5	0.001	-0.001	-0.016	0.096	**1.000**	
Comp 6	0.006	-0.042	0.008	0.028	0.181	**1.000**

13 July 2002

	Band 1	*Band 2*	*Band 3*	*Band 4*	*Band 5*	*Band 7*
Band 1	**1.000**					
Band 2	0.751	**1.000**				
Band 3	0.655	0.915	**1.000**			
Band 4	-0.098	0.322	0.467	**1.000**		
Band 5	0.084	0.451	0.680	0.831	**1.000**	
Band 7	0.202	0.515	0.743	0.694	0.955	**1.000**

	Comp 1	*Comp 2*	*Comp 3*	*Comp 4*	*Comp 5*	*Comp 6*
Comp 1	**1.000**					
Comp 2	0.000	**1.000**				
Comp 3	0.000	0.000	**1.000**			
Comp 4	-0.003	-0.002	-0.015	**1.000**		
Comp 5	0.013	0.000	0.007	0.018	**1.000**	
Comp 6	0.009	-0.004	-0.002	0.047	0.215	**1.000**

15 September 2002

	Band 1	*Band 2*	*Band 3*	*Band 4*	*Band 5*	*Band 7*
Band 1	**1.000**					
Band 2	0.865	**1.000**				
Band 3	0.753	0.936	**1.000**			
Band 4	-0.145	0.223	0.242	**1.000**		
Band 5	-0.014	0.284	0.380	0.805	**1.000**	
Band 7	0.099	0.341	0.461	0.621	0.943	**1.000**

	Comp 1	*Comp 2*	*Comp 3*	*Comp 4*	*Comp 5*	*Comp 6*
Comp 1	**1.000**					
Comp 2	0.000	**1.000**				
Comp 3	0.000	0.000	**1.000**			
Comp 4	-0.008	0.002	-0.011	**1.000**		
Comp 5	0.006	0.018	0.004	-0.073	**1.000**	
Comp 6	-0.013	-0.006	-0.072	-0.045	0.024	**1.000**

17 October 2002

	Band 1	*Band 2*	*Band 3*	*Band 4*	*Band 5*	*Band 7*
Band 1	1.000					
Band 2	0.768	1.000				
Band 3	0.703	0.954	1.000			
Band 4	-0.359	0.194	0.186	1.000		
Band 5	-0.164	0.272	0.329	0.799	1.000	
Band 7	-0.168	0.269	0.326	0.801	0.998	1.000

	Comp 1	*Comp 2*	*Comp 3*	*Comp 4*	*Comp 5*	*Comp 6*
Comp 1	1.000					
Comp 2	-0.001	1.000				
Comp 3	0.001	0.003	1.000			
Comp 4	0.013	0.009	0.044	1.000		
Comp 5	0.000	0.065	-0.018	0.493	1.000	
Comp 6	0.101	-0.027	0.018	-0.002	-0.026	1.000

Appendix 4: Unsupervised Cluster Classifications

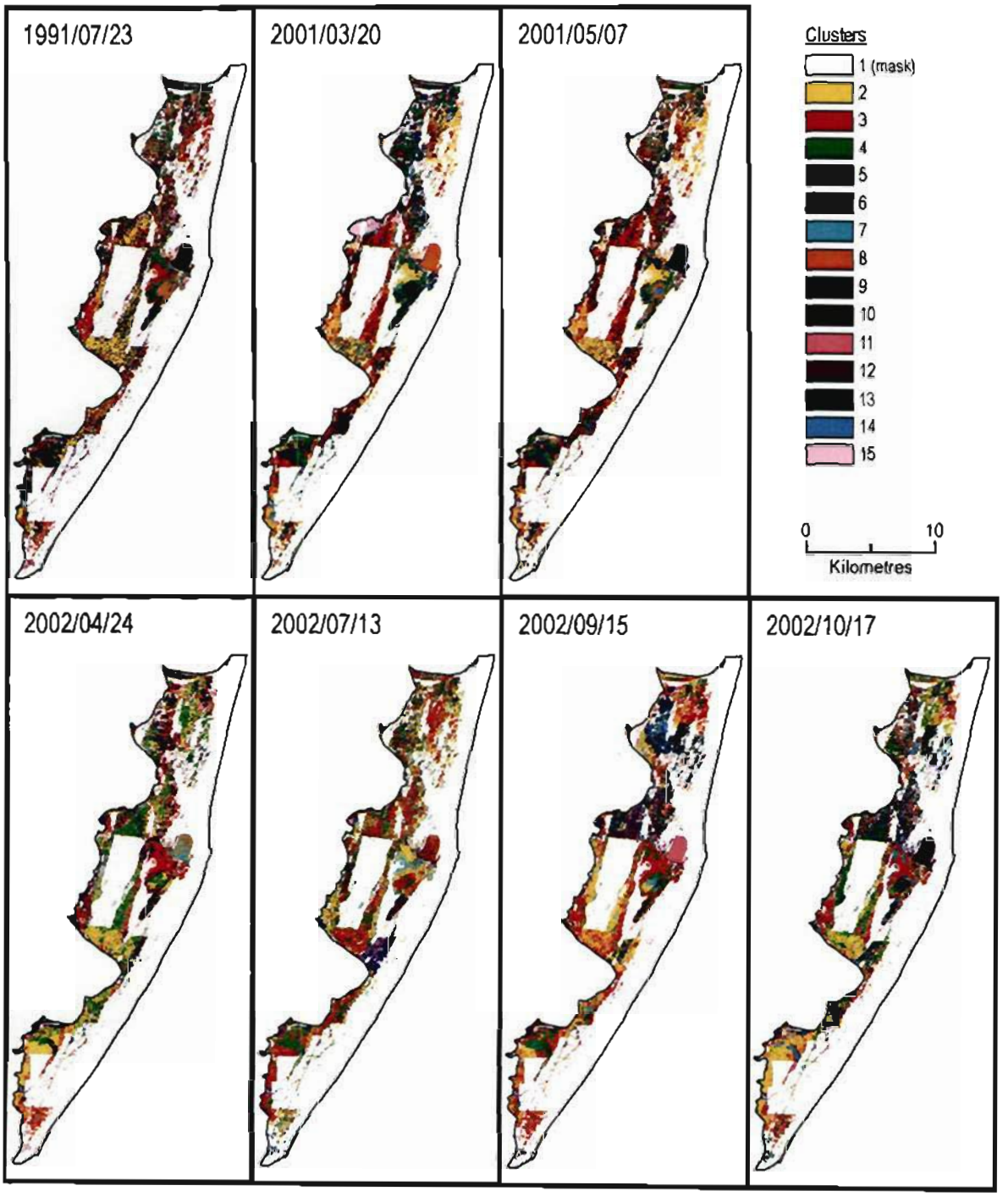

Figure A4.1: Clusters produced from the spectral data.

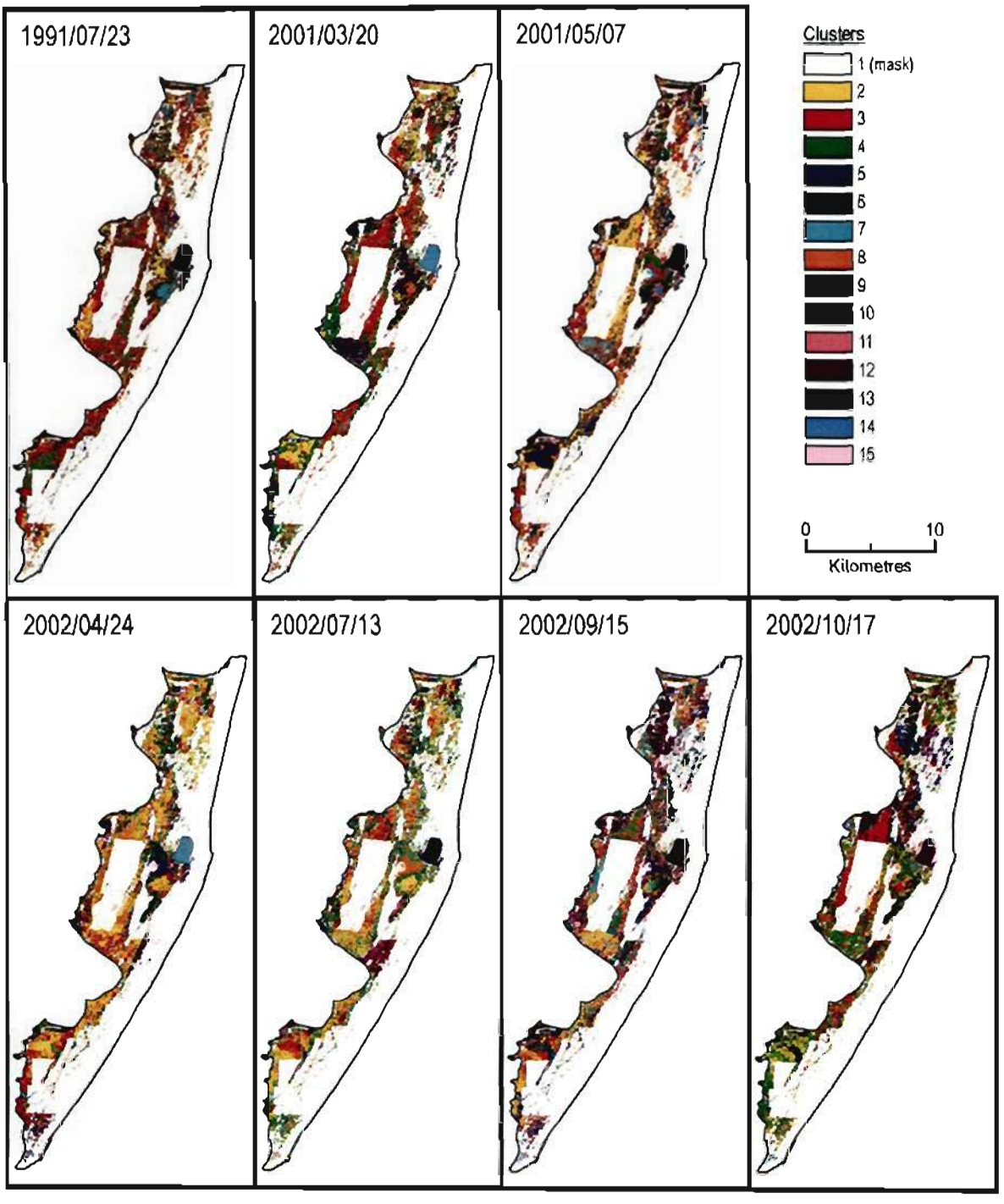

Figure A4.2: Clusters produced from the component data.

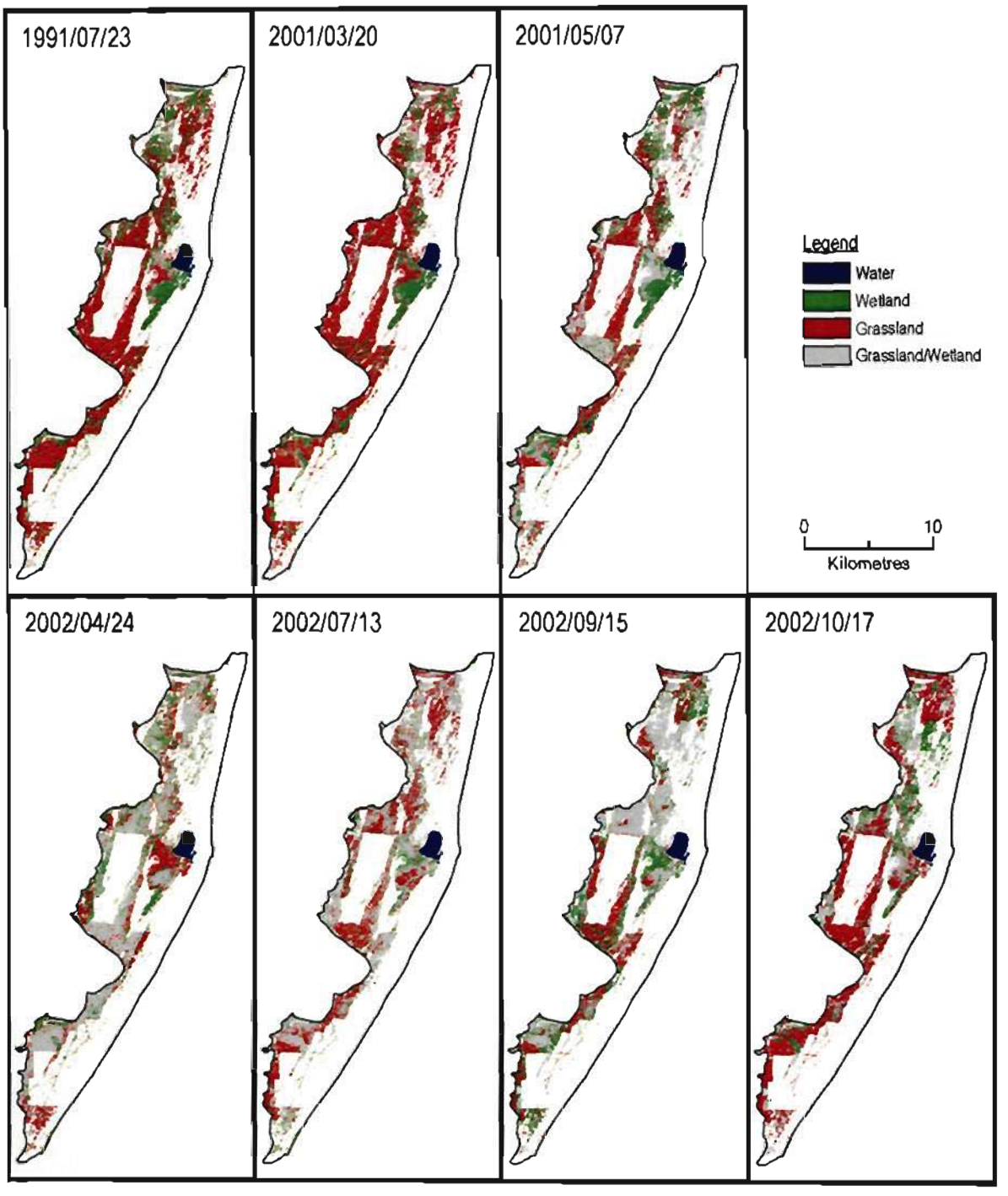

Figure A4.3: Classification of clusters produced from the spectral data.

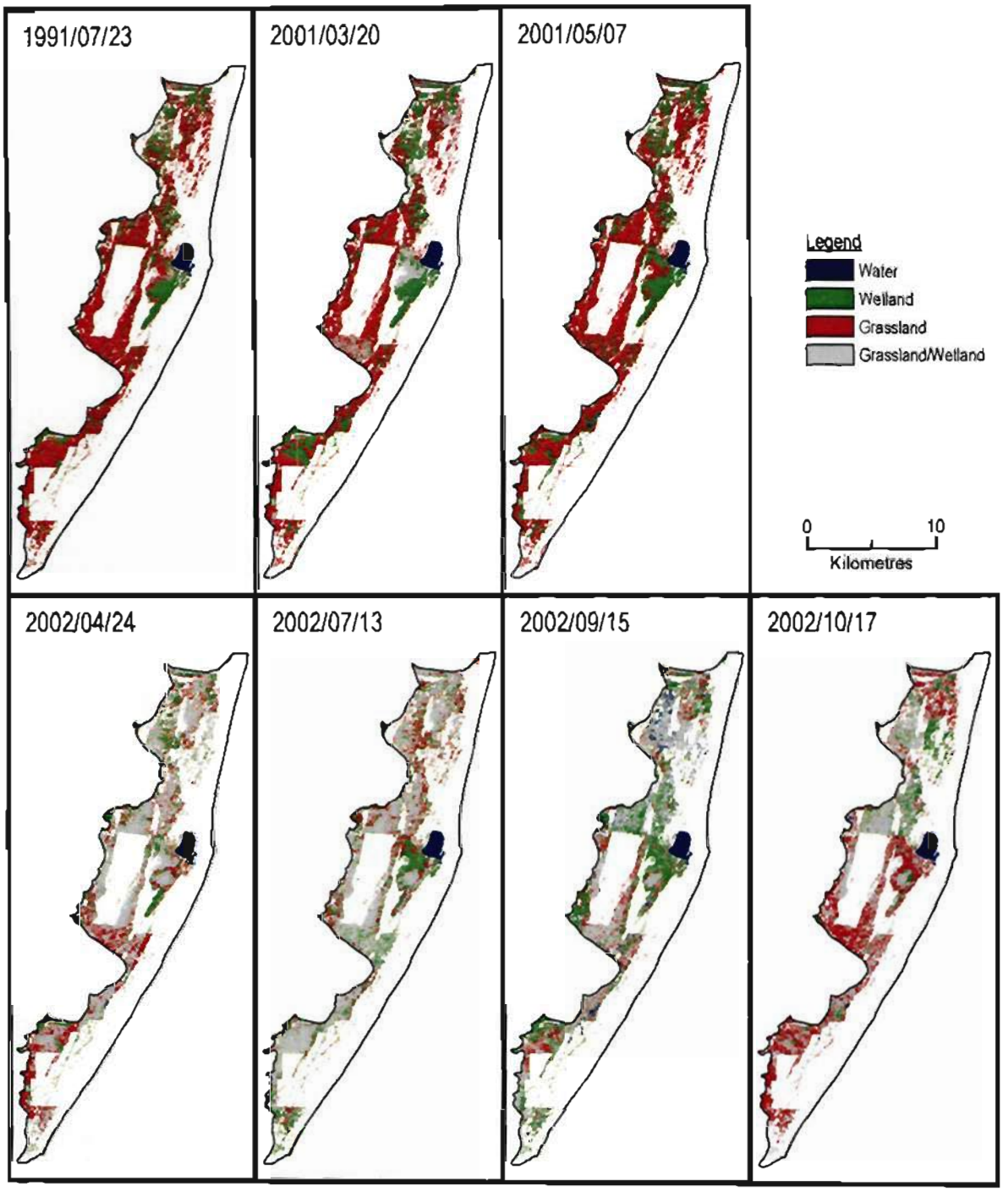

Figure A4.4: Classification of clusters produced from the component data.

Appendix 5: Supervised Maximum Likelihood Classifications

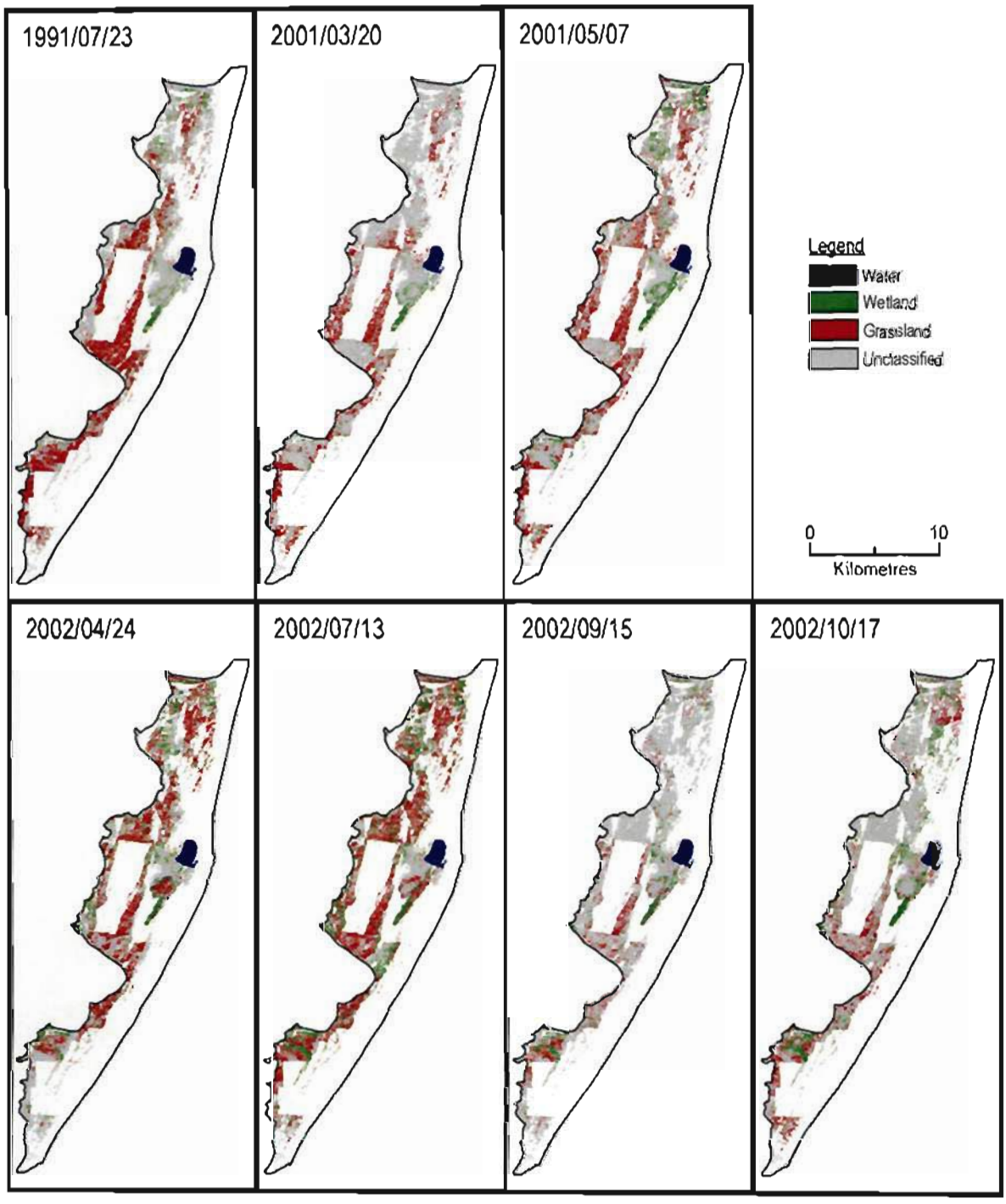

Figure A5.1: Maximum likelihood classification of the spectral data.

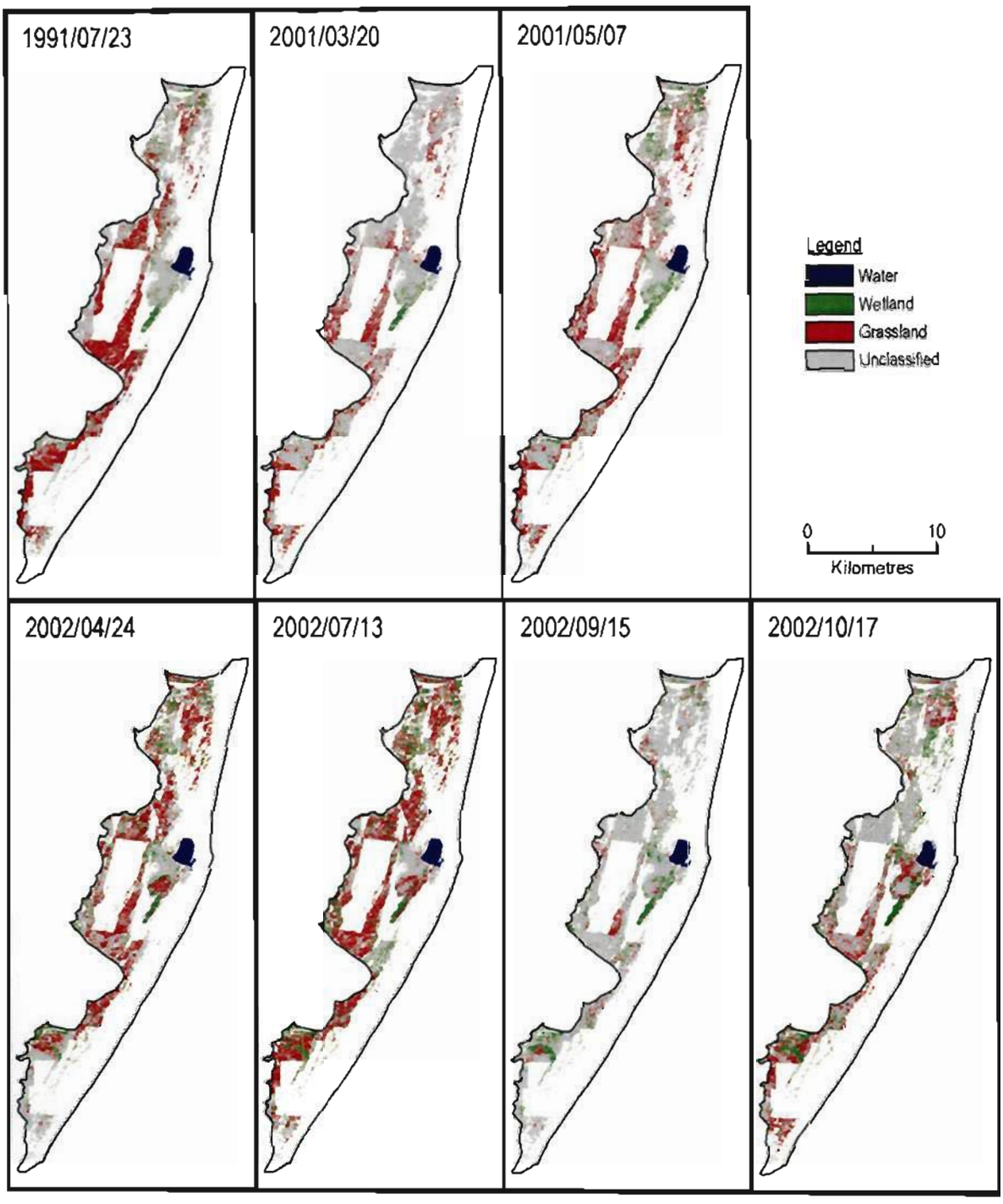

Figure A5.2: Maximum likelihood classification of the component data.

Appendix 6: Calculation of Mixture Analysis Residuals

The following example illustrates the calculation of the residual value (also known as the RMS error value) for a single pixel. Three endmembers were used to model the fraction of forest, grassland and water in the pixel.

Spectral mixture analysis applied to the band values of this pixel

using these endmember values

resulted in these fractions being obtained

Actual pixel values	
Band	***Value***
Band 2	7
Band 3	10
Band 4	16
Band 5	13

Endmember values			
Band	***Forest***	***Grassland***	***Water***
Band 2	3	8	3
Band 3	2	12	5
Band 4	39	32	2
Band 5	12	38	0

Endmember fractions	
Endmember	***Fraction***
Forest	0.1
Grassland	0.3
Water	0.6

Multiplying the endmember values by the corresponding endmember fraction gives the modelled values
e.g. 3 x 0.6 = 1.8

Band	***Forest***	***Grassland***	***Water***	***Sum***
Band 2	0.3	2.4	1.8	4.5
Band 3	0.2	3.6	3.0	6.8
Band 4	3.9	9.6	1.2	14.7
Band 5	1.2	11.4	0.0	12.6

Residuals
2.5
3.2
1.3
0.4
7.4

Band residuals are the absolute difference between the modelled and actual pixel values
e.g. | 4.5 - 7 | = 2.5

Modelled pixel values are obtained by summing the endmember modelled values
e.g. 1.2 + 11.4 + 0.0 = 12.6

Adding the band residuals gives the residual value [also known as the RMS error value]